2023

Aspects of damping in correlated quantum systems

BOSTON UNIVERSITY

GRADUATE SCHOOL OF ARTS AND SCIENCES

Dissertation

ASPECTS OF DAMPING IN CORRELATED QUANTUM SYSTEMS

by

MATTEO BELLITTI

B.S., University of Trento, 2014
M.S., University of Trento, 2016

Submitted in partial fulfillment of the

requirements for the degree of

Doctor of Philosophy

2023

Approved by

First Reader

Chris R. Laumann, PhD
Associate Professor of Physics

Second Reader

Claudio Chamon, PhD
Professor of Physics

ASPECTS OF DAMPING IN CORRELATED QUANTUM SYSTEMS

MATTEO BELLITTI

Boston University, Graduate School of Arts and Sciences, 2023

Major Professor: Chris R. Laumann, PhD
Associate Professor of Physics

ABSTRACT

In this work we discuss three problems connected to the damping of oscillations in quantum systems: dynamics and decay in a random matrix model with conserved quantities, energy redistribution and decay of the amplitude mode in a superconductor, and the decay of the gapped mode in a molecular condensate, a bosonic analog to the superconductor. These problems highlight different aspects of damping and energy redistribution in quantum dynamics, while being simple enough that analytic control is possible.

The first system captures the idea of a "partially conserved" quantity: in ergodic quantum systems, physical observables have a non-relaxing component if they overlap with a conserved quantity, but how to isolate the non-relaxing component is in general unclear. We compute exact dynamical correlators governed by a Hamiltonian composed of two large interacting random matrices, $H = A + B$, and we analytically obtain the late-time value of $\langle A(t)A(0)\rangle$, which quantifies the non-relaxing part of the observable A. We show that the relaxation to this value is governed by a power-law determined by the spectrum of the Hamiltonian H, independent of the observable A, while the long–time value and the amplitude of the oscillations depend on the trace–overlap between

the operator and the Hamiltonian. For Gaussian matrices, we further compute out-of-time-ordered-correlators (OTOCs) and find that the existence of a non-relaxing part of A leads to modifications of the late time values and exponents. Our results follow from exact resummation of a diagrammatic expansion and hyperoperator techniques.

The above problem deals with energy redistribution in a system with a complex internal structure, but without any spatial dependence nor many–body effects. In the second part of this work we discuss energy relaxation in a system with both: a BCS superconductor. In particular, we study the excitation of the collective Higgs oscillations of the order parameter by incoherent short pulses of light with frequency much larger than the superconducting gap. We find that the excitation amplitude of the Higgs mode is controlled by a single parameter, determined by the total number of quasiparticles excited by the pulse, which we trace back to the universality of the shape of the light-induced quasiparticle cascade at energy below the Debye frequency and above the gap. Our analysis is primarily based on the Keldysh technique for non–equilibrium field theory and the Boltzmann kinetic equation.

Finally, we study the damping of the gapped mode in a molecular Bose–Einstein condensate, the Bosonic analogue of a BCS superconductor. This system has the advantage of giving the experimentalist fine control over the interatomic interactions using Feshbach resonances, and is the object of renewed interest as the molecular superfluid phase has only very recently been realized in the lab. We discuss damping in the nontrivial thermodynamic phases: in the molecular superfluid phase the gapped excitation is protected by parity, and is damped only above a threshold momentum –as in the Cherenkov effect–, while in the atomic superfluid phase the gapped mode is damped at all momentum scales. We propose a class of experiments where our results are measurable: transmission (and reflection) of an atom beam through a molecular condensate cloud.

Contents

List of Tables

List of Figures

List of Abbreviations

ASF	.....	Atomic Superfluid
BCS	.....	Bardeen–Cooper–Schrieffer
BEC	.....	Bose-Einstein Condensate
BIN	.....	Binary Spectrum Ensemble
ETH	.....	Eigenstate Thermalization Hypothesis
GUE	.....	Gaussian Unitary Ensemble
MP	.....	Marchenko–Pastur
MSF	.....	Molecular Superfluid
OTOC	.....	Out–of–time–order Correlator
RKA	.....	Retarded Keldysh Advanced
RMT	.....	Random Matrix Theory
SYK	.....	Sachdev–Ye–Kitaev

Chapter 1

Introduction

In recent years, the effort directed at realizing a universal quantum computer has shifted the focus of many physicists: rather than trying to understand the details of naturally occurring quantum system, the challenge is to gain finer and more reliable control over synthetic ones.

The remarkable improvement in experimental techniques that followed this effort has opened the door to probing physical regimes that have been out of reach before. Two impressive examples relevant to this work are ultrafast spectroscopy, which allows the experimentalist to follow the dynamics of a quantum many–body system on the picosecond scale, and high precision manipulation of Feshbach resonances in ultracold atoms, that as we will see in chapter 4 gave access to a new thermodynamical phase of the dilute Bose gas.

It is interesting how these developments, inspired by quantum computation, have fed back into many–body physics at large, and stimulated a renewed interest in natural systems that can now be realistically measured. This exchange is the inspiration of this thesis: real experiments are noisy and dissipative, so it is essential to include the effect of damping in our dynamical predictions if we want to connect to experiments.

The three topics we treat follow the logic we just described: prompted by some questions related to the Quantum Satisfiability problem, we extended the scope to any generic quantum system without spatial structure but very complex spectrum, and asked how energy is redistributed in such a system. Our work quantifies the idea

behind the common wisdom that "conserved quantities diffuse slowly". The other two problems are also about energy redistribution and damping, but introduce many–body correlations in the form of Cooper pairing and superfluidity in a paired bosonic gas.

We tried to keep each chapter as self contained as possible, introducing enough technical background necessary to follow our steps.

Chapter 2

Conservation Laws and Decay in a Random Matrix Model

An earlier version of this chapter appeared before in (Bellitti et al., 2019).

2.1 Introduction

Consider an isolated quantum system whose Hamiltonian can be decomposed into two terms

$$H = A + B \tag{2.1}$$

Under what conditions does the observable A have a non-relaxing component? There are many more or less exotic mechanisms for the connected correlation function $\langle A(t)A(0)\rangle_c$ (the expectation $\langle\circ\rangle$ may include thermal and disorder averaging, the distinction is not important at this level of discussion) to approach a non-zero constant at late time: A could commute with H, or the whole system could be localized (Anderson, 1958a; Gornyi et al., 2005; Basko et al., 2006; Serbyn et al., 2013; Huse et al., 2014; Nandkishore and Huse, 2015), scarred (Bernien et al., 2017; Turner et al., 2018; Lin and Motrunich, 2019; Choi et al., 2019), shattered (Khemani and Nandkishore, 2019), or otherwise mistreated by theorists.

However, even in the simple case in which H is ergodic and A does not commute with it, the operator A appears to be "part" of the conserved energy and we expect it

to have a non-relaxing component.

This intuition is misleading. For any operator O and any Hamiltonian H, one could write $H = (H - O) + O$ and formally reproduce the decomposition in Eq. (2.1) without learning anything. For Eq. (2.1) to be nontrivial, there must be some physical sense in which the decomposition is defined. We consider the case in which A and B are large independent random matrices of dimension N with arbitrary spectra. They need not obey Wigner's celebrated semicircle law (Wigner, 1958), but the eigenvectors of A must be in generic position with respect to those of B. While this choice appears technical, it is a natural model if H, A and B each satisfy the eigenstate thermalization hypothesis (ETH) (Srednicki, 1999) and A and B are built out of physically distinct local operators.

Our primary result is an exact integral representation of the dynamical correlator $\langle A(t)A(0)\rangle_c$ at large N (Eq. (2.41)). From this representation we derive the asymptotic structure at late time,

$$\langle A(t)A(0)\rangle_c \underset{t\to\infty}{\sim} A_\infty^2 + C_{A,H}\left|\left\langle e^{iHt}\right\rangle\right|^2 \tag{2.2}$$

where A_∞^2 and $C_{A,H}$ are two constants that will be discussed in detail in Sec. 2.3.

For now, notice that this form has two important features: first, the late-time value A_∞^2 of the correlator quantifies the non-relaxing component of A. It has a definite integral representation in terms of the densities of states of A and H (see Eq. (2.50)). In general, A_∞^2 is not zero –this accords with the intuition that A is part of the energy– however it is not given by a simple trace overlap.

Second, $\langle A(t)A(0)\rangle_c$ approaches its late-time value with a form governed by the characteristic function of H alone. The particular operator A only enters through the constant rescaling $C_{A,H}$. This implies that the late time power laws come from the singularities in the density of states of H and do not depend on any detailed

structure of A. For the many random matrix ensembles where the density of states of H has square-root singularities –the semicircle law is one example– Eq. (2.2) predicts $1/t^3$ decay. Still, other possibilities exist: if A and B are projectors, for example, the resulting Hamiltonian has different singularities which produce a slower $1/t$ decay.

The reader may be surprised by the apparent lack of thermalization in a system whose Hamiltonian is *random*. For extended ergodic systems of volume V, we indeed expect the infinite time value A^2_∞ to be a quantity of order $1/V$. Here, the system is composed of a single (N dimensional) degree of freedom and $V = 1$. Nonetheless, Eq.(2.50) predicts a precise value for the constant that can be compared with numerics on ETH-satisfying systems.

We set up the calculation at infinite temperature, but once we have those results the full temperature dependence can be derived introducing Boltzmann weights in appropriate places (Sec.2.4). In the zero temperature limit the power law approach of Eq. (2.2) is modified and typically the decay exponents are reduced by a factor of 2. This behavior is reminiscent of the SYK model at times $t > N$ (Kitaev, 2015; Kitaev and Suh, 2018; Maldacena and Stanford, 2016; Cotler et al., 2017; Bagrets et al., 2016), where N is the number of fermions, but $t < e^{Ns}$, the level spacing.

In the special case where A and B are both Gaussian random matrices, and thus satisfy the semi-circle law, these results simplify significantly: the late time value A^2_∞ is given by a trace overlap between A and H (Eq. (2.81)), as one might have guessed, and the asymptotic form Eq. (2.2) holds exactly for all times t. We derive these simplified forms both from our general diagrammatic formalism, and from a more direct hyperoperator approach.

There has been a lot of recent interest in computing out of time ordered correlators (OTOCs) as a rough characterization of quantum chaos (Kitaev, 2015; Kitaev and Suh, 2018; Nahum et al., 2018; Maldacena et al., 2016; Khemani et al., 2018; Vijay

and Vishwanath, 2018; von Keyserlingk et al., 2018; Chan et al., 2018) among other possible characterizations (Kowalewska-Kudłaszyk et al., 2009; Weinstein et al., 2002; Kowalewska-Kudłaszyk et al., 2008; Bruzda et al., 2010). For Gaussian A and B we use the hyperoperator technique to compute the OTOC,

$$\frac{1}{2}\langle [A(t), A(0)]^2 \rangle \tag{2.3}$$

and find that it decays asymptotically more slowly than if it did not contain a conserved piece.

It is worthwhile noting that much recent analytical progress on dynamics in many-body systems has been made in the setting of random unitary circuits.(Chandran and Laumann, 2015; Nahum et al., 2017; Nahum et al., 2018; von Keyserlingk et al., 2018) These models do not naturally have conservation laws, and introducing the extra structure to create them (Khemani et al., 2018; Rakovszky et al., 2018) makes calculations significantly harder. On the contrary, Hamiltonian models automatically come with a conserved energy, but deriving exact results there is difficult in the absence of further structure like conformal symmetry, integrability, or a large-N limit. Our work falls in this last class: we treat a Hamiltonian system exactly, at the price of introducing large-N random matrices.

All of our results are at infinite temperature and averaged over the random matrix ensemble; for the rest of the chapter, the "expectation value" symbol means

$$\langle \circ \rangle := \frac{1}{N}\mathbb{E}_{A,B}\left[\mathrm{Tr}\left(\circ\right)\right] \tag{2.4}$$

and the normalization is such that the $N \times N$ identity matrix has expectation equal to 1. The requirement of infinite temperature is not necessary, in Sec.2.4 we discuss how to deal with finite temperature systems.

The ensemble for A and B is fairly general: we just need their densities of states

ρ_A and ρ_B to be well defined in the limit $N \to \infty$, and their eigenspaces to be in generic position. One way to realize such matrices is

$$A = U^\dagger \Lambda U \tag{2.5}$$

where Λ is a diagonal matrix and U is a Haar unitary.

2.2 Autocorrelation

2.2.1 Frequency space representation of correlators

We want to understand the dynamics of the two point function

$$G(t) = \langle A(t)A(0)\rangle = \left\langle e^{iHt} A e^{-iHt} A \right\rangle \tag{2.6}$$

It is convenient to reformulate the problem in frequency space, using the Cauchy representation of the time evolution operator:

$$e^{iHt} = \oint \frac{dz}{2\pi i} \frac{e^{izt}}{z - H} \tag{2.7}$$

where the integral is over any contour that encloses the full spectrum of H (see fig. 2·1). At any finite Hilbert space size N this contour is closed, and in the thermodynamic limit it can be closed at infinity.

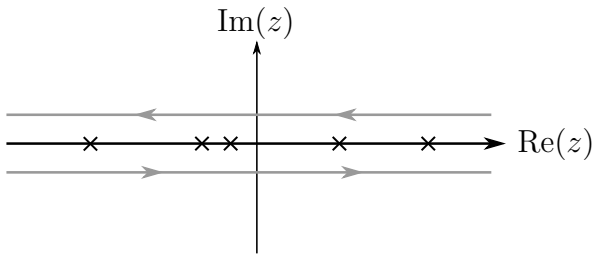

Figure 2·1: Integration contour for the Cauchy transform in Eq. (2.7). The crosses are eigenvalues of H.

Using the integral representation just introduced, we can rewrite Eq. (2.6) as

$$G(t) = \oint \frac{dz}{2\pi i}\frac{dw}{2\pi i} e^{i(z-w)t} \left\langle \frac{1}{z-H} A \frac{1}{w-H} A \right\rangle \tag{2.8}$$

$$= \oint \frac{dz}{2\pi i}\frac{dw}{2\pi i} e^{i(z-w)t} G(z,w) \tag{2.9}$$

which defines the frequency space correlator:

$$G(z,w) \coloneqq \left\langle \frac{1}{z-H} A \frac{1}{w-H} A \right\rangle \tag{2.10}$$

$$= \sum_{m=0}^{\infty}\sum_{n=0}^{\infty} \frac{1}{z^{n+1}}\frac{1}{w^{m+1}} \left\langle H^n A H^m A \right\rangle \tag{2.11}$$

The last formal manipulation involving the geometric series shows that we can reduce the problem of determining $G(z,w)$ to the calculation of mixed moments of A and H:

$$\left\langle H^n A H^m A \right\rangle = \left\langle (A+B)^n A (A+B)^m A \right\rangle \tag{2.12}$$

For practical purposes it is better to write the calculation in terms of the matrices A and B, as they are the independent objects in the problem.

2.2.2 Free cumulant expansion

If A and B are Gaussian random matrices, the evaluation of the moments in Eq.(2.12) is readily accomplished using Wick's theorem. For the more general matrices we treat here, the *free cumulant expansion* plays the role of a generalized Wick's theorem for non-commuting matrices. Given a set of non-commuting random variables X_i, we can recursively define their *free cumulants* (denoted with curly braces) through the formula

$$\left\langle X_1 \dots X_n \right\rangle =: \sum_{\pi \in \mathrm{NC}(n)} \prod_{b \in \pi} \left\{ X_{i_1} \dots X_{i_{|b|}} \right\} \tag{2.13}$$

where NC(k) denotes the set non–crossing partitions of k objects, and b is a block in the partition π.

Free cumulants were originally introduced in the context of free probability theory (Voiculescu, 1986), to easily compute the statistical properties of the sum of two non–commuting random variables. For our purposes we need three fundamental facts about free probability theory:

1. The free cumulants of simple distributions are known, and are an input to our derivations. We will make explicit examples using Gaussian random matrices;

2. The mixed free cumulants of *freely independent* random matrices vanish;

3. Random matrices whose eigenbases are in generic position become freely independent in the large N limit.

We refer the reader to (Nica and Speicher, 2006) for an in–depth explanation of these properties. These three statements make the evaluation of the moments in Eq.(2.12) possible, but the free cumulant expansion of of Eq.(2.13) is impractical to use in its algebraic form in all but the simplest cases, so we translate it to a set of diagrammatic rules.

2.2.3 Diagrammatic Approach

In section 2.2.1 we reduced the calculation of the $\langle A(t)A(0)\rangle$ correlator to the evaluation of a mixed moment, which proceeds using the free cumulant expansion Eq. (2.13) in diagrammatic form. The diagrammatics are similar to those of (Brézin et al., 1993; Brézin and Zee, 1994; Morampudi and Laumann, 2018) although our interpretation in terms of free cumulants is somewhat more recent (Nica and Speicher, 2006; Morampudi and Laumann, 2018).

We are computing trace moments, so it is natural to represent them with a circular diagram. Factors of A will be represented by the insertion of a full dot ($\bullet$) along the circle and B factors by insertions of an empty one ($\circ$).

Notice that two of the A insertions are not like the others: they do not come from the expansion of H^n. Each diagram is then naturally split in two halves by those special A insertions, one half associated to the H^n/z^{n+1} term and the other one to the H^m/w^{m+1} term of Eq.(2.10).

We associate single lines (—) to factors of $1/z$ and $1/w$: lines in the upper semicircle represent factors of $1/z$ and lines in the lower semicircle factors of $1/w$.

A vertex with double line legs (=) that connects a set of insertions represents the free cumulant of those operators. Notice that all the insertions participating in a given vertex must be of the same kind, as mixed free cumulants of A and B vanish.

Let us summarize the diagrammatic rules we have just introduced:

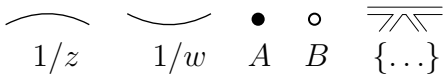

Finally, in the free cumulant expansion we only need noncrossing partitions, so these diagrams are *planar*. The planar nature of these diagrams makes them easy to classify, which will be very useful later in this section, when we compute the perturbative resummation of infinitely many diagrams. For aficionados of planar perturbation theory, we point out that the free cumulants of a random matrix X are closely related to the fully renormalized vertices of X.

Our aim is the following: to compute $G(z,w)$ to leading order in $O(1/N)$ we must *sum over all planar diagrams with at least two A insertions and any number of A and B insertions in the upper and lower halves.* There are no extra combinatorial factors.

As an example of the application of these rules, let us calculate a diagram that will be included in the expansion of $G(z,w)$:

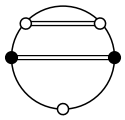

$$= \frac{1}{z^3 w^2} \{A^2\} \{B^2\} \{B\} \tag{2.14}$$

In this simple case there are only vertices with one or two legs, but in general a vertex can have any number of legs. Without loss of generality, we assume that $\{A\} = \{B\} = 0$. This does not change the dynamics, as it corresponds to a constant energy shift, but makes the diagrammatics much simpler.

In the next few sections we introduce some partial results, which are the building blocks of the main result we present in Sec.2.2.9.

2.2.4 Propagator

The *full propagator* of H, $f_H(z)$, is

$$f_H(z) \coloneqq \left\langle \frac{1}{z - H} \right\rangle = \sum_{n=0}^{\infty} \frac{\langle H^n \rangle}{z^{n+1}}. \tag{2.15}$$

Below, we suppress the subscript H when there is no risk of confusion. As usual, the complex analytic features of the propagator encode the spectrum of H. For example, the mean spectral density $\rho(x)$ can be obtained by inserting the Sokhotski–Plemelj formula

$$\lim_{\delta \to 0^+} \frac{1}{x \pm i\delta} = P\frac{1}{x} \mp i\pi\delta(x) \tag{2.16}$$

into the definition of the propagator,

$$f_H(x \pm i\delta) = \left\langle \frac{1}{x - H \pm i\delta} \right\rangle \tag{2.17}$$

$$= \phi_H(x) \mp i\pi\rho_H(x) \tag{2.18}$$

gives the the spectral density $\rho_H(x)$ and its Hilbert transform

$$\phi_H(x) \coloneqq \left\langle P\frac{1}{x - H} \right\rangle = P \int d\lambda \, \frac{\rho_H(\lambda)}{x - \lambda} \tag{2.19}$$

where the symbol P means that the integral uses Cauchy's principal part prescription.

2.2.5 1PI Diagrams

We write a diagrammatic representation of Eq. (2.15) by introducing a thick line to represent $f(z)$:

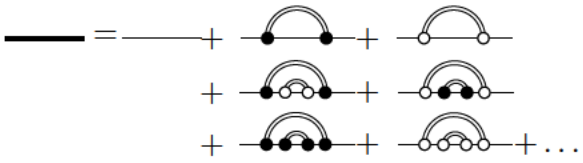

(2.20)

This series can be organized into a Schwinger-Dyson equation,

(2.21)

where we have introduced two kinds of one–particle irreducible diagrams (1PI) – those with an A or a B as their outermost insertion. We remind the reader that 1PI diagrams are the amputated diagrams which cannot be disconnected by cutting a single $1/z$ line. We solve Eq. (2.21) by introducing the 'self-energy' $\Sigma_H(z)$,

$$f_H(z) = \frac{1}{z - \Sigma_H(z)} \tag{2.22}$$

Comparing to Eq. (2.21), we have

$$\Sigma_H(z) = \Sigma_A(z) + \Sigma_B(z) \tag{2.23}$$

where

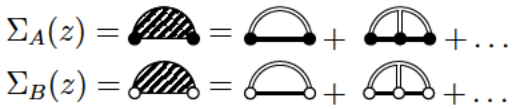

(2.24)

Let us pause and make several connections between planar perturbation theory and free probability theory explicit. The self-energies in Eq. (2.24) are given algebraically

by[1]

$$\Sigma_A(z) \equiv R_A(f(z)) \equiv \sum_{p=0}^{\infty} \left\{A^{n+1}\right\} f_H(z)^n \tag{2.25}$$

and similarly for Σ_B. That is, the self energy Σ_A is given by the free cumulant generating function R_A evaluated at $f_H(z)$. Thus, additivity of the self-energy in planar perturbation theory is equivalent to the additivity of the free cumulants of freely independent random variables (Zee, 1996).

The Cartesian decomposition of $f(x)$ (Eq.(2.18)) induces a similar structure in Σ_A (see Eq.(2.25)):

$$\Sigma_A(x \pm i\delta) = \sum_{n=1}^{\infty} \{A^n\} \left(\phi(x) \mp i\pi\rho(x)\right)^n \tag{2.26}$$

$$\equiv \Sigma_A^R(x) \mp i\Sigma_A^I(x) \tag{2.27}$$

where $\Sigma_A^R(x)$ and $\Sigma_A^I(x)$ are real functions.

2.2.6 2PI Diagrams

It is useful at this point to introduce the analog of the two–particle irreducible diagrams familiar in the context of field theory: they are (amputated) diagrams that cannot be separated into two disconnected pieces by cutting at most one z and one w line. Notice that all the vertices at the boundary of a 2PI diagram must be of the same type, either A or B.

We will denote $\pi_A(z, w)$ the sum of all 2PI diagrams with the most external interaction of type A:

$\pi_A(w, z) =$ 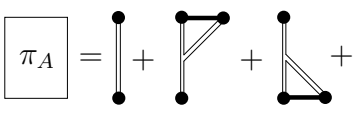 (2.28)

[1] This is a definition of R_A, as a formal power series with coefficients equal to the free cumulant of A.

and define analogously $\pi_B(z,w)$. The series corresponding to Eq. (2.28) is

$$\pi_A(z,w) = \sum_{n=0}^{\infty}\{A^{n+2}\}\sum_{t=0}^{n} f(z)^t f(w)^{n-t} \tag{2.29}$$

$$= \frac{\Sigma_A(z) - \Sigma_A(w)}{f(z) - f(w)} \tag{2.30}$$

The linearity of the self–energy contributions guarantees the linearity of this quantity as well:

$$\pi_H(z,w) = \pi_A(z,w) + \pi_B(z,w) \tag{2.31}$$

2.2.7 Box Resummation

In the diagrammatic expansion of $G(z,w)$ we need a set of disconnected diagrams that is closely related to the 2PI we just introduced: they are composed of a $1/z$ line, a $1/w$ line and any number of vertices possibly connecting those two lines. We call the sum $h(z,w)$ of this class of diagrams the *box*, and represent it with a gray shaded area[2]. The resummation of these diagrams proceeds in a way analogous to what we did for the propagator.

Before writing the self–consistent equation we show a few of the diagrams that contribute to the box:

$h(w,z) =$ 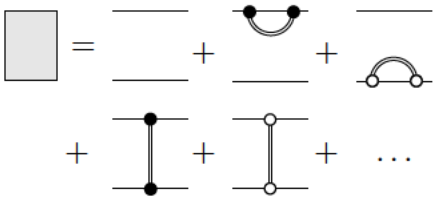 (2.32)

where we can imagine that the first line of this equation contains all the disconnected diagrams and the second line all the connected ones.

The disconnected diagrams can be summed using the results of Sec. 2.2.5, while

[2]The actual shape does not matter, as long as it has four sides: one side must contain only $1/z$ lines and the opposite one only contains $1/w$ lines

the connected diagrams can be written in terms of π_H and the box itself:

$h(w,z) =$ 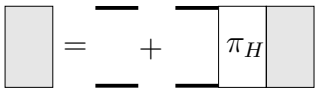 (2.33)

which can be solved for $h(z,w)$ to give

$$h(z,w) = \frac{f(z)f(w)}{1-\pi_H(z,w)f(z)f(w)} \tag{2.34}$$

We can further simplify this expression using Eq. (2.30) and Eq. (2.22), so that after some algebra we obtain

$$h(z,w) = -\frac{f(z)-f(w)}{z-w} \tag{2.35}$$

2.2.8 Triangle Resummation

There is another pattern that is important for the computation of the two–point function: (amputated) diagrams in which one of the two special insertions of A participates in a vertex with at least three legs, and it connects to both a z and a w line. The sum of all diagrams of this kind is

$T(z,w) =$ 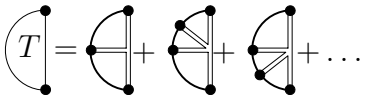 (2.36)

which can be written in a simple form using Eq. (2.25):

$$T(z,w) = \sum_{n=0}^{\infty}\{A^{n+3}\}f(z)f(w)\sum_{t=0}^{n} f(z)^t f(w)^{n-t} \tag{2.37}$$

$$= \frac{f(w)\Sigma_A(z) - f(z)\Sigma_A(w)}{f(z)-f(w)} \tag{2.38}$$

As a simple consistency check, notice that if A is from one of the Gaussian ensembles we have $\Sigma_A(z) = \{A^2\}f(z)$ and thus $T(z,w)$ vanishes identically. This

is consistent with the diagrammatic statement that Gaussian matrices do not have vertices with more than two legs.

2.2.9 Two–point correlation function: complete resummation

We are now ready to compute the two–points function $G(z, w)$: as stated in Sec. 2.2.3, we must sum over all the circular planar diagrams with at least two A insertions.

Using the objects Σ_A, h, and T we can sum all diagrams in which the two special A insertions do not connect to each other.

We organize the remaining diagrams by the kind of interaction the two A participate in:

$G(z,w) =$ 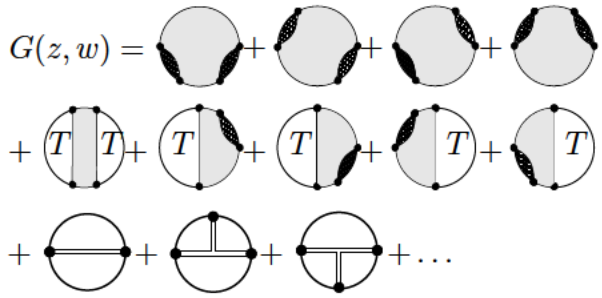

(2.39)

which is the diagrammatic representation of

$$\begin{aligned} G(z,w) = h(z,w)\left(T(z,w) + \Sigma_A(z) + \Sigma_A(w)\right)^2 \\ + \sum_{n=0}^{\infty} \left\{A^{n+2}\right\} f(z) f(w) \sum_{t=0}^{n} f(z)^t f(w)^{n-t} \end{aligned} \tag{2.40}$$

and the series appearing in the last term can be summed as usual using Eq. (2.25):

$$\begin{aligned} G(w,z) = f(z)f(w)\frac{\Sigma_A(w) - \Sigma_A(z)}{f(w) - f(z)} \\ - \frac{f(z) - f(w)}{z - w}\left(\frac{f(z)\Sigma_A(z) - f(w)\Sigma_A(w)}{f(z) - f(w)}\right)^2 \end{aligned} \tag{2.41}$$

This is our main result about the two–point function: once we fix the probability distributions of A and B, we can compute (Novak and LaCroix, 2012; Zee, 1996) $f(z)$ and $\Sigma_A(z)$, so they can be considered inputs to the problem.

2.2.10 Example: A, B Gaussian

If A and B are sampled from the GUE ensemble, all their free cumulants vanish after the second one. Without loss of generality we can set

$$\{A\} = \{B\} = 0, \tag{2.42}$$

while a convenient choice for the second free cumulant is

$$\{A^2\} = \lambda, \quad \{B^2\} = 1 - \lambda \tag{2.43}$$

with $0 \leq \lambda \leq 1$. For these random variables the self–energy series terminates after just one term:

$$\Sigma_A(z) = \lambda f(z) \qquad \Sigma_B(z) = (1-\lambda) f(z). \tag{2.44}$$

where $f(z)$ is the full propagator for H. In the infinite N limit, independent GUE variables are also freely independent (Nica and Speicher, 2006), so we can use Eq. (2.23) and Eq. (2.22) to compute

$$f(z) = \frac{1}{2}\left(z - \sqrt{z^2 - 4}\right) \tag{2.45}$$

and plugging f and Σ_A in Eq. (2.41) we have

$$G(w,z) = \lambda f(z) f(w) - \lambda^2 \frac{f(z) - f(w)}{z - w} \left(f(w) + f(z)\right)^2 . \tag{2.46}$$

The real time correlator is (Eq. (2.9)):

$$\langle A(t) A(0) \rangle = \oint \frac{dz}{2\pi i} \frac{dw}{2\pi i} e^{i(z-w)t} G(z,w) \tag{2.47}$$

which has a closed form[3] in terms of the Bessel function J_1:

$$\frac{1}{\lambda}\langle A(t)A(0)\rangle = \lambda + (1-\lambda)\left(\frac{J_1(2t)}{t}\right)^2 \tag{2.48}$$

2.3 Late Time Asymptotics

2.3.1 General Case

The integral in Eq. (2.9) can not be expressed in terms of elementary functions except in a few special cases. In this section we prove that for a large class of Haar–invariant ensembles we have the asymptotic result

$$\langle A(t)A(0)\rangle \sim A_\infty^2 + C_{A,H}\left|\left\langle e^{iHt}\right\rangle\right|^2 \quad t\to\infty \tag{2.49}$$

where $C_{A,H}$ is a real constant and (see Eq. (2.17) and Eq.(2.25) for the definitions of the quantities involved)

$$A_\infty^2 \equiv \int dx\ \rho_H(x)\left(\mathrm{Re}\Sigma_A(x) + \phi_H(x)\frac{\mathrm{Im}\Sigma_A(x)}{\pi\rho_H(x)}\right)^2 \tag{2.50}$$

This integral expression lets us compute the long–time value of the correlator, and the second term in Eq.(2.49) contains the non–trivial result that the decay is controlled by the Hamiltonian only.

To derive Eq. (2.49), we deform the integration contours in Eq. (2.9) to run infinitesimally close to the real axis:

$$z =: x \pm i\delta \qquad w =: y \pm i\delta \qquad x, y, \delta \in \mathbb{R} \tag{2.51}$$

and for convenience we define the symbol

$$\Delta_x^\delta f(x) \coloneqq \lim_{\delta\to 0^+}\left(f(x+i\delta) - f(x-i\delta)\right) \tag{2.52}$$

[3]The factor $1/\lambda$ on the left–hand side is included for convenience: with the choices of this section $\langle A(0)A(0)\rangle/\lambda = 1$.

so that after parametrization the integral representation of the two–point correlator becomes

$$\langle A(t)A(0)\rangle = \int_{-\infty}^{\infty} \frac{dxdy}{(2\pi i)^2}\, e^{i(x-y)t}\Delta_x^\delta \Delta_y^\delta G(x,y). \tag{2.53}$$

Comparing with Eq. (2.41), it is clear that contributions to the long–time value of this integral only come from Dirac $\delta(x)$ terms in $f(z)$, and the divergence in $h(x+i\delta, y-i\delta)$ as x approaches y (see Eq.(2.35)) .

The first kind of constant is trivial, so we will assume that

$$\lim_{t\to\infty} \left\langle e^{iHt} \right\rangle = 0 \tag{2.54}$$

and focus on the second kind.

The asymptotic behavior of the inverse Fourier transform $\mathcal{F}^{-1}\{\circ\}(t)$ is determined by singularities in frequency space (Lighthill, 1958a), with smaller positive powers $\alpha_i > 0$ corresponding to slower real time decay:

$$\mathcal{F}^{-1}\left\{ \sum_i |x - x_i|^{\alpha_i} \right\} \sim O\left(\frac{1}{|t|^{\min_i \alpha_i + 1}} \right) \quad t \to \infty. \tag{2.55}$$

For many common choices of A and B, including the Gaussian, the Orthogonal Polynomial (Brézin et al., 1993), and the Wishart ensemble, all the singularities in $\rho_H(x)$ are of the form

$$|x - x_i|^{\alpha_i}\, \theta(x - x_i) \qquad \alpha_i > 0 \tag{2.56}$$

which means that the density of states is small close to its edges. We obtain then the asymptotics of Eq. (2.53) expanding the integrand in powers of ρ and integrating term by term. The expansion coefficients depend on x and y, so they could in principle modify the singular behavior, but in hindsight we realize that this not the case.

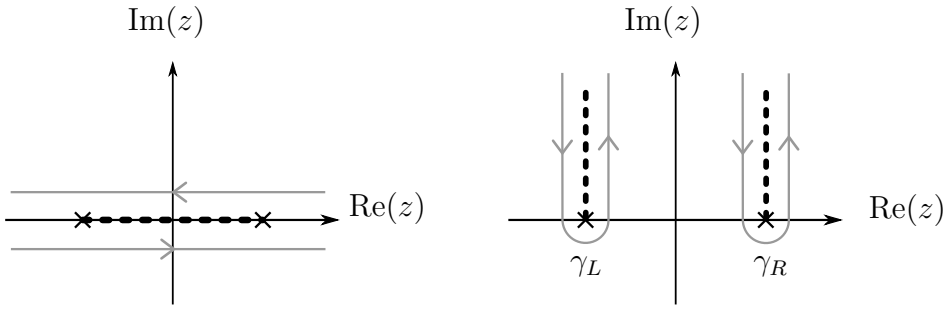

Figure 2·2: Branch cut (dashed line) and integration contour for Eq. (2.58). The same choices are made in the w plane.

Keeping terms up to $O(\rho(x)\rho(y))$ gives

$$\begin{aligned}\Delta_x^\delta \Delta_y^\delta G(x,y) \sim &(2\pi i)^2 \left(R_A(\phi(x)) + \phi(x) \frac{dR_A(\phi(x))}{d\phi(x)} \right)^2 \delta(x-y)\rho(x) \\ &+ (2\pi i)^2 \frac{d^2}{d\phi(x) d\phi(y)} \left(\phi(x)\phi(y) \frac{R_A(\phi(x)) - R_A(\phi(y))}{\phi(x) - \phi(y)} \right. \\ &\left. - \frac{\phi(x) - \phi(y)}{x-y} \left(\frac{\phi(x) R_A(\phi(x)) - \phi(y) R_A(\phi(y))}{\phi(x) - \phi(y)} \right)^2 \right) \rho(x)\rho(y).\end{aligned} \tag{2.57}$$

The first term is time–independent after integration, and gives an approximate value of $\langle A(\infty)A(0)\rangle$, but we can do better: using Eq. (2.16) *before* expanding in powers of ρ and collecting all terms proportional to $\delta(x-y)$, we obtain the exact expression presented in Eq. (2.50).

2.3.2 Example: Asymptotics for a $\sqrt{x}$ Edge

The square–root singularity at the edges of the GUE spectral density is very common, so we believe it is useful to analyze in detail this case. Using the same conventions as in section 2.2.10, Eq. (2.9) reads

$$\frac{\langle A(t)A(0)\rangle}{\lambda} = \oint \frac{dz}{2\pi i} \frac{dw}{2\pi i} e^{i(z-w)t} \left(f(z)f(w) - \lambda \frac{f(z) - f(w)}{z-w} \left(f(w) + f(z) \right)^2 \right) \tag{2.58}$$

The integrand has four branching points in $z = \pm 2$ and $w = \pm 2$ (see Eq. (2.45)), so we cut the complex plane and deform the integration contour as presented in fig. 2·2.

The first term in Eq. (2.58) is factorized and can be estimated using standard[4] methods of asymptotic analysis:

$$\int_{\gamma_L} \frac{dz}{2\pi i}\, e^{izt} f(z) \sim -\frac{e^{-i\pi/4}}{2\sqrt{\pi}} \frac{e^{-2it}}{t^{3/2}} \qquad \text{as } t \to \infty \tag{2.59}$$

$$\int_{\gamma_R} \frac{dz}{2\pi i}\, e^{izt} f(z) \sim -\frac{e^{i\pi/4}}{2\sqrt{\pi}} \frac{e^{2it}}{t^{3/2}} \qquad \text{as } t \to \infty \tag{2.60}$$

which gives

$$\oint dz\; e^{izt} f(z) \sim -\frac{1}{\sqrt{\pi}} \frac{1}{t^{3/2}} \cos\left(2t + \frac{\pi}{4}\right) \qquad \text{as } t \to \infty \tag{2.61}$$

Using Eq. (2.45), we can rewrite the remaining terms in Eq. (2.58) as

$$\frac{f(z) - f(w)}{z - w} \left(f(w) + f(z)\right)^2 = -1 + f(z)f(w) - \frac{z^2 f(z) - w^2 f(w)}{z - w} \tag{2.62}$$

During the calculation we drop all analytic terms from the sum, as they integrate to zero on a closed contour. The factorized term gives the same result as Eq. (2.61), and one proves that

$$\oint \frac{dz}{2\pi i} \frac{dw}{2\pi i}\, e^{i(z-w)t}\, \frac{z^2 f(z) - w^2 f(w)}{w - z} = 1 \tag{2.63}$$

Even without going into the details of integration, we can recognize that it must be constant, by taking the time derivative under the integral sign:

$$\frac{d}{dt} \oint \frac{dz}{2\pi i} \frac{dw}{2\pi i} e^{i(z-w)t} \frac{z^2 f(z) - w^2 f(w)}{w - z} \tag{2.64}$$

$$= \oint \frac{dz}{2\pi i} \frac{dw}{2\pi i} e^{i(z-w)t} i(z^2 f(z) - w^2 f(w)) = 0 \tag{2.65}$$

where the last equality holds because now each term in the sum factorizes. In

[4] We remind the reader that $\sqrt{-1} = \exp(-i\pi/2)$ with our choice of branch cut.

conclusion, we have proved that

$$\frac{\langle A(t)A(0)\rangle}{\lambda} \sim \lambda + \frac{1-\lambda}{\pi t^3}\cos^2\left(2t+\frac{\pi}{4}\right) \quad t\to\infty \tag{2.66}$$

which is consistent with the exact result Eq.(2.48), since

$$\frac{J_1(2t)}{t} \sim -\frac{1}{\sqrt{\pi}}\frac{1}{t^{3/2}}\cos\left(2t+\frac{\pi}{4}\right) \qquad t\to\infty \tag{2.67}$$

2.4 Finite temperature modifications

In order to extend our arguments from infinite to finite temperature β^{-1}, observe that the exact analysis of $G(w,z)$ is unmodified, so the results we have derived about $G(t)$ immediately transfer: it is sufficient to replace $t\to t+i\beta$ in appropriate locations, which induces some thermal reweighting of the integrals. Here, we point out the key modifications that need to be made in Secs. 2.2 and 2.3 for finite β.

At finite temperature, the dynamical autocorrelator is

$$\langle A(t)A(0)\rangle_\beta = \mathbb{E}\left[\frac{\mathrm{Tr}\left(e^{-\beta H}A(t)A(0)\right)}{\mathrm{Tr}\left(e^{-\beta H}\right)}\right] \tag{2.68}$$

At large N, the concentration of measure allows one to split the disorder average between numerator and denominator. Defining the partition function

$$Z \equiv \frac{1}{N}\mathbb{E}\left[\mathrm{Tr}\left(e^{-\beta H}\right)\right] \tag{2.69}$$

the correlator becomes

$$\langle A(t)A(0)\rangle_\beta = \frac{1}{Z}\langle e^{(it-\beta)H}Ae^{-iHt}A\rangle \tag{2.70}$$

where the average on the right is the usual disordered averaged trace from Eq. (2.4).

Retracing the steps of Sec.2.2, we find that all the information about temperature

disappears from $G(z,w)$, and is only contained in the integration measure:

$$\langle A(t)A(0)\rangle_\beta = \oint \frac{dw}{2\pi i}\frac{dz}{2\pi i}\frac{e^{(it-\beta)z}}{Z}e^{-iwt}G(w,z) \tag{2.71}$$

The exponential factor $e^{-\beta z}$ does not cause convergence problems if the density of states has bounded support, as in most random matrix ensembles.

In particular, the late time asymptotics of $\langle A(t)A(0)\rangle_\beta$ are still governed by the decomposition Eq. (2.57) of the exact $G(w,z)$. Plugging Eq. (2.57) into Eq. (2.71), we find the analog of Eq.(2.2):

$$\langle A(t)A(0)\rangle_\beta \underset{t\to\infty}{\sim} A^2_{\infty,\beta} + \frac{C_{A,H}}{Z}\left\langle e^{(it-\beta)H}\right\rangle\left\langle e^{-iHt}\right\rangle \tag{2.72}$$

The late time constant $A^2_{\infty,\beta}$ is the same as Eq.(2.50) reweighted by the Boltzmann weight,

$$A^2_{\infty,\beta} = \int dx \frac{e^{-\beta x}}{Z}\rho_H(x)\left(\mathrm{Re}\Sigma_A(x) + \phi(x)\frac{\mathrm{Im}\Sigma_A(x)}{\pi\rho_H(x)}\right)^2 \tag{2.73}$$

Somewhat more interesting is the approach to the constant: for any finite β the power law is the same as in infinite temperature case, while in the limit $\beta\to\infty$ the decay is slower since

$$\frac{1}{Z}\left\langle e^{(it-\beta)H}\right\rangle \to e^{itE_0} \tag{2.74}$$

where E_0 is the ground state energy. Thus, if the finite temperature relaxation follows a power law $1/t^\alpha$, the zero temperature system relaxes as $1/t^{\alpha/2}$.

2.5 The Gaussian Rotation Approach

If A and B are both Gaussian, there is an alternative approach that lets us compute any real–time correlator based on an orthogonal transformation.

If A and H are freely independent, we can easily compute the two–point function

$$\langle A(t)A(0)\rangle = \left\langle e^{iHt}Ae^{-iHt}A\right\rangle \tag{2.75}$$

using the non–crossing rules between A and H, but the problem is of course that we are interested in the case when they are not.

In section 2.2 we kept A fixed and expanded H in terms of A and B, which do have a non–crossing rule. Here we do the opposite: we hold H fixed, and seek a change of variables that turns A into something freely independent with H. This is easily done in the Gaussian case, but it is not clear how to construct such a transformation for general ensembles.

As in Sec.2.2.10, we use traceless matrices with second moments

$$\{A^2\} = \lambda \qquad \{B^2\} = 1 - \lambda \tag{2.76}$$

and it is convenient to extract the λ dependence defining the unit variance variables

$$\tilde{A} \equiv \frac{A}{\sqrt{\lambda}} \qquad \tilde{B} \equiv \frac{B}{\sqrt{1-\lambda}} \tag{2.77}$$

to make the algebra in the rest of the section a little cleaner.

We define the variable C through the orthogonal transformation

$$\begin{pmatrix} C \\ H \end{pmatrix} = \begin{pmatrix} \sqrt{1-\lambda} & -\sqrt{\lambda} \\ \sqrt{\lambda} & \sqrt{1-\lambda} \end{pmatrix} \begin{pmatrix} \tilde{A} \\ \tilde{B} \end{pmatrix} \tag{2.78}$$

which makes C Gaussian and independent with H. In the $N \to \infty$ limit, independent Gaussian variables become also freely independent(Nica and Speicher, 2006), so we have found a variable with the requested non–crossing rule with H.

The calculation of the correlator at this point is straightforward: we express A as

$$\tilde{A} = \frac{A}{\sqrt{\lambda}} = \sqrt{1-\lambda}C + \sqrt{\lambda}H \tag{2.79}$$

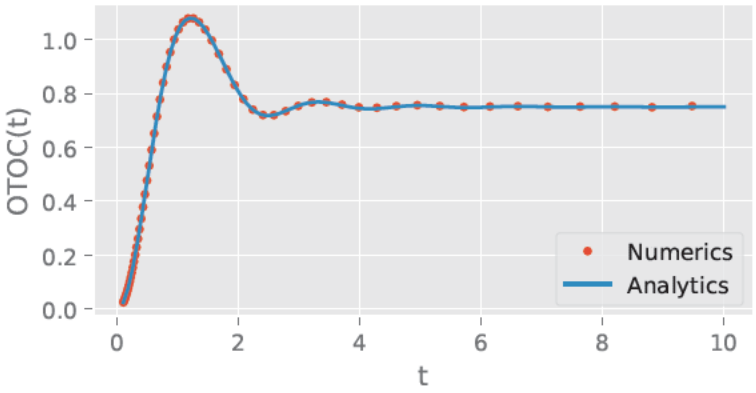

Figure 2·3: Gaussian OTOC, $N = 200$, disorder average over 10 samples.

and using the free cumulant expansion we get

$$\frac{\langle A(t)A(0)\rangle}{\lambda} = \left\langle \tilde{A}(t)\tilde{A}(0)\right\rangle \tag{2.80}$$

$$= \lambda \left\langle H^2\right\rangle + (1-\lambda)\left\langle C^2\right\rangle \left|\left\langle e^{iHt}\right\rangle\right|^2 \tag{2.81}$$

$$= \lambda + (1-\lambda)\left(\frac{J_1(2t)}{t}\right)^2 \tag{2.82}$$

which correctly reproduces the result we obtained through the diagrammatic formalism (Eq. (2.48)).

Using this method we can actually compute any correlator of Gaussian operators easily. For example, the out-of-time-order correlator of A with itself:

$$\begin{aligned} \mathrm{OTOC}(t) &\coloneqq \frac{1}{2}\left\langle |[A(t), A]|^2\right\rangle \\ &= \left\langle A(t)^2 A^2\right\rangle - \langle A(t)AA(t)A\rangle \end{aligned} \tag{2.83}$$

The free cumulant expansion gives in this case,

$$\begin{aligned}\frac{\mathrm{OTOC}(t)}{\lambda^2} = 1-\lambda^2 &+ \left(\frac{J_1(2t)}{t}\right)^2 (1-\lambda)(1-9\lambda) \\ &- \left(\frac{J_1(2t)}{t}\right)^2 \frac{J_1(4t)}{t}(1-\lambda)^2 \\ &+ \frac{J_1(2t)}{t}\frac{J_2(2t)}{t^2}12\lambda(1-\lambda) \\ &+ \left(\frac{J_2(2t)}{t}\right)^2 8\lambda(1-\lambda)\end{aligned} \tag{2.84}$$

This expression is in good agreement with numerics, as we can see from Fig. 2·3. The short time behavior is compatible with what is known in literature (Vijay and Vishwanath, 2018)

$$\frac{\mathrm{OTOC}(t)}{\lambda^2} = 5(1-\lambda)t^2 + O(t^3) \tag{2.85}$$

but we see a modification of the exponent in the long–time power law: if A is independent of H, previous work (Vijay and Vishwanath, 2018) finds a t^{-4} decay to the infinite time value. The partial conservation of A leads to a slower $1/t^3$ decay:

$$\begin{aligned}\frac{\mathrm{OTOC}(t)}{\lambda^2} =& 1-\lambda^2 + \frac{(1-\lambda)^2}{2\pi t^3} \\ &- (1-\lambda)(1-17\lambda)\frac{\sin(4t)}{2\pi t^3} + O\left(\frac{1}{t^4}\right)\end{aligned} \tag{2.86}$$

2.6 Numerical Confirmation

In this section we check the predictions of Eq. (2.41) in a few interesting cases. Table 2.1 contains a summary of the relevant functions and the resulting long–time constant, while Fig. 2·4 compares the analytical prediction with the numerical results.

In all three examples, A and B are sampled from the same ensemble simply because the resulting expressions are cleaner, but this is not necessary: our results work just as well in the mixed case.

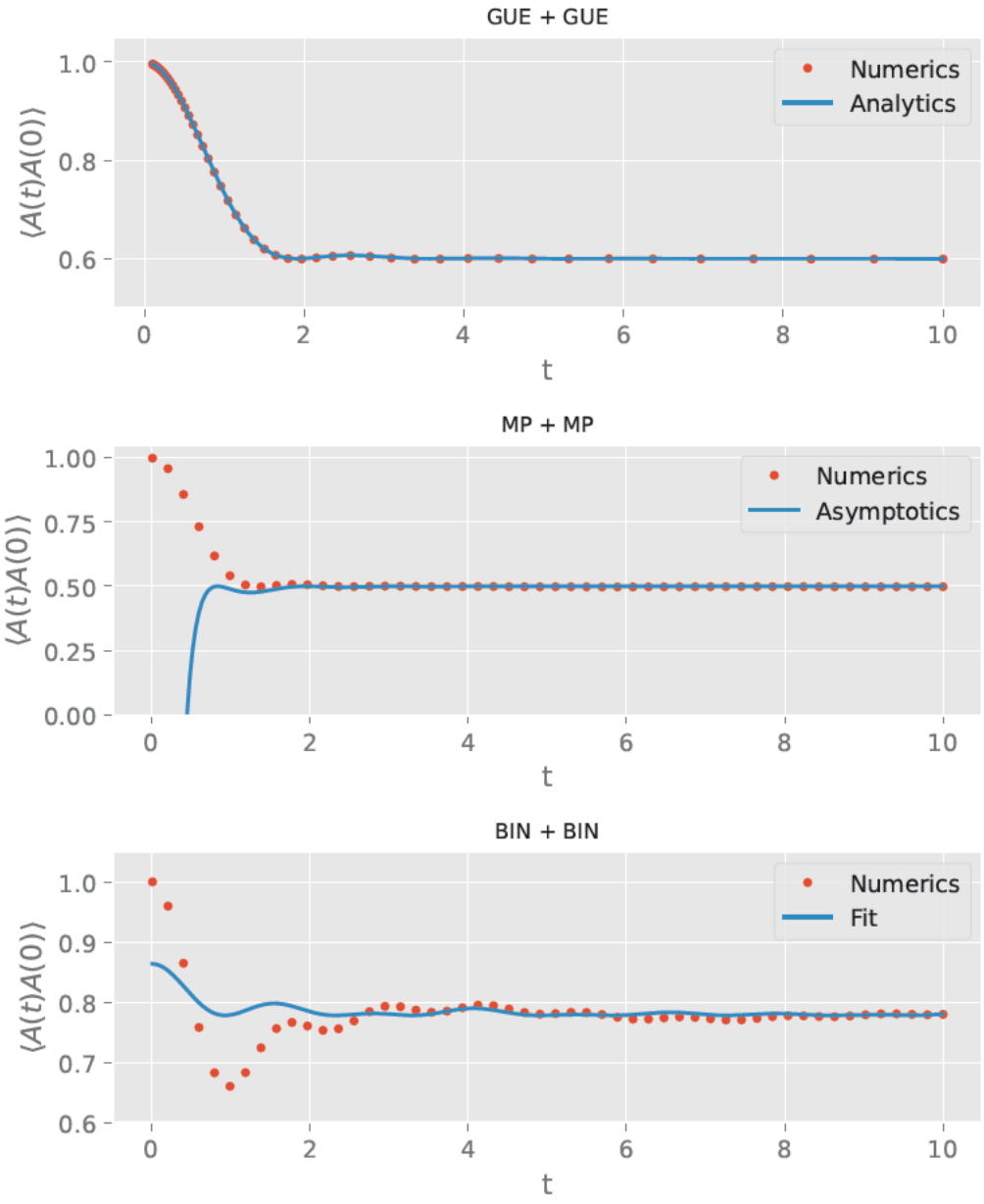

Figure 2·4: Numerical verification of the prediction of Eq.(2.41) with $N = 500$. See Sec.2.6 for details. The title of each panel indicates which ensemble A and B are sampled from.

Table 2.1: Summary of functions and result for a few examples we checked numerically.

A	B	$R_A(z)$	$f_H(z)$	$\langle A(t)A(0)\rangle$
GUE	GUE	λz	$\frac{1}{2}\left(z-\sqrt{z^2-4}\right)$	λ
MP	MP	$\frac{z}{1-z}$	$\frac{z+1-\sqrt{z^2-2z-7}}{2(z+2)}$	$\frac{1}{2}$
BIN	BIN	$\frac{z}{z^2-\lambda^2}$	$\frac{z}{\sqrt{(z^2-(\lambda+\mu)^2)(z^2-(\lambda-\mu)^2)}}$	$\max\left(\frac{1}{2}, 1-\frac{\mu^2}{2\lambda^2}\right)$

GUE We used the conventions of section 2.2.10.

Marchenko–Pastur (MP) To sample an MP matrix A we first sample a standard GUE matrix M with

$$\langle M\rangle = 0 \quad \left\langle M^2\right\rangle = 1 \tag{2.87}$$

and then we compute

$$A = M^2 - \left\langle M^2\right\rangle . \tag{2.88}$$

The same procedure is repeated for the matrix B.

Binary Matrices (BIN) These are matrices of the form

$$A = \lambda\, U_A^\dagger D U_A \quad B = \mu\, U_B^\dagger D U_B \quad \lambda,\mu > 0 \tag{2.89}$$

where U_i are Haar–random $N \times N$ unitaries and D is a diagonal matrix filled with half -1 and half $+1$ values.

While the result Eq. (2.41) is still valid for these matrices, the approximation that leads to Eq. (2.57) breaks down: $\rho_H(x)$ has $x^{-1/2}$ edges (see the second column in Table 2.1). This means that the value of the long–time constant Eq.(2.50) is correct,

as confirmed by numerics, but determining the approach requires more work.

We instead numerically compute the characteristic function $\langle e^{iHt} \rangle$ and fit

$$\langle A(t)A(0) \rangle = \langle A(\infty)A(0) \rangle + c \left| \langle e^{iHt} \rangle \right|^2 \tag{2.90}$$

to the numerics. Figure 2·4 shows that this approximation is not as clean as in the other two cases, but after a short time the error settles to $1/N$, which is the best we can hope for.

This suggests that even though the approximation of Eq. (2.57) is not valid in this case, the approach to the constant is still determined by the characteristic function of H.

2.7 Concluding Thoughts

There are two directions along which it would be interesting to extend the work discussed in this chapter to local, finite dimensional, ergodic quantum systems.

First, if A is a local operator and B is a sum of local operators which itself satisfies ETH, then we expect $H = A + B$ to satisfy ETH and the observable A to be partially conserved. This implies that $\langle A(t)A(0) \rangle \to c/L$ where L is the size of the extended system and c is a constant quantifying how conserved A is. This can be computed explicitly using Eq. (2.50) and the results tested against ETH systems.

More technically challenging is to extend the analysis here to chains of locally interacting random matrices where one might hope to compute the energy diffusion constant explicitly from the dynamical correlators. Here the exact resummations available in the random matrix case are complicated by the locality structure of the chain. Some technical steps along this axis have been developed in (Morampudi and Laumann, 2018).

The order of limits is important: $N \to \infty$ must be taken before $t \to \infty$. At

finite N, we expect corrections of order $1/N$ to the late time value of $\langle A(t)A(0)\rangle_c$, though we have not computed them. They can be calculated perturbatively by resumming diagrams that tessellate a torus with a hole. For A independent of H, the $1/N$ corrections can be computed non-perturbatively from dephasing the spectral representation:

$$\langle A(t)A(0)\rangle \to \frac{1}{N}\mathbb{E}\sum_{\alpha}|A_{\alpha\alpha}|^2 = \frac{1}{N}\langle A^2\rangle \tag{2.91}$$

where α runs over the energy eigenbasis. However, for A part of H, this diagonal ensemble calculation is not straightforward, as the $|\alpha\rangle$ are correlated with A. Indeed, these correlations must produce both the $O(1/N^0)$ late time value which we have computed and any $O(1/N)$ corrections.

Chapter 3

Excitation and Relaxation of the Amplitude mode in a Superconductor

An earlier version of this chapter was published in (Bellitti et al., 2022).

3.1 Introduction

The dynamics of the superconducting state, described by BCS theory (Bardeen et al., 1957), has been a subject of research for a long time (Volkov and Kogan, 1973; Abrahams and Tsuneto, 1966; Rothwarf and Taylor, 1967; Chang and Scalapino, 1978; Papenkort et al., 2007; Beck et al., 2011; Matsunaga et al., 2014; Pekker and Varma, 2015; Shimano and Tsuji, 2020), and while the first theoretical studies about the collective modes appeared soon after BCS, recent experimental developments in the field of time–resolved spectroscopy at the THz scale (Matsunaga et al., 2017; Katsumi et al., 2018; Matsunaga et al., 2014; Beck et al., 2013; Matsunaga and Shimano, 2012; Giannetti et al., 2016) rekindled the interest in the out-of-equilibrium dynamics of condensed matter systems. In the simple case of a conventional s–wave superconductor, the Landau–Ginzburg theory predicts the existence of two collective modes: a Goldstone mode left behind by the spontaneous breaking of U(1) symmetry, and an amplitude mode (see Fig.3·1). Once we couple the theory to electromagnetism, the Anderson–Higgs mechanism (Anderson, 1958b) gaps the Goldstone mode, pushing it to the plasma frequency. In a typical metal the plasma frequency is much larger than the superconducting gap, so that the amplitude mode is the lowest available

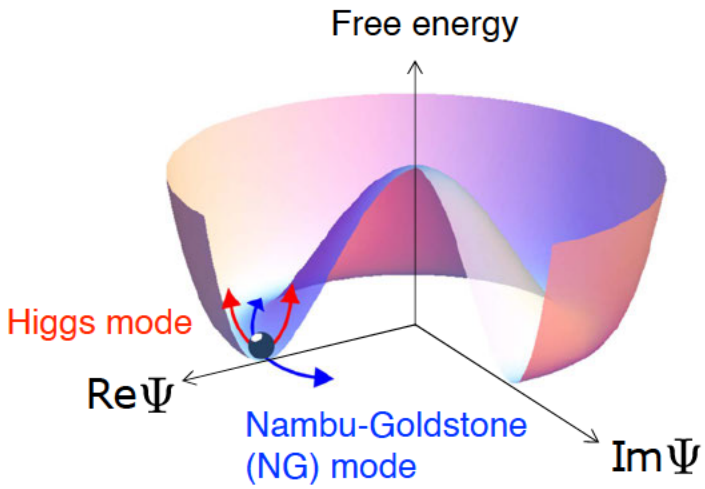

Figure 3·1: Landau–Ginzburg picture of the superconducting phase. The Nambu–Goldstone mode is gapped by the Anderson–Higgs mechanism. Ψ is the order parameter. Image reproduced from (Shimano and Tsuji, 2020).

excitation. It has been shown (Volkov and Kogan, 1973) that the amplitude mode oscillates at a frequency $2\Delta_0$ in the zero momentum limit, where Δ_0 is the equilibrium gap. This frequency coincides with the two–particle threshold in the superconductor (see Fig.3·2), which explains why the dynamics of the amplitude mode is nontrivial even neglecting the interaction between quasiparticles.

Since the Higgs mode is scalar, it cannot couple linearly to electromagnetic fields directly. Rather, several excitation mechanisms have been studied: via combined dynamics of the Higgs mode with charge density wave oscillations (Cea and Benfatto, 2014; Méasson et al., 2014; Littlewood and Varma, 1981; Littlewood and Varma, 1982), linear excitation by coherent THz electromagnetic waves in the presence of DC super-current (Moor et al., 2017; Nakamura et al., 2019; Wang et al., 2021), and nonlinear coherent excitation (Matsunaga et al., 2013; Matsunaga et al., 2014; Papenkort et al., 2007; Kemper et al., 2015) using high intensity THz light with frequency just above the superconducting gap.

In this chapter, we discuss excitation of the Higgs mode by incoherent short light

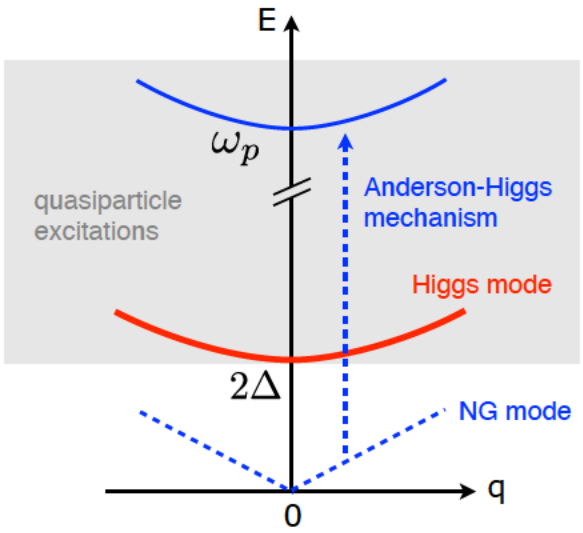

Figure 3·2: Qualitative picture of the spectrum in an s–wave superconductor. The amplitude (Higgs) mode is at the bottom of the multiparticle threshold. Image reproduced from (Shimano and Tsuji, 2020).

pulses with duration $\tau_p \ll 1/\Delta_0$ and high frequency $\Omega_0 \gg \Delta_0$ (ie. infrared, optical or higher). For a detailed discussion of the history and properties of the Higgs mode in superconductors, see the reviews (Pekker and Varma, 2015; Shimano and Tsuji, 2020).

3.2 Scales and physical picture

The two most important time scales characterizing the dynamics of the system are the quasiparticle inelastic relaxation time $\tau_{in}(\epsilon)$ and $1/\Delta_0$, where ϵ is the quasiparticle energy and Δ_0 is the equilibrium value of the order parameter. If the temperature T is not too close to the transition, the quasiparticle inelastic relaxation rate is much smaller than the superconducting energy gap:

$$\frac{1}{\tau_{in}(T)} \ll \Delta_0. \tag{3.1}$$

In this case, for processes with frequency $\omega \ll \Delta_0$, the density of states is a local function of time and the low frequency dynamics of the superconductor is described by

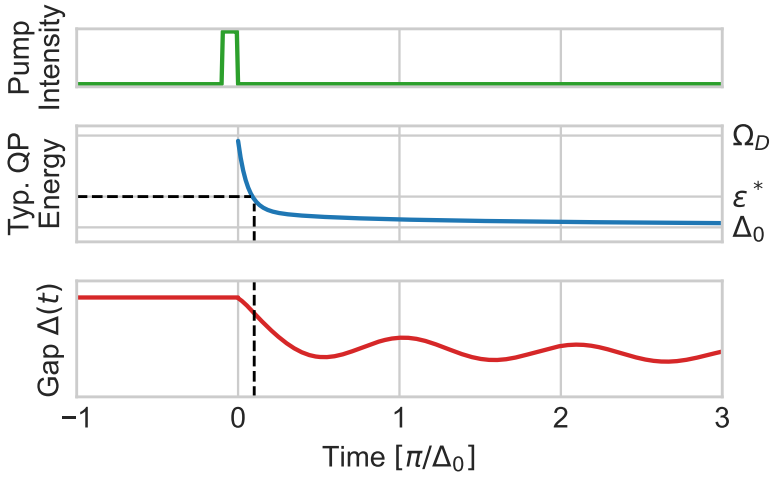

Figure 3·3: Qualitative picture of the Higgs excitation mechanism. A short incoherent pulse of high frequency light (eg. optical) excites a cloud of quasiparticles which rapidly cascade back to lower energy by emitting phonons. The cascade efficiently launches a Higgs oscillation when its relaxational rate of change matches the Higgs frequency, which occurs at the characteristic energy $\epsilon^* \gg \Delta_0$.

a kinetic equation for the quasiparticle distribution function $n(\epsilon, t)$ and a self-consistent equation for $\Delta(t)$ (Aronov et al., 1981).

At frequency $\omega \sim \Delta_0$, the kinetic approach fails. Rather, for time $t \ll \tau_{in}$, the dynamics are governed by non-dissipative equations which conserve both the entropy and the total energy. As a result, the system exhibits coherent oscillations of the order parameter (Volkov and Kogan, 1973), which in the linearized regime decay slowly

$$\delta\Delta(t) = B\frac{\cos(\omega_H t + \phi)}{\sqrt{\Delta_0 t}} \tag{3.2}$$

Here $\omega_H = 2\Delta_0$ is the Higgs frequency, Δ_0 is the equilibrium gap, and the parameters B and ϕ depend on the initial conditions. The physical picture of the mechanism is the following (see Fig.3·3): the pulse creates non-equilibrium quasiparticles with characteristic energy $\epsilon \gg \Delta_0$. Initially, these quasiparticles are not effective at exciting the Higgs mode because they have high energy and the relaxation rate $1/\tau_{in}$ of their

distribution is much faster than Δ_0. As their energy decreases due to various inelastic processes, the relaxation rate decreases as well. When the typical energy ϵ is smaller than the Debye energy Ω_D but still much larger than Δ_0, the relaxation is controlled by acoustic phonon emission with rate (Abrikosov, 2017)

$$\tau_{in}^{-1}(\epsilon) = \gamma\epsilon^3 \tag{3.3}$$

where $\gamma = \alpha/\Omega_D^2$, and α is a coefficient of order one, just as in a normal metal.

The optimal coupling between the quasiparticle cascade and the Higgs mode is achieved when the rate of change of the quasiparticle distribution function is of order ω_H. This provides an estimate of the characteristic energy at this stage of the relaxation process,

$$\epsilon^\star \equiv (2\Delta_0\Omega_D^2/\alpha)^{1/3} \tag{3.4}$$

It is important that $\epsilon^\star \gg \Delta_0$: at such high energy, superconducting correlations are negligible, and we may approximate $n(\epsilon, t)$ with the solution of the kinetic equation[1] for a normal metal with acoustic phonons (Abrikosov, 2017):

$$\frac{\partial n(\epsilon,t)}{\partial t} = \gamma\left(\int_\epsilon^\infty d\epsilon'(\epsilon-\epsilon')^2 n(\epsilon',t) - \frac{1}{3}\epsilon^3 n(\epsilon,t)\right) \tag{3.5}$$

We start modeling the quasiparticle cascade only when its typical energy reaches Ω_D, well after the fast processes driven by Coulomb interaction have completed. At $\epsilon^\star \ll \Omega_D$ these processes slow down enough that we neglect them entirely. See Fig.3·4 for a summary of the scattering rates and energy scales in the system.

We assume the intensity of the exciting pulse is small and neglect terms nonlinear in n as well as stimulated emission of phonons. Moreover, we assume that, due to rapid elastic relaxation, the quasiparticle distribution function is isotropic in momentum

[1] We will discuss this equation in detail in Sec.3.5.

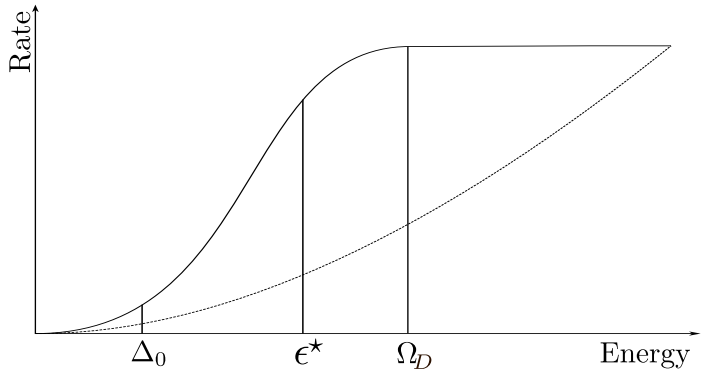

Figure 3·4: Energy scales and scattering rates in the superconductor. The solid line is the electron–phonon rate. The dashed line is the electron–electron rate, given by the Landau–Pomeranchuk form $\sim (\epsilon - \epsilon_F)^2/\epsilon_F$. The energy scale for optimal coupling to the Higgs mode is $\epsilon^\star$, where the Landau–Pomeranchuk rate is negligible with respect to the electron–phonon one. Figure modified from (Kozorezov et al., 2000).

and thus depends only on energy.

It is furthermore possible to neglect phonon reabsorption during the cascade down to ϵ^* indicating that the effect of heating is negligible on the excitation process, although it may matter at later times. This approximation is valid because the phonon reabsorption rate is much smaller than the inelastic electron relaxation rate $1/\tau_{ph} \ll 1/\tau_{in}$ in the energy interval $[\epsilon^*, \Omega_D]$. Indeed, the phonon reabsorption rate is $1/\tau_{ph} \sim \omega c/v_F$ at $ql \ll 1$ and $1/\tau_{ph} \sim \omega^2\tau$ at $ql \gg 1$. Here ω and q are the frequency and the wave vector of phonons, c and v_F are the speed of sound and the Fermi velocity, l and τ are the electron mean free path and mean free time. The desired inequality follows from the fact that $c \ll v_F$.

At $\epsilon \ll \Omega_0 < \Omega_D$ the dynamics described by equation (3.5) has no scales, and the distribution function approaches a scaling form

$$n(\epsilon, t) = C\Omega_D(\gamma t)^{1/3}\mathcal{N}\left([\frac{t}{\tau_{in}(\epsilon)}]^{1/3}\right) \tag{3.6}$$

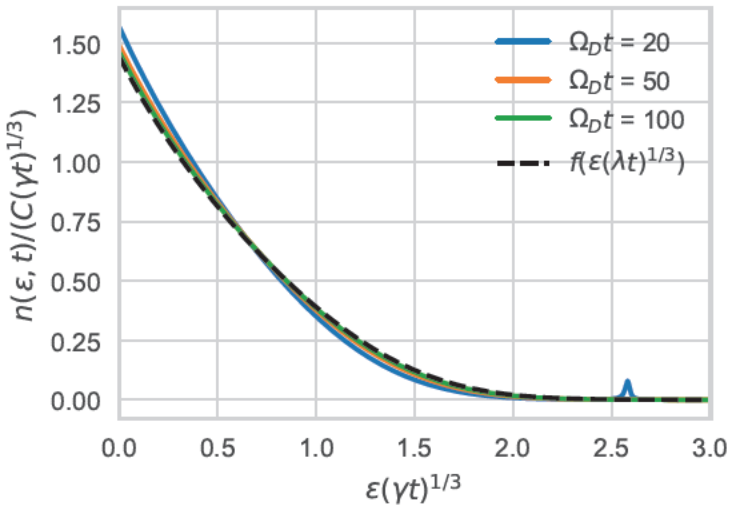

Figure 3·5: Scaling collapse of the quasiparticle distribution function under the dynamics of Eq.(3.5). In this simulation we started with the quasiparticle population narrowly peaked at Ω_D: the small peak around $\epsilon(\gamma t)^{1/3} = 2.5$ is a signature of the initial conditions. As time progresses the distribution approaches the smooth scaling form of Eq.(3.6) (dashed black curve, solution of Eq. (3.7)) and the peak disappears.

where $\mathcal{N}(u)$ is a scaling function satisfying the equation

$$u\mathcal{N}'(u) + \left(1+u^3\right)\mathcal{N}(u) = 3\int_u^\infty du'\,(u-u')^2\mathcal{N}(u') \tag{3.7}$$

In Eq. (3.6), C is a normalization constant fixing the total number of quasiparticles, which is effectively conserved over the time scale relevant for excitation of the Higgs mode. We fix $\int du\mathcal{N}(u) = 1$. Then $C = N/(\Omega_D\nu(0))$ where N is the number of quasiparticles per unit volume created by the pulse, and $\nu(0)$ is the density of states per unit volume at the Fermi energy. The solution for $\mathcal{N}$ is shown in Fig. 3·5: starting with a quasiparticle distribution sharply peaked around Ω_D, we numerically solve Eq.(3.5) and compare to the scaling form predicted by Eq.(3.7). After a time of a few Ω_D^{-1} has passed, the initial condition is forgotten, and the dynamics is in its scaling

regime.

Explaining the derivation of our results requires a fair amount of mathematical machinery, which we introduce in the next sections. To help the reader, we give a bird's eye view of the chapter: in Sec.3.3 we introduce the Keldysh formalism, express the mean–field BCS theory in this language and discuss the electron–phonon coupling. Then, in Sec.3.5 we review the derivation of the Kinetic equation for a metal from the Keldysh language. This showcases the techniques we use in the derivation of the important Eq.(3.145) without being too verbose, and justifies Eq.(3.116). In Sec.3.7 we derive the equations of motion that govern the dynamics of $\Delta(t)$: they are a closed set of inhomogeneous differential equations, with source terms given by two generalized collision integrals. We feed the metallic quasiparticle avalanche (the solution of Eq.(3.116)) to these collision integrals, and compute the asymptotic behavior of $\Delta(t)$.

3.3 Keldysh Formalism

Our main analytical tool is the Keldysh technique (Keldysh, 1965). This approach to field theory is able to deal with out–of–equilibrium systems, at the price of introducing more Green functions than the traditional equilibrium technique (presented for example in the classic (Abrikosov, 1963)). Strictly speaking, the Keldysh technique only needs two Green functions to give a complete description, but the formalism is mathematically easier to deal with if we work with a redundant description that uses four. The central object in the technique is the contour–ordered Green function, which for a field ψ is defined as

$$G(x,y) = -i\left\langle \mathcal{T}_C \psi(x)\psi(y)^\dagger \right\rangle \tag{3.8}$$

where the variables x, y contain spacetime and spin information. The redundancy is introduced attaching an extra index to the time variable, thinking of it as a point on

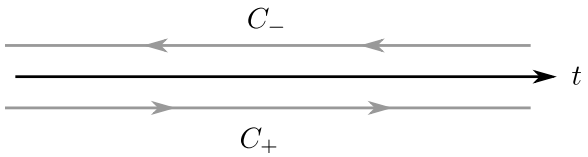

Figure 3·6: The Keldysh contour. The grey lines are separated from the t axis only for graphical clarity, there is no "small imaginary part" as in some other field theoretic approaches.

the Keldysh contour:

$$C = C_+ \cup C_- = (-\infty, \infty) \cup (\infty, -\infty) \tag{3.9}$$

which covers the time axis twice (see Fig.3·6). Every point t on the time axis then needs an extra label to distinguish if we consider it on the forward (t_+) or backward (t_-) branch[2]. The "contour ordering" symbol $\mathcal{T}_C$ is analogous to the usual time ordering $\mathcal{T}$, with the difference that

- Points on the backward branch always follow points on the foward branch;
- Points on the backward branch are in reverse time order $\tilde{\mathcal{T}}$.

When $\mathcal{C}$ is the real line, the contour ordered Green function is identical to the usual time–ordered one. In practice, the Keldysh contour is a useful theoretical tool when deriving the Feynman rules, but all the time integrals one actually has to compute are simply over the real line.

The fundamental relation that enables the use of perturbation theory is

$$\left\langle \mathcal{T}\psi(t)\psi(t')^\dagger \right\rangle = \mathrm{Tr}\left(\rho_0 \mathcal{T}_C\{S_C \psi_0(t_+)\psi_0(t'_+)^\dagger\}\right) \tag{3.10}$$

where the operators on the left–hand side are in the Heisenberg Picture initialized at $t = 0$ (so the average is taken with respect to $\rho(0) = \rho_0$), while the quantities on the

[2]This is the opposite convention as Landau's (Lifshitz and Pitaevskii, 1981) course in theoretical physics.

right–hand side are in Interaction picture. The two pictures coincide at $t = 0$. The state before the adiabatic switching of interactions is

$$\rho_0 = \rho(-\infty) \tag{3.11}$$

The symbol S_C denotes the interaction picture evolution operator over the whole contour. When inside a contour ordering prescription it should be broken up whenever there is an operator insertion.

3.3.1 Basic properties of the Green Functions and Independent Content of the Theory

The set of Green functions most commonly used in the Keldysh technique for a degree of freedom ψ is

$$G^{ff}(t,t') = \left\langle \mathcal{T}_C \psi(t_+)\psi(t'_+)^\dagger \right\rangle = \left\langle \mathcal{T}\psi(t)\psi(t')^\dagger \right\rangle \tag{3.12a}$$

$$G^{bf}(t,t') = \left\langle \mathcal{T}_C \psi(t_-)\psi(t'_+)^\dagger \right\rangle = \left\langle \psi(t)\psi(t')^\dagger \right\rangle \tag{3.12b}$$

$$G^{bb}(t,t') = \left\langle \mathcal{T}_C \psi(t_-)\psi(t'_-)^\dagger \right\rangle = \left\langle \tilde{\mathcal{T}}\psi(t)\psi(t')^\dagger \right\rangle \tag{3.12c}$$

$$G^{fb}(t,t') = \left\langle \mathcal{T}_C \psi(t_+)\psi(t'_-)^\dagger \right\rangle = \pm \left\langle \psi(t')\psi(t)^\dagger \right\rangle \tag{3.12d}$$

Where the minus sign in the lower right expression applies if the operators are fermionic, and $\tilde{\mathcal{T}}$ is the reverse time ordering symbol. The apices f and b stand for "forward" and "backward". Notice that the times on the right–hand side of these expressions do not have a contour index anymore.

From the definition of the Green function immediately follows a linear relation:

$$G^{ff} + G^{bb} = G^{fb} + G^{bf} \tag{3.13}$$

which is true for both Bosons and Fermions. This brings the number of independent Green functions down to three, and it is also possble to build G^{ff} and G^{bb} out of the

two remaining Green functions

$$G^{ff}(x_1, x_2) = \theta(t_1 - t_2)G^{bf}(x_1, x_2) + \theta(t_2 - t_1)G^{fb}(x_1, x_2) \tag{3.14a}$$

$$G^{bb}(x_1, x_2) = \theta(t_1 - t_2)G^{fb}(x_1, x_2) + \theta(t_2 - t_1)G^{bf}(x_1, x_2) \tag{3.14b}$$

showing that the number of independent functions is just two, as mentioned in Sec.3.3.

It is useful to define three more Green functions:[3]

$$G^R(x, x') \equiv -i\theta(t - t') \left\langle \{\psi(x), \psi^\dagger(x')\} \right\rangle \tag{3.15}$$

$$G^A(x, x') \equiv i\theta(t' - t) \left\langle \{\psi(x), \psi^\dagger(x')\} \right\rangle \tag{3.16}$$

$$G^K(x, x') \equiv -i \left\langle [\psi(x), \psi^\dagger(x')] \right\rangle \tag{3.17}$$

and the analogous Bosonic ones

$$D^R(x, x') \equiv -i\theta(t - t') \left\langle [\varphi(x), \varphi(x')] \right\rangle \tag{3.18}$$

$$D^A(x, x') \equiv i\theta(t' - t) \left\langle [\varphi(x), \varphi(x')] \right\rangle \tag{3.19}$$

$$D^K(x, x') \equiv -i \left\langle \{\varphi(x), \varphi(x')\} \right\rangle \tag{3.20}$$

They are not independent:

$$(G^R)^\dagger = G^A \qquad (G^K)^\dagger = -G^K \tag{3.21}$$

where the adjoint symbol swaps the spacetime index and takes the complex conjugate: $G(x, y)^\dagger = G(y, x)^*$. We refer to this set as the "RKA" representation. They are

[3] In Keldysh's original paper the definitions of G^R and G^A are swapped (maybe a misprint?), the convention adopted here is much more common.

related to the original forward–backward definitions of Eq.(3.14) by

$$G^R = G^{ff} - G^{fb} = G^{bf} - G^{bb} \tag{3.22a}$$

$$G^A = G^{ff} - G^{bf} = G^{fb} - G^{bb} \tag{3.22b}$$

$$G^K = G^{ff} + G^{bb} = G^{fb} + G^{bf} \tag{3.22c}$$

There are analogous definitions for the self energy, which we report here for reference:

$$\Sigma^R = \Sigma^{ff} + \Sigma^{fb} = -\Sigma^{bf} - \Sigma^{bb} \tag{3.23a}$$

$$\Sigma^A = \Sigma^{ff} + \Sigma^{bf} = -\Sigma^{fb} - \Sigma^{bb} \tag{3.23b}$$

$$\Sigma^K = \Sigma^{ff} + \Sigma^{bb} = -\Sigma^{fb} - \Sigma^{bf} \tag{3.23c}$$

The reason we introduced both the $(G^{ff}, G^{fb}, G^{bf}, G^{bb})$ and the (G^R, G^A, G^K) sets is practical: when evaluating Feynman diagrams it is much easier to work with the first set, but the physical meaning of expressions is often clearer in terms of the second. For example, in equilibrium G^K is the only function that carries information about the populations, while G^R gives the retarded one particle response. This information is harder to disentangle in the forward–backward notation.

3.3.2 Some Exact Green functions

Free Electrons in equilibrium

We give the expressions for the Green functions of non–interacting free spinless fermions. This is the simplest example and should give the reader some intuition about the Green functions. It also serves as a simple check for the superconducting case, which must reduce to the free case when the gap vanishes. The Hamiltonian is

$$H = \sum_{\boldsymbol{p}} \xi_{\boldsymbol{p}} c^\dagger_{\boldsymbol{p}} c_{\boldsymbol{p}} \tag{3.24}$$

and the correlators defining the Green functions are easiest to evaluate in momentum space. We find

$$G_0^R(\boldsymbol{p},\xi) = G_0^A(\boldsymbol{p},\xi)^\star = \frac{1}{\xi - \xi_{\boldsymbol{p}} + i\delta} \tag{3.25}$$

$$G_0^{fb}(\boldsymbol{p},\xi) = 2\pi i n_{\boldsymbol{p}} \delta(\xi - \xi_{\boldsymbol{p}}) \tag{3.26}$$

$$G_0^{bf}(\boldsymbol{p},\xi) = -2\pi i (1 - n_{\boldsymbol{p}}) \delta(\xi - \xi_{\boldsymbol{p}}) \tag{3.27}$$

$$G_0^K(\boldsymbol{p},\xi) = 2\pi i (2n_{\boldsymbol{p}} - 1) \delta(\xi - \xi_{\boldsymbol{p}}) \tag{3.28}$$

where the electron distribution function in equilibrium is (μ is the chemical potential and β the inverse temperature)

$$n_{\boldsymbol{p}} = \frac{1}{e^{\beta \xi_{\boldsymbol{p}}} + 1} \qquad \xi_{\boldsymbol{p}} = \frac{p^2}{2m} - \mu \tag{3.29}$$

In real spacetime these functions are sinc–like (we are taking the inverse Fourier transform of a "box", the Fermi surface): they oscillate with a period fixed by the properties of the Fermi surface and decay as power laws. For example, in one dimension at zero temperature we have

$$G_0^{fb}(x, t=0) = i \int \frac{dp}{2\pi} e^{ipx} [|p| < p_F] \int d\varepsilon \; \delta(\varepsilon - \varepsilon_p) = \frac{i p_F}{\pi} \frac{\sin(p_F x)}{x} \tag{3.30}$$

while at equal spacetime points

$$G_0^{fb}(x=0, t) = i \int \frac{dp}{2\pi} e^{i\frac{p^2}{2m}t} [|p| < p_F] = i\sqrt{\frac{m}{\pi}} \frac{S(\sqrt{2\varepsilon_F t/\pi}) + iC(\sqrt{2\varepsilon_F t/\pi})}{\sqrt{t}} \tag{3.31}$$

where S and C are Fresnel integrals. Both $S(t)$ and $C(t)$ are oscillating bounded functions that approach a constant at large $|t|$. The square brackets denote the Heaviside theta function: $[x]$ evaluates to one if x is true, and zero otherwise.

Notice how the Green functions follow the Fermionic fluctuation–dissipation relation

at inverse temperature β

$$G^K(\epsilon,p)=\tanh\left(\frac{\beta\epsilon}{2}\right)(G^R(\epsilon,p)-G^A(\epsilon,p)) \tag{3.32}$$

when we use Eq.(3.29) for the population. This relation is the reason why in equilibrium we only need a single Green function.

Equilibrium BCS theory

Our main result will follow from a perturbative correction to the mean–field BCS description of an s–wave superconductor. To set it up, in this section we introduce the BCS mean–field theory in Keldysh language. The Hamiltonian is

$$H=\sum_{\boldsymbol{p}\sigma}\xi_{\boldsymbol{p}}c^\dagger_{\boldsymbol{p}\sigma}c_{\boldsymbol{p}\sigma}-\sum_{\boldsymbol{p}}(\Delta c^\dagger_{-\boldsymbol{p}\downarrow}c^\dagger_{\boldsymbol{p}\uparrow}+\Delta^* c_{\boldsymbol{p}\uparrow}c_{-\boldsymbol{p}\downarrow}) \tag{3.33}$$

and it is diagonalized by the Bogoliubov transformation

$$c_{\boldsymbol{k}\uparrow}=u_{\boldsymbol{k}}\gamma_{\boldsymbol{k}\uparrow}-v_{\boldsymbol{k}}\gamma^\dagger_{-\boldsymbol{k}\downarrow} \tag{3.34a}$$

$$c^\dagger_{-\boldsymbol{k}\downarrow}=v_{\boldsymbol{k}}\gamma_{\boldsymbol{k}\uparrow}+u_{\boldsymbol{k}}\gamma^\dagger_{-\boldsymbol{k}\downarrow} \tag{3.34b}$$

transforming the bare fermions $c_{\boldsymbol{p}\sigma}$ to the quasiparticle operators $\gamma_{\boldsymbol{p}\sigma}$. We could compute the Green functions for the quasiparticles, but it is easier to work with the original degrees of freedom: it is not obvious at this stage, but switching to $\gamma_{\boldsymbol{p}\sigma}$ would make the interaction terms with the phonons much more complicated. We will encounter the same problem in chapter 4, where we compute some perturbative corrections to the Bogoliubov theory of a molecular superfluid. Using Eq.(3.34) all the electronic Green functions are straightforward to compute explicitly. The quasiparticle dispersion is

$$\varepsilon_p=\sqrt{\xi_p^2+\Delta^2}\qquad \xi_p=\frac{p^2}{2m}-\mu \tag{3.35}$$

and and the quasiparticle number at fixed spin polarization is

$$n_p = \left\langle \gamma^\dagger_{p\uparrow}\gamma_{p\uparrow} \right\rangle = \left\langle \gamma^\dagger_{p\downarrow}\gamma_{p\downarrow} \right\rangle \tag{3.36}$$

Notice that this is the *quasiparticle* number, so that at zero temperature $n_p = 0$ identically. It is convenient to introduce Nambu spinors (Nambu, 1960)

$$\Psi_{\boldsymbol{p}} = \begin{pmatrix} c_{\boldsymbol{p}\uparrow} \\ c^\dagger_{-\boldsymbol{p}\downarrow} \end{pmatrix} \tag{3.37}$$

which gives two extra indices $G_{\alpha\beta}$ to the Green function, beyond the contour indices G^{ij} which take values in $\{f, b\}$). A complete description of the s–wave superconductor in Nambu–Keldysh formalism requires then the four–index Green function

$$G^{ij}_{\alpha\beta}(x,y) = -i\left\langle \mathcal{T}_{\mathcal{C}}\Psi(x)\Psi(y)^\dagger \right\rangle = -i\begin{pmatrix} G^{ij}_{11}(x,y) & G^{ij}_{12}(x,y) \\ G^{ij}_{21}(x,y) & G^{ij}_{22}(x,y) \end{pmatrix} \tag{3.38}$$

We will refer to G_{11} and G_{22} as the "normal" components of the Green function, since they are finite even in a normal metal, and to G_{12} and G_{21} as "anomalous", as they vanish when the gap does. For simplicity we work in the absence of a magnetic field, so we are allowed to choose $u_p, v_p, \Delta \in \mathbb{R}$ without loss of generality. In this case the Green functions are

$$G^{fb}_{11}(\boldsymbol{p},\varepsilon) = 2\pi i\left(u_p^2 n_p \delta(\varepsilon - \varepsilon_p) + v_p^2(1-n_p)\delta(\varepsilon+\varepsilon_p)\right) \tag{3.39}$$

$$G^{bf}_{11}(\boldsymbol{p},\varepsilon) = -2\pi i\left(u_p^2(1-n_p)\delta(\varepsilon - \varepsilon_p) + v_p^2 n_p\delta(\varepsilon+\varepsilon_p)\right) \tag{3.40}$$

$$G^{ff}_{11}(\boldsymbol{p},\varepsilon) = \frac{u_p^2(1-n_p)}{\varepsilon - \varepsilon_p + i\delta} + \frac{v_p^2 n_p}{\varepsilon+\varepsilon_p+i\delta} + \frac{u_p^2 n_p}{\varepsilon-\varepsilon_p-i\delta} + \frac{v_p^2(1-n_p)}{\varepsilon+\varepsilon_p-i\delta} \tag{3.41}$$

$$G_{12}^{fb}(\boldsymbol{p},\varepsilon) = -2\pi i u_p v_p \left(-n_p \delta(\varepsilon-\varepsilon_p) + (1-n_p)\delta(\varepsilon+\varepsilon_p)\right) \tag{3.42}$$

$$G_{12}^{bf}(\boldsymbol{p},\varepsilon) = -2\pi i u_p v_p \left(-n_p \delta(\varepsilon+\varepsilon_p) + (1-n_p)\delta(\varepsilon-\varepsilon_p)\right) \tag{3.43}$$

$$G_{12}^{ff}(\boldsymbol{p},\varepsilon) = -u_p v_p \left(\frac{n_p}{\varepsilon+\varepsilon_p+i\delta} - \frac{(1-n_p)}{\varepsilon-\varepsilon_p+i\delta} - \frac{n_p}{\varepsilon-\varepsilon_p-i\delta} + \frac{(1-n_p)}{\varepsilon+\varepsilon_p-i\delta}\right) \tag{3.44}$$

In RKA representation we have instead

$$G_{11}^{R}(\boldsymbol{p},\varepsilon) = \frac{u_p^2}{\varepsilon-\varepsilon_p+i\delta} + \frac{v_p^2}{\varepsilon+\varepsilon_p+i\delta} \tag{3.45}$$

$$G_{11}^{A}(\boldsymbol{p},\varepsilon) = \frac{u_p^2}{\varepsilon-\varepsilon_p-i\delta} + \frac{v_p^2}{\varepsilon+\varepsilon_p-i\delta} \tag{3.46}$$

$$G_{11}^{K}(\boldsymbol{p},\varepsilon) = -2\pi i(1-2n_p)\left(u_p^2\delta(\varepsilon-\varepsilon_p) - v_p^2\delta(\varepsilon+\varepsilon_p)\right) \tag{3.47}$$

$$G_{12}^{R}(\boldsymbol{p},\varepsilon) = -u_p v_p \left(\frac{1}{\varepsilon+\varepsilon_p+i\delta} - \frac{1}{\varepsilon-\varepsilon_p+i\delta}\right) \tag{3.48}$$

$$G_{12}^{A}(\boldsymbol{p},\varepsilon) = -u_p v_p \left(\frac{1}{\varepsilon+\varepsilon_p-i\delta} - \frac{1}{\varepsilon-\varepsilon_p-i\delta}\right) \tag{3.49}$$

$$G_{12}^{K}(\boldsymbol{p},\varepsilon) = -2\pi i u_p v_p (1-2n_p)\left(\delta(\varepsilon+\varepsilon_p) + \delta(\varepsilon-\varepsilon_p)\right) \tag{3.50}$$

A simple consistency check on these functions is that they should reduce to the metallic ones when $\Delta = 0$. The replacements

$$\varepsilon_p \to |\xi_p| \qquad u_p \to [p < p_F] \qquad v_p \to [p > p_F] \qquad n_p \to 0 \tag{3.51}$$

indeed reproduce the normal state Green functions we have already encountered.

Phonons and Electron–Phonon coupling

To discuss energy relaxation in the superconductor we must couple the quasiparticles to phonons. In this section we discuss the Keldysh description of Frölich phonons, following the conventions of (Mahan, 2013). For simplicity we restrict the discussion

to a single longitudinal phonon

$$H_{ph} = \sum_{\boldsymbol{q}} \omega_q a^\dagger_{\boldsymbol{q}} a_{\boldsymbol{q}} \tag{3.52}$$

with linear dispersion $\omega_q = cq$, where c is the speed of sound. In Fourier space we have the equilibrium phonon Green functions at inverse temperature β (Keldysh, 1965)

$$D^{fb}(\boldsymbol{k},\omega) = -i\pi \left|m_k\right|^2 \left((N_k+1)\delta(\omega+\omega_k) + N_k\delta(\omega-\omega_k)\right) \tag{3.53}$$

$$D^{bf}(\boldsymbol{k},\omega) = -i\pi \left|m_k\right|^2 \left((N_k+1)\delta(\omega-\omega_k) + N_k\delta(\omega+\omega_k)\right) \tag{3.54}$$

$$D^{ff}(\boldsymbol{k},\omega) = \left|m_k\right|^2 \left((N_k+1)\frac{\omega_k}{\omega^2-\omega_k^2+i0^+} - N_k\frac{\omega_k}{\omega^2-\omega_k^2-i0^+}\right) \tag{3.55}$$

$$D^{R}(\boldsymbol{k},\omega) = \left|m_k\right|^2 \frac{\omega_k}{(\omega+i0^+)^2-\omega_k^2} \tag{3.56}$$

$$D^{A}(\boldsymbol{k},\omega) = \left|m_k\right|^2 \frac{\omega_k}{(\omega-i0^+)^2-\omega_k^2} \tag{3.57}$$

$$D^{K}(\boldsymbol{k},\omega) = -i\pi \left|m_k\right|^2 (2N_k+1)(\delta(\omega+\omega_k)+\delta(\omega-\omega_k)) \tag{3.58}$$

with population factors

$$N_k = \frac{1}{e^{\beta\omega_k}-1} \tag{3.59}$$

and (squared) electron–phonon matrix element $\left|m_k\right|^2$. Notice that these functions have the correct Hermiticity properties

$$D^R(p)^\star = D^A(p) \qquad D^K(p)^\star = -D^K(p) \tag{3.60}$$

and respect the bosonic fluctuation-dissipation theorem

$$D^K(p) = \frac{1}{\tanh(\beta\omega/2)}\left(D^R(p) - D^A(p)\right) \tag{3.61}$$

With these conventions, the the deformation potential coupling the phonon opera-

tor φ to the electrons ψ is

$$H_{el-ph} = g \sum_{\sigma} \int d\boldsymbol{r}\ \psi^{\dagger}_{\sigma}(\boldsymbol{r})\psi_{\sigma}(\boldsymbol{r})\varphi(\boldsymbol{r}) \tag{3.62}$$

where the coupling constant g does not depend on momentum.

3.4 Diagrammatics

In this section we introduce the diagrammatic rules we need to compute the perturbative corrections on top of the BCS mean–field theory.

3.4.1 The Green Functions

Green functions are represented by lines. By convention, the arrows on charged particles follow the current, and reading the labels left to right gives them in the order they should be written as arguments of the Green functions. This is the same set of convention adopted in (Abrikosov, 1963). The electronic Green function is

$$\mathbf{r}t_i\alpha \twoheadleftarrow \mathbf{r}'t'_j\beta \ = iG^{ij}_{\alpha,\beta}(\mathbf{r}t, \mathbf{r}'t') \tag{3.63}$$

The real bosonic Green function is

$$\mathbf{r}t_i \text{ ---- } \mathbf{r}'t'_j \ = iD^{ij}(\mathbf{r}t, \mathbf{r}'t') \tag{3.64}$$

3.4.2 Electron–Phonon Vertex

While the Feynman rules for the Green functions are the same as in the equilibrium technique, the Feynman rule for the vertex associated to the interaction Eq.(3.62) has an extra minus sign if the time is on the backward contour. This is clear from a

path–integral argument:

$$e^{-iS_{\text{int}}} = \exp\left(-i\int_C dt' H_{\text{int}}(t')\right) = \exp\left(-i\int_{-\infty}^{\infty} dt' \left(H_{\text{int}}(t'_f) - H_{\text{int}}(t'_b)\right)\right) \tag{3.65}$$

This sign flip is taken into account by attaching an appropriate tensor to the vertex[4]

$$\gamma^k_{ij} = \delta_{ij}(\sigma^z)_{jk} \qquad i,j,k \in (f,b) \tag{3.66}$$

the Feynman rule for the vertex is then simply

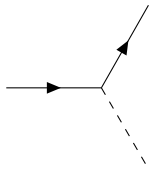

$$= -ig\gamma^k_{ij} \tag{3.67}$$

The Keldysh indices must be summed at internal vertices as any other index.

3.4.3 Electron Self Energy in the Superconductor

We compute the self-energy Σ to leading order in the self–consistent Born approximation (Abrikosov et al., 2012). We include only the electron–phonon interaction, which is the leading scattering mechanism at the energies we consider. To leading order in the coupling g, the self energy consists of only one diagram

$$-i\Sigma(x,y) = x$$  $$y \tag{3.68}$$

where the endpoints x, y include spacetime, Nambu and Keldysh information. In symbols this equation reads

$$\Sigma^{ij}_{\alpha\beta} = i(-1)^{\alpha+\beta+i+j} G^{ij}_{\alpha\beta}(xy) D^{ij}(xy) \tag{3.69}$$

[4]Lower indices are fermionic legs and upper indices bosonic ones, no summation implied

Or, in terms of the RKA representation (there is no sum over spacetime in these expressions)

$$\Sigma^R(xy) = i(-1)^{\alpha+\beta} g^2 \left(G^{11}_{\alpha\beta}(xy) D^{11}(xy) - G^{12}_{\alpha\beta}(xy) D^{12}(xy) \right) \tag{3.70a}$$

$$\Sigma^A(xy) = i(-1)^{\alpha+\beta} g^2 \left(G^{11}_{\alpha\beta}(xy) D^{11}(xy) - G^{21}_{\alpha\beta}(xy) D^{21}(xy) \right) \tag{3.70b}$$

$$\Sigma^K(xy) = i(-1)^{\alpha+\beta} g^2 \left(G^{11}_{\alpha\beta}(xy) D^{11}(xy) + G^{22}_{\alpha\beta}(xy) D^{22}(xy) \right) \tag{3.70c}$$

In momentum space, assuming translational invariance these read

$$\Sigma^K_{\alpha\beta}(\boldsymbol{p}, \varepsilon) = \frac{ig^2}{2}(-1)^{\alpha+\beta}(G^K_{\alpha\beta} \star D^K + G^A_{\alpha\beta} \star D^A + G^R_{\alpha\beta} \star D^R) \tag{3.71a}$$

$$\Sigma^R_{\alpha\beta}(\boldsymbol{p}, \varepsilon) = \frac{ig^2}{2}(-1)^{\alpha+\beta}(G^K_{\alpha\beta} \star D^R + G^R_{\alpha\beta} \star D^K) \tag{3.71b}$$

$$\Sigma^A_{\alpha\beta}(\boldsymbol{p}, \varepsilon) = \frac{ig^2}{2}(-1)^{\alpha+\beta}(G^K_{\alpha\beta} \star D^A + G^A_{\alpha\beta} \star D^K) \tag{3.71c}$$

where the symbol $\star$ denotes the convolution product. Notice that these expression have the correct hermiticity properties.

3.4.4 The Dyson equation in Differential Form

At operator level the Dyson equation is

$$G = G_0 \mathbb{1} + G_0 \Sigma G = G_0 \mathbb{1} + G \Sigma G_0 \tag{3.72}$$

where the products in this expression are contractions over spacetime, Nambu, and Keldysh indices. Formally, acting with G_0^{-1} we obtain the Dyson differential equations

$$G_0^{-1} G = \mathbb{1} + \Sigma G \tag{3.73a}$$

$$G G_0^{-1} = \mathbb{1} + G \Sigma \tag{3.73b}$$

Writing the spacetime dependence explicitly we have

$$G_0^{-1}(x_1)G(x_1,x_2) = \delta(x_1-x_2)\mathbb{1} + \int dy\ \Sigma(x_1,y)G(y,x_2) \tag{3.74}$$

and for the second one, after transferring the derivatives appearing in G_0^{-1} to G

$$G_0^{-1}(x')^\star G(x,x') = \delta(x-x') + \int dy\ G(x,y)\Sigma(y,x') \tag{3.75}$$

To understand better the structure of the G_0^{-1} operator, we introduce the single particle operator

$$g_0^{-1}(x) = i\partial_t - H(x) \tag{3.76}$$

where $H(x)$ is the single particle Hamiltonian. It is straightforward to verify that the free Green functions have the properties

$$g_0^{-1}(x)G_0^{fb,bf}(x,x') = 0 \tag{3.77}$$

$$g_0^{-1}(x)G_0^{ff}(x,x') = \delta(x-x') \tag{3.78}$$

$$g_0^{-1}(x)G_0^{bb}(x,x') = -\delta(x-x') \tag{3.79}$$

so that the matrix

$$G_0^{-1}(x) \equiv \begin{pmatrix} g_0^{-1}(x) & 0 \\ 0 & -g_0^{-1}(x) \end{pmatrix} \tag{3.80}$$

is the inverse of the noninteracting matrix Green function:

$$G_0^{-1}(x)G_0(x,x') = \delta(x-x')\mathbb{1}_{2\times 2} \tag{3.81a}$$

$$G_0^{-1}(x')^\star G_0(x,x') = \delta(x-x')\mathbb{1}_{2\times 2} \tag{3.81b}$$

The two equations (3.74) and (3.75) are closely related to the (quantum) kinetic equation, as we explain in Sec.3.5.

3.5 From Keldysh to the Kinetic Equation for Metals

We want to derive an equation for the dynamics of the quasiparticle population f. It turns out (Keldysh, 1965) that it is sufficient to focus on the entry of the Dyson equation corresponding to G^{fb}. Consider the upper right entry in Eq. 3.74 (remember that G still has Keldysh and Nambu indices):

$$g_0^{-1}(x_1)G^{fb}(x_1,x_2) = \int dx_3 \ \left(\Sigma^{ff}(x_1,x_3)G^{fb}(x_3,x_2) + \Sigma^{fb}(x_1,x_3)G^{bb}(x_3,x_2)\right) \tag{3.82}$$

and the analog equation obtained from Eq.(3.75)

$$-\, g_0^{-1}(x_2)^\star G^{fb}(x_1,x_2) = \int dx_3 \ \left(G^{ff}(x_1,x_3)\Sigma^{fb}(x_3,x_2) + G^{fb}(x_1,x_3)\Sigma^{bb}(x_3,x_2)\right) \tag{3.83}$$

Adding up these equations we obtain

$$\begin{aligned}(i\partial_{t_1} + i\partial_{t_2} - H(x_1) + H(x_2)^\star)G^{fb}(x_1,x_2) = \\ \int dx_3 \ \Sigma^{ff}_{13}G^{fb}_{32} + \Sigma^{fb}_{13}G^{bb}_{32} + \{\Sigma \leftrightarrow G\}\end{aligned} \tag{3.84}$$

which is the Quantum kinetic equation, an exact result. We are ultimately interested in dynamics that happens on slow spacetime scales (compared to the Fermi energy and momentum), so it is useful to change coordinates for two–points objects $G(x_1,x_2)$ from $x_1 = (\boldsymbol{r}_1 t_1)$ and $x_2 = (\boldsymbol{r}_2 t_2)$ to center-of-mass $x = (t, \boldsymbol{r})$ and relative coordinates $\xi = (\tau, \boldsymbol{\xi})$

$$x \equiv \frac{1}{2}(x_1 + x_2) \qquad \xi \equiv x_1 - x_2 \tag{3.85}$$

This lets us separate the slow motion in $(\boldsymbol{r}, t)$ dependence from the fast oscillations of the relative coordinates. To obtain the kinetic equation from Eq.(3.84) we

1. Change variables to relative and center–of–mass;

2. Take the Fourier transform from ξ to p;

3. Use a variational ansatz for G^{fb}: parametrize it as in Eq.(3.26), but allow the population to depend on t.

4. Set $\tau = 0$, by taking the Fourier transform to ϵ and then integrating over all values of ϵ.

At this point the connection between the G^{fb} function and the quasiparticle distribution function becomes clear: comparing to Eq.(3.26) we find, as promised, the relation between G^{fb} and the distribution function

$$f(\boldsymbol{r}, \boldsymbol{p}, t) = -iG^{fb}(\boldsymbol{r}, \boldsymbol{p}, t, \tau = 0) = \int \frac{d\varepsilon}{2\pi i} G^{fb}(\boldsymbol{r}, \boldsymbol{p}, t, \varepsilon) \tag{3.86}$$

and Eq.(3.84) becomes a differential equation for the distribution function f

$$\left(\partial_t + \frac{\boldsymbol{p}}{m} \cdot \nabla_{\boldsymbol{r}}\right) f(\boldsymbol{r}, \boldsymbol{p}, t) = \int \frac{d\varepsilon}{2\pi i} dx_3 \left(\Sigma^{ff}_{13} G^{fb}_{32} + \Sigma^{fb}_{13} G^{bb}_{32} + G^{ff}_{13} \Sigma^{fb}_{32} + G^{fb}_{13} \Sigma^{bb}_{32}\right) \tag{3.87}$$

The right–hand side of this equation is the collision integral, but its structure is still opaque. All the terms are schematically of the form

$$\int dx_3 \; \Sigma(x_1, x_3) G(x_3, x_2) \tag{3.88}$$

and since we are working with the new coordinates (x, ξ), it is best to redefine all functions as

$$f(x_1, x_2) \to f\left(\frac{1}{2}(x_1 + x_2), x_1 - x_2\right) \tag{3.89}$$

With this redefinition the integrals we have to compute become

$$\int dx_3 \; \Sigma_{13} G_{32} \to \int dx_3 \; \Sigma\left(\frac{x_1 + x_3}{2}, x_1 - x_3\right) G\left(\frac{x_3 + x_2}{2}, x_3 - x_2\right) \tag{3.90}$$

Assuming that the scales (t_A, L_A) over which the macroscopic properties of the system fluctuate are much larger than the Fermi microscopic scales

$$L_A \gg \lambda_F \qquad t_A \gg \frac{1}{\varepsilon_F} \tag{3.91}$$

the integral simplifies: the Green function is a peaked function of width λ_F in terms of its relative coordinate, so the integrand is only nonzero if (r_1, r_2) are within a few λ_F from each other and (r_2, r_3) are as well. This implies that r_1 and r_2 must be close to each other, and since all quantities vary slowly as a function of their center of mass argument, it is an acceptable approximation to replace

$$\begin{aligned} \int dx_3 \, \Sigma\left(\frac{x_1+x_3}{2}, x_1-x_3\right) G\left(\frac{x_3+x_2}{2}, x_3-x_2\right) \\ \to \int dx_3 \, \Sigma\left(x, x_1-x_3\right) G\left(x, x_3-x_2\right) \end{aligned} \tag{3.92}$$

In this form the integral over x_3 is a convolution, so the Fourier transform is trivial:

$$\int d(x_1-x_2) dx_3 e^{ip(x_1-x_2)} \Sigma\left(x, x_1-x_3\right) G\left(x, x_3-x_2\right) = \Sigma(x,p) G(x,p) \tag{3.93}$$

Repeating this argument for all terms on the right–hand side of the kinetic equation, and exploiting the linear relations Eq.(3.13) we get

$$\left(\partial_t + \frac{\boldsymbol{p}}{m} \cdot \nabla_{\boldsymbol{r}}\right) f(\boldsymbol{r}, \boldsymbol{p}, t) = \int \frac{d\varepsilon}{2\pi} \left(G^{fb}(x,p)\Sigma^{bf}(x,p) - \Sigma^{fb}(x,p)G^{bf}(x,p)\right) \tag{3.94}$$

Working at $O(g^2)$ it is consistent to replace G on the right–hand side with G_0, since the self energy contains a factor g^2. With this approximation the kinetic equation becomes

$$\left(\partial_t + \frac{\boldsymbol{p}}{m} \cdot \nabla_{\boldsymbol{r}}\right) f = f(\boldsymbol{r}, \boldsymbol{p}, t) i\Sigma^{bf}(\boldsymbol{r}, \boldsymbol{p}, t, \varepsilon_p) + (1 - f(\boldsymbol{r}, \boldsymbol{p}, t)) i\Sigma^{fb}(\boldsymbol{r}, \boldsymbol{p}, t, \varepsilon_p) \tag{3.95}$$

and we still need to evaluate the self energy. Working at leading order we have

$$-i\Sigma^{fb}(x,y) = x_f \quad y_b \tag{3.96}$$

which in x, ξ coordinates reads[5]

$$-i\Sigma^{fb}(x,\xi) = -g^2 G_0^{fb}(x,\xi) D_0^{fb}(x,\xi) \tag{3.97}$$

The Fourier transform over the relative variables is

$$i\Sigma^{fb}(x,p) = g^2 \int \frac{dp_1}{(2\pi)^4} D_0^{fb}(x,p_1) G_0^{fb}(x,p-p_1) \tag{3.98}$$

Repeating the same for the bf component of the self–energy we find

$$-i\Sigma^{bf}(x,\xi) = -g^2 G_0^{bf}(x,\xi) D_0^{bf}(x,\xi) \tag{3.99}$$

and its Fourier transform

$$i\Sigma^{bf}(x,p) = g^2 \int \frac{dp_1}{(2\pi)^4} D_0^{bf}(x,p_1) G_0^{bf}(x,p-p_1) \tag{3.100}$$

We are ready to plug everything in. We assume the phonon to be in thermal equilibrium, so we use the equilibrium expression for D_0^{ij}. We also suppress the dependence on $\boldsymbol{r}$ and t on the right–hand side to keep the notation marginally more compact

$$\begin{aligned}\left(\partial_t + \frac{\boldsymbol{p}}{m}\cdot\nabla_{\boldsymbol{r}}\right) f(\boldsymbol{r},\boldsymbol{p},t) = 2\pi^2 g^2 \int \frac{d\boldsymbol{k}}{(2\pi)^3} |m_{\boldsymbol{k}}|^2 \\ \big(f_{\boldsymbol{p}+\boldsymbol{k}}(1-f_{\boldsymbol{p}})\big[(N_{\boldsymbol{k}}+1)\delta(\xi_{\boldsymbol{p}}-\xi_{\boldsymbol{p}+\boldsymbol{k}}+\omega_{\boldsymbol{k}}) + N_{\boldsymbol{k}}\delta(\xi_{\boldsymbol{p}}-\xi_{\boldsymbol{p}+\boldsymbol{k}}-\omega_{\boldsymbol{k}})\big] \\ -(1-f_{\boldsymbol{p}+\boldsymbol{k}})f_{\boldsymbol{p}}\big[(N_{\boldsymbol{k}}+1)\delta(\xi_{\boldsymbol{p}}-\xi_{\boldsymbol{p}+\boldsymbol{k}}-\omega_{\boldsymbol{k}}) + N_{\boldsymbol{k}}\delta(\xi_{\boldsymbol{p}}-\xi_{\boldsymbol{p}+\boldsymbol{k}}+\omega_{\boldsymbol{k}})\big]\big)\end{aligned} \tag{3.101}$$

This is the well–known form of the kinetic equation for a metal (Abrikosov, 2017).

[5]The minus sign comes from the vertex rule for vertices on the backward contour

3.5.1 Simplest model of avalanche in a metal

Eventually we want to describe the relaxation of quasiparticles in a superconductor after an initial short pulse. At energies much higher than the gap the system is indistinguishable from a normal metal, so we approximate the quasiparticle relaxation using the metallic result.

As explained in Sec.3.2, we ignore phonon reabsorption. An electron in any given state can only fall to states of lower energy. We assume the electron population remains isotropic at all times, so that it is parametrized only by energy. Since the deviation from the equilibrium population is small, we linearize the kinetic equation (3.101) and for simplicity work at zero temperature. The kinetic equation reduces to

$$\begin{aligned}\delta\dot{n}_p = 2\pi^2 g^2 \int \frac{d\boldsymbol{k}}{(2\pi)^3} |m_k|^2 \big(&\delta(\xi_p - \xi_{|\boldsymbol{p}+\boldsymbol{k}|} + \omega_k)(\delta n_{|\boldsymbol{p}+\boldsymbol{k}|}(1-n_p^0) - n^0_{|\boldsymbol{p}+\boldsymbol{k}|}\delta n_p) \\ &-\delta(\xi_p - \xi_{|\boldsymbol{p}+\boldsymbol{k}|} - \omega_k)\big)(\delta n_p(1-n^0_{|\boldsymbol{p}+\boldsymbol{k}|}) - n_p^0 \delta n_{|\boldsymbol{p}+\boldsymbol{k}|})\big)\end{aligned} \tag{3.102}$$

where in equilibrium at zero temperature $n_p^0 = [\xi_p < 0]$. As estimate for the matrix element we use the one given in (Lifshitz and Pitaevskii, 1981),

$$2\pi^2 g^2 |m_k|^2 \simeq \Omega_D v_F k d^3 \equiv \alpha k \tag{3.103}$$

where d is the lattice spacing. The exact value of α is unimportant, the essential feature is the linear dependence on k. The initial excitations are above the Fermi surface, and all the states below it are filled. This means that we only need to consider n_p for $p > p_F$. The linearized kinetic equation becomes

$$\begin{aligned}\delta\dot{n}_p = 2\pi^2 g^2 \int \frac{d\boldsymbol{k}}{(2\pi)^3} |m_k|^2 \big(&\delta(\xi_p - \xi_{|\boldsymbol{p}+\boldsymbol{k}|} + \omega_k)(\delta n_{|\boldsymbol{p}+\boldsymbol{k}|} - \delta n_p[\xi_{|\boldsymbol{p}+\boldsymbol{k}|} < 0]) \\ &-\delta(\xi_p - \xi_{|\boldsymbol{p}+\boldsymbol{k}|} - \omega_k)\delta n_p[\xi_{|\boldsymbol{p}+\boldsymbol{k}|} > 0]\big)\end{aligned} \tag{3.104}$$

It is convenient to work on the "diagonal" and "off–diagonal" parts of this equation separately. The off–diagonal part is

$$\delta\dot{n}_p^{\rm off} = \frac{\alpha}{(2\pi)^3}\int d\Omega_k k^3 dk\ \delta n_{|\boldsymbol{p}+\boldsymbol{k}|}\delta(\xi_p - \xi_{|\boldsymbol{p}+\boldsymbol{k}|} + \omega_k) \tag{3.105}$$

where the argument of the Dirac delta is

$$\xi_p - \xi_{|\boldsymbol{p}+\boldsymbol{k}|} + \omega_k = -\frac{k^2}{2m} - \frac{pk}{m}\cos\theta + ck \tag{3.106}$$

and we write it in the equivalent form

$$\delta(\xi_p - \xi_{|\boldsymbol{p}+\boldsymbol{k}|} + \omega_k) = \frac{m}{pk}\delta\left(\cos\theta - \left(\frac{mc}{p} - \frac{k}{2p}\right)\right) \tag{3.107}$$

Using the Dirac delta in terms of $\cos\theta$ we rewrite

$$|\boldsymbol{p}+\boldsymbol{k}| = \sqrt{p^2 + k^2 + 2pk\cos\theta} = \sqrt{2m(\xi_p + \omega + \mu)} \tag{3.108}$$

which is just the statement of energy conservation. The population appearing in the integrand is then a function of the final energy only:

$$\delta n_{|\boldsymbol{p}+\boldsymbol{k}|} \equiv \delta n_{\xi_p+\omega_k} \tag{3.109}$$

Integrating over $d\phi$ and $d\cos\theta$ we have

$$\dot{n}_p^{\rm off} = \frac{\alpha}{(2\pi)^2}\frac{m}{p}\int_0^{\Omega_D/c} dk k^2 \delta n_{\xi_p+\omega_k}\left[-1 < \frac{mc}{p} - \frac{k}{2p} < 1\right] \tag{3.110}$$

The expression in square brackets is equivalent to

$$[2(mc-p) < k < 2(mc+p)] \tag{3.111}$$

The lower bound is $k > 2(mc-p) \simeq -2p_F$, so it must be replaced with the more

restrictive integration limit $k > 0$. The upper bound $k < 2(mc + p_F) \simeq 2p_F \simeq \Omega_D/c$ is nonrestrictive, we keep the upper cutoff at the Debye frequency. It is convenient at this point to relabel $\varepsilon_p \equiv \varepsilon$ and change the variable of integration to $\xi' \equiv \xi + ck$. The off diagonal contribution to the kinetic equation is finally

$$\dot{n}_\xi^{\rm off} = \frac{\alpha}{(2\pi)^2}\frac{m}{pc^3}\int_\xi^{\Omega_D} d\xi(\xi - \xi')^2 \delta n_{\xi'} \tag{3.112}$$

The diagonal contribution to the kinetic equation is analogous. After the same steps we arrive at the expression

$$\delta\dot{n}_p^{\rm diag} = -\frac{\alpha}{(2\pi)^2}\frac{m}{p}\delta n_p \int_0^{\Omega_D/c} k^2 dk[\omega_k < \xi_p]\left[-1 < \frac{k}{2p} + \frac{mc}{p} < 1\right] \tag{3.113}$$

The restriction imposed by the integration over the Dirac delta is equivalent to

$$[-2(p + mc) < k < 2(p + mc)] \tag{3.114}$$

so the lower bound of the integral is unchanged (it is still $k = 0$), while the upper bound is the smallest between $(\Omega_D/c, 2(p + mc), \sqrt{2m\xi_p}/c)$, which is the last one of the list. The resulting integral over dk is elementary. Collecting the diagonal and off–diagonal parts together we obtain

$$\delta\dot{n}_\xi = \frac{\alpha m}{(2\pi)^2 pc^3}\left(-\frac{1}{3}\xi^3\delta n_\xi + \int_\xi^{\Omega_D} d\xi'\ (\xi - \xi')^2\delta n_{\xi'}\right) \tag{3.115}$$

Using the Landau estimate for $\alpha \simeq \Omega_D v_F d^3$, approximate $m/p \simeq 1/v_F$, and $d/c \simeq 1/\Omega_D$ we have

$$\delta\dot{n}_\xi = \frac{\alpha'}{\Omega_D^2}\left(-\frac{1}{3}\xi^3\delta n_\xi + \int_\xi^{\Omega_D} d\xi'\ (\xi - \xi')^2\delta n_{\xi'}\right) \tag{3.116}$$

where the constant α' is a pure number of order one. The first term describes particles

coming in from higher energy, while the second one counts particles leaving the state at energy ξ.

Initializing the system with a peak around the Debye energy, over a time of a few $1/\Omega_D$ the quasiparticle weight is redistributed over the spectrum down to the Fermi energy. The shape of $n_\varepsilon(t)$ approaches a scaling form for large t (see Fig.3·5).

$$n_\varepsilon(t) = ct^\alpha f(\varepsilon t^\alpha) \qquad t \to \infty \tag{3.117}$$

where the constant c is the total quasiparticle weight:

$$c \equiv \int_0^1 d\varepsilon \; n_\varepsilon(t) \Longrightarrow \int_0^{t^\alpha} dx \; f(x) = 1 \tag{3.118}$$

Plugging this ansatz into Eq.(3.116) and changing variable to $u \equiv \varepsilon t^\alpha$ we have

$$uf'(u) + \left(1 + \frac{u^3}{3\alpha t^{3\alpha-1}}\right) f(u) = \frac{1}{\alpha t^{3\alpha-1}} \int_u^{t^\alpha} du' \; (u-u')^2 f(u') \tag{3.119}$$

For this equation to be verified at large t, it is necessary that $\alpha = 1/3$. Then

$$uf'(u) + \left(1 + u^3\right) f(u) = 3 \int_u^\infty du' \; (u-u')^2 f(u') \tag{3.120}$$

in which we extended the integration bound to $t = \infty$, where the scaling form should be asymptotically exact. Evaluated at $u = 0$ this equation imposes a constraint on the value of $f(0)$:

$$f(0) = 3 \int_0^\infty dx \; x^2 f(x) \tag{3.121}$$

Given these results about quasiparticle dynamics in the metal, we are ready to discuss the superconducting case.

3.6 Equations of motions with quasiparticle relaxation

Let us now turn to the description of the superconducting dynamics induced by the quasiparticle cascade. In the absence of magnetic field and in the mean field approximation, the non-equilibrium superconducting dynamics at frequencies of order Δ_0 is described by four equations of motions for Green functions (normal Keldysh, normal retarded, anomalous Keldysh, anomalous retarded) together with one self-consistent equation for the order parameter $\Delta(t)$. It has been shown (Volkov and Kogan, 1973), however, that in the uniform, isotropic case and in the absence of inelastic scattering, the four equations for the Green functions can be reduced to just two for the equal-time Keldysh functions,

$$g(\xi,t) \equiv \int \frac{d\omega}{2\pi}\, G^K_{11}(t;\xi,\omega) \tag{3.122a}$$

$$f(\xi,t) \equiv \int \frac{d\omega}{2\pi}\, G^K_{12}(t;\xi,\omega) \tag{3.122b}$$

where $\xi = p^2/2m - \epsilon_F$ parameterizes the momentum dependence. In this section, we derive the equations of motion for the normal and anomalous Keldysh Green functions using the Keldysh technique (Keldysh, 1965) in the spatially uniform case for an isotropic BCS superconductor coupled to Fröhlich (acoustic) phonons. These equations of motion were derived in (Volkov and Kogan, 1973) ignoring the quasiparticle relaxation processes, which we include to leading order in perturbation theory. The starting point is the Dyson equation:

$$G = G_0 + G_0 \Sigma G \tag{3.123}$$

where the objects have Keldysh, Nambu and spacetime indices, all of them contracted. Reading it entry by entry, the Dyson equation is equivalent to

$$G^A = G_0^A + G_0^A \Sigma^A G^A \tag{3.124}$$

$$G^R = G_0^R + G_0^R \Sigma^R G^R \tag{3.125}$$

$$G^K = G_0^K + G_0^R \Sigma^K G^A + G_0^R \Sigma^R G^K + G_0^K \Sigma^K G^A \tag{3.126}$$

As it was shown in (Volkov and Kogan, 1973), to describe the oscillations of the order parameter it is sufficient to focus on the Keldysh Green functions only. The equations of motion for G_{11}^K and G_{12}^K follow applying $(G_0^R)^{-1}$ on Eq.(3.126)

$$(G_0^R)^{-1} G^K = \Sigma^K G^A + \Sigma^R G^K \tag{3.127}$$

since $(G_0^R)^{-1} G_0^K = 0$. These are still 2×2 Nambu matrices

$$(G_0^R)^{-1} = \begin{pmatrix} i\partial_t - H & 0 \\ 0 & i\partial_t + H^\star \end{pmatrix} \qquad G^R = \begin{pmatrix} G_{11}^R & G_{12}^R \\ G_{12}^R & G_{22}^R \end{pmatrix} \tag{3.128}$$

where the notation $i\partial_t - H$ is shorthand for the two–point operator $i\delta'(t-t')\delta(\boldsymbol{r} - \boldsymbol{r'}) - H(x, x')$ and H is the single particle Hamiltonian for free Fermions. The two entries in the top row of Eq.(3.127) are

$$(i\partial_t - H) G_{12}^K = \Sigma_{11}^K G_{12}^A + \Sigma_{12}^K G_{22}^A + \Sigma_{11}^R G_{12}^K + \Sigma_{12}^R G_{22}^K \tag{3.129}$$

$$(i\partial_t - H) G_{11}^K = \Sigma_{11}^K G_{11}^A + \Sigma_{12}^K G_{21}^A + \Sigma_{11}^R G_{11}^K + \Sigma_{12}^R G_{21}^K \tag{3.130}$$

To isolate the slow dynamics, we follow the same steps that led to Eq.(3.84): we isolate from the alternative form of the Dyson equation

$$G = G_0 + G\Sigma G_0 \tag{3.131}$$

the appropriate entries and add them to the equations of motion we already have.

The Keldysh entries are

$$G^K_{12}(i\partial_t + H^\star) = G^K_{11}\Sigma^A_{12} + G^K_{12}\Sigma^A_{22} + G^R_{11}\Sigma^K_{12} + G^R_{12}\Sigma^K_{22} \tag{3.132}$$

$$G^K_{11}(i\partial_t - H) = G^K_{11}\Sigma^A_{11} + G^K_{12}\Sigma^A_{21} + G^R_{11}\Sigma^K_{11} + G^R_{12}\Sigma^K_{21} \tag{3.133}$$

where the notation $G^K_{12}i\partial_t$ means

$$\int dx'' G^K_{12}(x,x'')i\delta'(t''-t')\delta(\boldsymbol{r}-\boldsymbol{r'}) = -i\partial_{t'}G^K_{12}(x,x') \tag{3.134}$$

and the minus sign comes from integration by parts over dt''. The same applies to terms of the form $G^K_{11}H$: since derivatives always appear multiplied by an i, we have after integration by parts

$$(G^K_{11}H)(x,x') = H^\star(x')G^K_{11}(x,x') \tag{3.135}$$

Combining two set of equations and defining $T = (t+t')/2$ we obtain

$$\begin{aligned}(i\partial_T - H(x) + H^\star(x'))G^K_{11}(x,x') = {}& \Sigma^K_{11}G^A_{11} + \Sigma^K_{12}G^A_{21} + \Sigma^R_{11}G^K_{11} + \Sigma^R_{12}G^K_{21} \\ & -G^K_{11}\Sigma^A_{11} - G^K_{12}\Sigma^A_{21} - G^R_{11}\Sigma^K_{11} - G^R_{12}\Sigma^K_{21}\end{aligned} \tag{3.136}$$

$$\begin{aligned}(i\partial_T - H(x) - H(x'))G^K_{12}(x,x') = {}& \Sigma^K_{11}G^A_{12} + \Sigma^K_{12}G^A_{22} + \Sigma^R_{11}G^K_{12} + \Sigma^R_{12}G^K_{22} \\ & -G^K_{11}\Sigma^A_{12} - G^K_{12}\Sigma^A_{22} - G^R_{11}\Sigma^K_{12} - G^R_{12}\Sigma^K_{22}\end{aligned} \tag{3.137}$$

These equations become simpler if we use the symmetries of G and Σ to eliminate all quantities with Nambu indices 21 and 22:

$$\begin{pmatrix}(G^R_{11}(x_1,x_2))^\star & (G^R_{12}(x_1,x_2))^\star \\ (G^R_{21}(x_1,x_2))^\star & (G^R_{22}(x_1,x_2))^\star\end{pmatrix} = \begin{pmatrix}-G^R_{22}(x_1,x_2) & G^R_{21}(x_1,x_2) \\ G^R_{12}(x_1,x_2) & -G^R_{11}(x_1,x_2)\end{pmatrix} \tag{3.138}$$

The self energies transform exactly as their corresponding Green function (Σ^R trans-

forms as G^R and so on). We introduce the order parameter Δ through[6]

$$\Delta \equiv \frac{1}{2}\left(\Sigma^R_{12} + \Sigma^A_{12}\right) \tag{3.139}$$

and assume it does not have any spatial structure: $\Delta(x, x') \propto \delta(x - x')$. This gives

$$i\partial_T G^K_{11} + \Delta G^{K*}_{12} + G^K_{12}\Delta^* = I_{11} \tag{3.140a}$$

$$(i\partial_T - 2\xi)G^K_{12} - \Delta G^{K*}_{11} + G^K_{11}\Delta = I_{12} \tag{3.140b}$$

where $\xi = p^2/(2m) - \epsilon_F$. The source terms I_{11} and I_{12} encode the effect of inelastic processes on the dynamics: I_{11} yields the collision integral in the metal when $\Delta \to 0$ ($I_{12} \to 0$ in this limit). They are formally given by

$$\begin{aligned} I_{11} \equiv{}& \Sigma^K_{11}G^A_{11} - G^R_{11}\Sigma^K_{11} + \Sigma^R_{11}G^K_{11} - G^K_{11}\Sigma^A_{11} \\ &+ \Sigma^K_{12}G^{A\star}_{12} + G^R_{12}\Sigma^{K\star}_{12} + G^K_{12}\frac{\Sigma^{R\star}_{12} - \Sigma^{A\star}_{12}}{2} - \frac{\Sigma^R_{12} - \Sigma^A_{12}}{2}G^{K\star}_{12} \end{aligned} \tag{3.141a}$$

$$\begin{aligned} I_{12} \equiv{}& \Sigma^K_{11}G^A_{12} - G^R_{12}\Sigma^{K\star}_{11} - \Sigma^K_{12}G^{A\star}_{11} - G^R_{11}\Sigma^K_{12} + \Sigma^R_{11}G^K_{12} \\ &+ G^K_{12}\Sigma^{A\star}_{11} + \frac{\Sigma^R_{12} - \Sigma^A_{12}}{2}G^{K\star}_{11} + G^K_{11}\frac{\Sigma^R_{12} - \Sigma^A_{12}}{2} \end{aligned} \tag{3.141b}$$

The products in these equations are still spacetime contractions. To focus on the equal time dynamics $t = t_1 = t_2$, we take the Fourier transform over τ of Eqs. (3.140)-(3.141) and then integrate over the relative frequency.

In order to evaluate I_{11} and I_{12} we need the self–energy computed in 3.4.3. Looking at Eq.(3.71) we see that the set of differential equations (3.140) is not closed, unlike in the analysis of (Volkov and Kogan, 1973); the source terms need the electronic retarded Green functions and all the phononic ones. To close the system, we work at the same level of approximation used in the derivation of the kinetic equation

[6]Notice that Δ does not have neither Keldysh nor Nambu indices, it is a scalar function of spacetime.

(Sec.3.101). We take the Green functions in Eq. (3.141) to be in quasiequilibrium form: the retarded and advanced functions are assumed to always remain in equilibrium BCS form, while the Keldysh ones depend on the average time t only through the quasiparticle distribution function $n(\xi, t)$. We have assumed that the elastic relaxation time is the shortest time in the problem so that the Green functions are independent of the direction of $\boldsymbol{p}$ and can be parametrized by ξ alone, $G^K_{\alpha\beta}(t; \boldsymbol{p}, \omega) = G^K_{\alpha\beta}(t; \xi, \omega)$. The quasiequilibrium form we use is

$$G^R_{11}(\xi;\omega) = (G^A_{11}(\xi;\omega))^* = \frac{u_\xi^2}{\omega - \varepsilon + i0^+} + \frac{v_\xi^2}{\omega + \varepsilon + i0^+} \tag{3.142a}$$

$$G^K_{11}(\xi;\omega,t) = -2\pi i(1 - 2n(\xi,t))\left(u_\xi^2\delta(\omega-\varepsilon) - v_\xi^2\delta(\omega+\varepsilon)\right) \tag{3.142b}$$

$$G^R_{12}(\xi;\omega) = (G^A_{12}(\xi;\omega))^* = -\frac{u_\xi v_\xi}{\omega + \varepsilon + i0^+} + \frac{u_\xi v_\xi}{\omega - \varepsilon + i0^+} \tag{3.142c}$$

$$G^K_{12}(\xi;\omega,t) = -2\pi i u_\xi v_\xi(1 - 2n(\xi,t))\left(\delta(\omega+\varepsilon) + \delta(\omega-\varepsilon)\right) \tag{3.142d}$$

$$D^R(k;\omega) = (D^A(k;\omega))^* = |m_k|^2 \frac{\omega_k}{(\omega + i0)^2 - \omega_k^2} \tag{3.142e}$$

$$D^K(k;\omega,t) = -i\pi\,|m_k|^2\left(\delta(\omega+\omega_k) + \delta(\omega-\omega_k)\right) \tag{3.142f}$$

where

$$u_\xi^2 = \frac{1}{2}\left(1 + \frac{\xi}{\varepsilon}\right) \qquad v_\xi^2 = \frac{1}{2}\left(1 - \frac{\xi}{\varepsilon}\right) \qquad \varepsilon = \sqrt{\xi^2 + \Delta_0^2} \tag{3.143}$$

In these expressions, $|m_k|^2$ is the squared electron–phonon matrix element (which is linear in k), and $\omega_k = ck$ is the phonon dispersion. We also assume that the phonons remain in equilibrium at all times.

Finally, linearizing the resulting equations, we obtain

$$i\partial_t \delta g + 2\Delta_0 \mathrm{Re}[\delta f] = \delta I_{11} \tag{3.144a}$$

$$(i\partial_t - 2\xi)\,\delta f + 2g_{eq}\delta\Delta + 2\Delta_0 \delta g = \delta I_{12} \tag{3.144b}$$

$$\delta\Delta = -\frac{\lambda_{\mathrm{BCS}}}{2}\int d\xi\, \mathrm{Im}[\delta f] \tag{3.144c}$$

where λ_{BCS} is the dimensionless BCS coupling, and

$$\delta I_{11} = 2\gamma\, \mathrm{sign}(\xi)\left(\frac{1}{3}\epsilon^3 n(\epsilon,t) - \int_{\epsilon}^{\infty} d\epsilon'\,(\epsilon-\epsilon')^2 n(\epsilon',t)\right) \tag{3.145a}$$

$$\delta I_{12} = 2\gamma\Delta_0\left(n(\epsilon,t)\int_0^{\epsilon} d\epsilon'\,(\epsilon-\epsilon')^2\left(\frac{1}{\epsilon}-\frac{1}{\epsilon'}\right) - \int_{\epsilon}^{\infty} d\epsilon'\,(\epsilon-\epsilon')^2\left(\frac{1}{\epsilon}-\frac{1}{\epsilon'}\right) n(\epsilon',t)\right) \tag{3.145b}$$

Eqs. (3.144) and (3.145) describe the linearized dynamics of small deviations around the equilibrium solution (Volkov and Kogan, 1973)

$$f_{eq} = -i\frac{\Delta_0}{\epsilon}(1-2n_F(T)) \tag{3.146a}$$

$$g_{eq} = -i\frac{\xi}{\epsilon}(1-2n_F(T)) \tag{3.146b}$$

where $n_F(T) = (1+\exp(\epsilon/T))^{-1}$ is the equilibrium Fermi distribution and $\epsilon = \sqrt{\xi^2+\Delta_0^2}$. Eq. (3.145) is valid for energies $\epsilon \gg \Delta$, where we need not distinguish the quasiparticle energy ϵ from $|\xi|$. We also take into consideration that, for optical excitation, the quasiparticle distribution n is even in ξ and follows the metallic cascade governed by Eq. (3.6).

3.7 Oscillations of the order parameter

As we are interested in the case $T \ll \Delta_0$, we approximate $1-2n_F(T) \simeq 1$. Furthermore, for optical excitation, $\mathrm{Re}[\delta f]$ is odd in ξ, while $\mathrm{Im}[\delta f]$ and δg are even in ξ at all times.

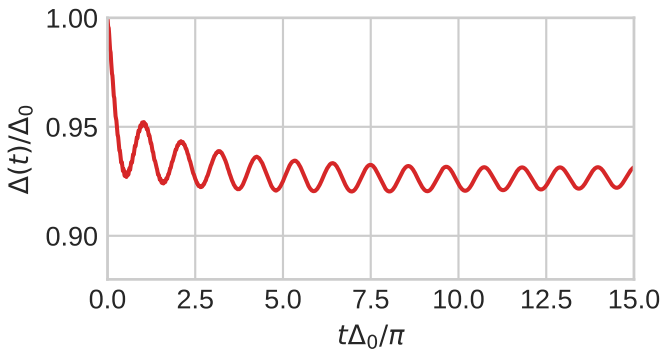

Figure 3·7: Example solution of Eq.(3.144). The units on the horizontal axis are chosen so that a period of one unit corresponds to $\omega = 2\Delta_0$. In this simulation we started from an equlibrium initial condition with $\Delta_0 = 0.05\Omega_D$, and driven the system with the quasiparticle dynamics presented in Fig.3·5. This figure only gives a qualitative picture of the dynamics predicted by our model: in particular, the long time average value is not accurately modeled as we are not including phonon reabsorption. The focus is on the amplitude of the excited oscillations.

As the excitation of $\Delta(t)$ is controlled by energies $\epsilon \sim \epsilon^* \gg \Delta$, we can substitute the solution for the quasiparticle cascade in the normal metal (Eq. (3.6)) into the right–hand side of Eq. (3.145).

Taking the Fourier transform of Eq. (3.144), solving for δf in Eqs. (3.144)(a,b) and substituting the result into Eq. (3.144)c, we obtain

$$\delta\Delta(\omega) = \frac{1}{i\omega F(\omega)}\left(\frac{4\Delta_0}{\omega^2 - 4\Delta_0^2}\left\langle\frac{\xi\delta I_{11}(\xi,\omega)}{\omega^2-4\epsilon^2}\right\rangle - \left\langle\frac{\delta I_{12}(\xi,\omega)}{\omega^2-4\epsilon^2}\right\rangle\right) \tag{3.147}$$

where the angle brackets are shorthand for

$$\langle\ldots\rangle \equiv \frac{\lambda_{\rm BCS}}{2}\int_{-\Omega_D}^{\Omega_D} d\xi\ldots \tag{3.148}$$

and following Ref. (Volkov and Kogan, 1973) we define the auxiliary function

$$F(\omega) \equiv \left\langle\frac{1}{\epsilon}\frac{1}{\omega^2-4\epsilon^2}\right\rangle \tag{3.149}$$

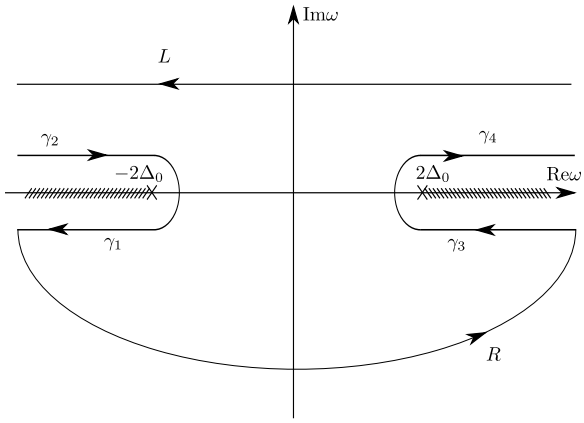

Figure 3·8: Contour in the complex ω plane for the solution of Eq. (3.151). The semicircle R has radius approaching infinity, while the the semicircles surrounding the branch points at $\pm 2\Delta_0$ have vanishing radius.

For a discussion of the analytic properties of this function see Ref.(Volkov and Kogan, 1973). The most important feature is the pair of branch points on the real axis at $\omega = \pm 2\Delta_0$, which is the origin of the $1/\sqrt{t}$ decay of the $\delta\Delta(t)$ oscillation amplitude at long times(Lighthill, 1958b) in Eq. (3.2).

To obtain the amplitude of oscillations, we take the inverse Fourier transform

$$\delta\Delta(t) = \int_{-\infty}^{\infty} \frac{d\omega}{2\pi} e^{-i\omega t} \delta\Delta(\omega) \tag{3.150}$$

which is equivalent to the integral along the contour L in Fig. 3·8. Using the Cauchy residue theorem we have

$$\delta\Delta(t) = i\mathrm{Res}(\delta\Delta(\omega), 0) + \int_{\cup_i \gamma_i} \frac{d\omega}{2\pi} e^{-i\omega t} \delta\Delta(\omega) \tag{3.151}$$

We focus on the second term in Eq. (3.151) which describes the oscillating part of $\Delta(t)$. The first term describes the mean value of $\Delta(t)$ at late time, which is determined physically by quasiparticle processes at energies of order the gap Δ where our perturbative expressions for I_{11} and I_{12} are no longer valid.

Close to the branch points of $F(\omega)$, we have

$$\left\langle \frac{4\Delta_0 \xi I_{11}(\xi,\omega)}{\omega^2 - 4\epsilon^2} \right\rangle \simeq i\pi \frac{\gamma}{4} \frac{C}{\epsilon^\star} \mathcal{N}(0) a(\omega) \tag{3.152}$$

where C is the normalization constant in Eq. (3.6) and

$$a(\omega) = -\frac{\pi}{\Gamma(-1/3)} + i\frac{\Gamma(1/3)}{6} \mathrm{sign}(\mathrm{Re}\,\omega) \tag{3.153}$$

The dependence on the sign of ω is due to I_{11} being the Fourier transform of a real function.

It turns out that the term including I_{12} gives a subleading contribution at long times – the amplitude decays as $1/t$, which is negligible compared to $1/\sqrt{t}$ as $t \to \infty$. Taking the inverse Fourier transform of Eq. (3.147), we arrive at

$$\delta\Delta(t) = B \frac{\cos(2\Delta_0 + \phi)}{\sqrt{\Delta_0 t}} \tag{3.154}$$

where the values of the parameters B, ϕ are

$$B = \left(\frac{2}{\pi}\right)^{3/2} \frac{\pi |a| N \mathcal{N}(0)}{\nu(0)\Omega_D} \frac{\Omega_D}{\epsilon^\star} \qquad \phi = \pi/4 + \arg(a) \tag{3.155}$$

where $a = -\pi/\Gamma(-1/3) + i\Gamma(1/3)/6$ so that $|a| \simeq 0.893$. With our choice of normalization, $\mathcal{N}(0) \simeq 1.44$.

3.8 Concluding Thoughts

We arrived at the conclusion that short pulses of incoherent light at very high frequency efficiently produce coherent oscillations of the Higgs mode in superconductors. The amplitude of oscillation is controlled by a single parameter N – the total number of quasiparticles at Ω_D after the initial rapid stages of quasiparticle relaxation. One might have worried that the complicated high energy dynamics of quasiparticles would

kick the Higgs mode in "random" ways and thus be ineffective at exciting it. Indeed, at very high energies, the quasiparticles are ineffective, but the simple scaling dynamics once they reach the characteristic energy scale ϵ^* lead to coherent excitation. Large energy excitation may eventually lead to heating (although it need not in thin films well coupled to substrates), but the time scale for phonon reabsorption is much larger than the time on which oscillations should be visible and we expect our mechanism to lead to observable Higgs oscillations.

Chapter 4

Damping of the Gapped Mode in a Molecular Condensate

4.1 Introduction

The study of the Molecular Superfluid (MSF) phase of weakly interacting ultracold Bose atoms, first analyzed theoretically some two decades ago (Radzihovsky et al., 2004; Radzihovsky et al., 2008), has recently heated up again (Zhang et al., 2022; Malla et al., 2022; Lam et al., 2022) due to groundbreaking experimental progress (Zhang et al., 2021b) in coherently trapping ultracold cesium atoms and controlling their Feshbach resonances to produce cesium molecules (Cs_2) (Chin et al., 2010; Berninger et al., 2013; Mark et al., 2007; Chin et al., 2003; Köhler et al., 2006). The refinement of these trapping techniques enables a new generation of experiments probing both equilibrium and dynamical properties of both the MSF and proximate Atomic Superfluid (ASF) phase. While the thermodynamics of the MSF-ASF system are well-known theoretically (Radzihovsky et al., 2008; Romans et al., 2004) (see Fig. 4·1 for a phase diagram), its dynamical responses are more complicated. A full dynamical theory of the system requires an understanding of both the quasiparticle content and their dissipative scattering properties.

In this chapter, we compute the near equilibrium decay rates of the quasiparticles in the ASF and MSF phases to one-loop order at zero temperature. The quasiparticle decay rate determines the width of the spectral function, schematically illustrated in

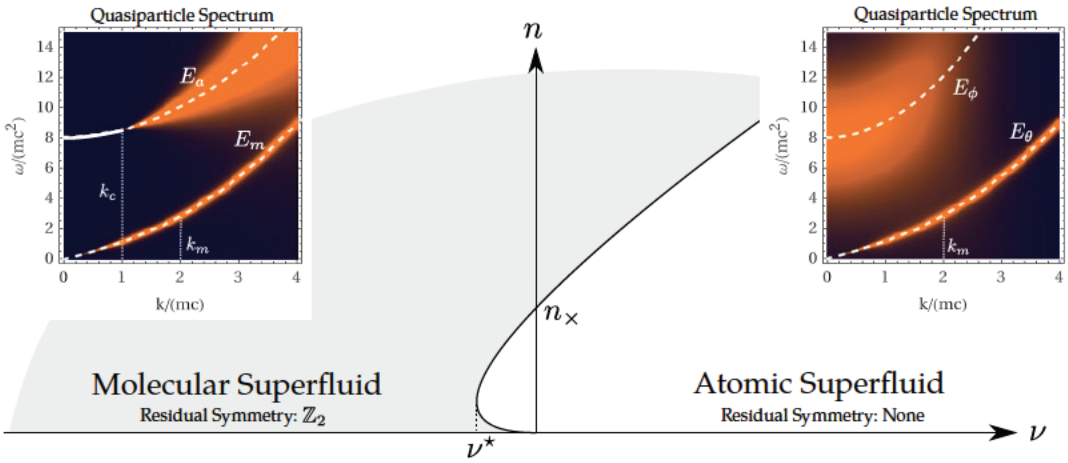

Figure 4·1: The mean field phase diagram as a function of the binding energy ν and total condensate density $n = n_a + 2n_m$, with two insets showing the quasiparticle spectral weight. The white lines are the mean field results for the quasiparticle dispersion discussed in Sec.4.4. The solid white line in the MSF side inset indicates that the excitation is infinitely long lived: in the MSF phase the $\mathbb{Z}_2$ symmetry keeps the spectral line for the gapped excitation sharp up to a threshold momentum k_c, above which decay by phonon emission is allowed. In the ASF phase there is no such symmetry protection, the gapped mode is damped at arbitrarily low momenta and is in fact very diffuse. In both phases the gapless mode is always damped. To give the reader a reference for the momentum scales we marked k_m on the k axis: it is the scale where the gapless excitation changes nature from predominantly phonon–like to particle–like. The phase boundary depicted assumes $2g_{am} > g_m$, see Eq.(4.16).

the insets of Fig. 4·1. In principle, this is directly measurable by tunneling experiments in which a micro-trap is placed in tunnel contact with the MSF (Micheli et al., 2004).

Single atom transmission spectroscopy provides an alternative, and perhaps more striking, experimental signature of the quasiparticle dynamics in the MSF phase. An incident atom evolves into the gapped quasiparticle mode, which is sharp up to a critical momentum k_c. Beyond this threshold, the quasiparticle Cherenkov radiates phonons (the gapless mode). Thus, a slow atom fired through a MSF cloud propagates without dissipation, while faster atoms slow down until they drop below the Cherenkov threshold. This leads to a sharp feature in the energy spectrum of the transmitted atoms as the incident energy crosses the threshold – assuming the cloud is "optically dense" enough to slow the atom before it passes through. Using our computed scattering rates, we estimate that the stopping power of a typical molecular cloud is sufficient to observe these features (see Fig. 4·3). The existence of k_c follows from the symmetry structure of the MSF phase, as we discuss below. Deep in the MSF phase $k_c \simeq mc$, where m is the atomic mass and c the speed of sound (see Eq.(4.42)).

We summarize here the equilibrium properties of the system to contextualize our work and keep the presentation self–contained. The system has a global $U(1)$ symmetry associated with total atom number conservation $n = N_a + 2N_m$, where N_a is the number of atoms and N_m is the number of molecules. The simplest model Hamiltonian for the system (Tommasini et al., 1998) includes kinetic contributions, density–density interactions, and a Feshbach interaction that coherently converts two atoms into a molecule and vice versa - see equations (4.1) through (4.6). This interconversion occurs thanks to the hyperfine interactions between the closed and open scattering channels for atomic collisions (Timmermans et al., 1999; Chin et al., 2010; Duine and Stoof, 2004).

With the formation of the condensate the global $U(1)$ is spontaneously broken.

At low temperature there are two distinct scenarios for this $U(1)$ breaking: 1. when just the molecules condense the phase is known as molecular superfluid (MSF), and 2. when both the atoms and the molecules condense as atomic superfluid (ASF). Due to the coherent interconversion process, the condensation of the atoms forces a condensation of the molecules, and thus there is no phase where the atoms are condensed but the molecules are not. In the MSF phase the global $U(1)$ is reduced to a global $\mathbb{Z}_2$, where the $\mathbb{Z}_2$ charge is the parity of the atom number, while in the ASF phase there is no remaining symmetry. Prior work has argued (Lee and Lee, 2004; Radzihovsky et al., 2004) that the zero temperature quantum phase transition between the MSF and ASF phases is continuous and lies in the quantum Ising class.

There are two experimentally tunable parameters which control the phase diagram: the total number of atoms n and the molecular binding energy ν. When ν is large and positive, the molecular state is anti–bound, so we expect ASF to be the equilibrium phase, while for large and negative ν forming a molecule is energetically favorable and we expect MSF. No such simple argument can be made for the effect of the particle number n on the phase. Indeed, the transition is re-entrant as a function of particle number at the mean–field level (see Fig. 4·1).

The quasiparticle content of the ASF and MSF phases is as follows. Since the $U(1)$ symmetry is broken in both the ASF and MSF phases, there is one Goldstone boson on each side of the transition. In the MSF phase, the molecules are at lower energy than the atoms and the Goldstone mode is molecular in nature, carrying a $\mathbb{Z}_2$ even charge. A second, gapped branch of the spectrum is atom-like, carrying odd $\mathbb{Z}_2$ charge. By $\mathbb{Z}_2$ conservation, the upper mode can lose energy and momentum into the Goldstone mode, but cannot disappear. At zero temperature, such emission can only happen above a Cherenkov momentum k_c, where the group velocity matches the Goldstone velocity. The decay width above the Cherenkov transition is proportional

to $\sim (k - k_c)^3$ and is given by Eq.(4.52). The gapless mode in the MSF phase has a similar lifetime to that of a single component BEC (Beliaev, 1958) and is given by Eq.(4.55).

In the ASF phase the Goldstone mode has mostly atomic character while the high energy mode has mostly molecular character. However, there is no $\mathbb{Z}_2$ conservation so no decays are forbidden. The decay rate of the high energy mode scales with the gap, Δ, as Δ^4 and is given by Eq.(4.70). The decay rate of the Goldstone mode in the ASF phase is of similar form to Eq.(4.55) however with $2m \to m$.

To obtain these results, we derive a low energy effective theory on each side of the transition from the microscopic theory of Eq.(4.1). This approach significantly simplifies the calculation compared to using the microscopic theory directly, and is applicable as long as we restrict our attention to excitations with wavelengths longer than the healing length of the condensate and energies below the multiparticle threshold. Using the effective theory, we compute for each excitation the one–loop imaginary part of the self energy in the on–shell approximation, and thus estimate the decay rates of the gapped modes.

The chapter is organized as follows: in Sec.4.2 we set up the problem, then in Sec.4.3 we briefly review the mean–field phase diagram. In Sec.4.4 we review the Bogoliubov mean field theory of the spectrum and in Sec.4.5 we summarize our results for the decay rates of the gapped mode in each phase. The interested reader will find details of the calculation of certain integrals in Sec.4.7.

4.2 Euclidean Action and Symmetries

The number of atoms N_a and the number of molecules N_m are not separately conserved, only the total number $N = N_a + 2N_m$. The Euclidean action of the system is

$$S = \int d\mathbf{r} d\tau \left(\mathcal{T} + \mathcal{H}_a + \mathcal{H}_m + \mathcal{H}_{am} + \mathcal{H}_F \right) \tag{4.1}$$

$$\mathcal{T} = \bar{\Psi}_m \partial_\tau \Psi_m + \bar{\Psi}_a \partial_\tau \Psi_a \tag{4.2}$$

$$\mathcal{H}_m = \bar{\Psi}_m \left(-\frac{\nabla^2}{4m} - 2\mu + \nu \right) \Psi_m + \frac{g_m}{2} |\Psi_m|^4 \tag{4.3}$$

$$\mathcal{H}_a = \bar{\Psi}_a \left(-\frac{\nabla^2}{2m} - \mu \right) \Psi_a + \frac{g_a}{2} |\Psi_a|^4 \tag{4.4}$$

$$\mathcal{H}_{am} = g_{am} |\Psi_a|^2 |\Psi_m|^2 \tag{4.5}$$

$$\mathcal{H}_F = -\alpha \left(\bar{\Psi}_a^2 \Psi_m + \bar{\Psi}_m \Psi_a^2 \right) \tag{4.6}$$

The subscript a denotes the atoms and m the molecules. Here ν is the molecular binding energy; a negative ν means it is energetically favorable to make bound states. The minus sign in front of the Feshbach term is chosen so that $\alpha > 0$ in equilibrium the phases of the condensates are locked to the same value; Without loss of generality we assume $\alpha > 0$, as it is always possible to absorb its sign with the field redefinition $\Psi_m \to -\Psi_m$. The coefficient α only depends on the properties of the Feshbach resonance under consideration, we assume it is given. The exact relation to is discussed in (Radzihovsky et al., 2008). The chemical potential μ appears with a factor of 2 in the molecular part because two atoms bind to form a molecule and only the total number is conserved. Under the $U(1)$ symmetry associated to this conservation law the atomic field transforms with unit charge and the molecular one

with double charge

$$\Psi_a \to e^{i\theta}\Psi_a \qquad \Psi_m \to e^{i2\theta}\Psi_m \tag{4.7}$$

The system has two nontrivial low–temperature phases: the atomic superfluid (ASF) phase, in which the $U(1)$ symmetry is completely broken –both Ψ_a and Ψ_m condense–, and the molecular superfluid (MSF) phase, in which the $U(1)$ breaks down to $\mathbb{Z}_2$

$$\Psi_a \to -\Psi_a \qquad \Psi_m \to \Psi_m \tag{4.8}$$

As such we expect any continuous transition between the two phases to be Ising class (Radzihovsky et al., 2008).

4.3 Mean Field phase diagram

We briefly review the mean field phase diagram (see Fig.4·1) of the system, to provide context for our calculations. We map the phase diagram in terms of the total density $n = n_a + 2n_m$ and the binding energy ν, which are experimentally tunable. As anticipated, there are two stable thermodynamic phases at zero temperature (ASF and MSF), separated by an Ising class transition line (Radzihovsky et al., 2004; Lee and Lee, 2004). If $2g_{am} > g_m$ the transition is reentrant as a function of n for small negative ν (see Eq.(4.16)). Parametrizing the fields in polar form

$$\Psi_j = \sqrt{n_j}e^{i\theta_j} \qquad j = a, m \tag{4.9}$$

clarifies the role of the relative phase between the condensates. In the absence of an external potential the equilibrium solution is uniform, so we drop the gradient terms.

The mean field energy density is then

$$\begin{aligned}\mathcal{E}_{MF} = &\frac{1}{2}g_a n_a^2 + \frac{1}{2}g_m n_m^2 + g_{am} n_a n_m \\ &-2\alpha n_a \sqrt{n_m}\cos\left(2\theta_a - \theta_m\right) \\ &-\mu(n_a + 2n_m - n) + \nu n_m\end{aligned} \tag{4.10}$$

which is minimized by

$$0 = \alpha n_a \sqrt{n_m}\sin(2\theta_a - \theta_m) \tag{4.11}$$

$$\mu = g_a n_a + g_{am} n_m - 2\alpha\sqrt{n_m}\cos(2\theta_a - \theta_m) \tag{4.12}$$

$$2\mu - \nu = g_m n_m + g_{am} n_a - \alpha\frac{n_a}{\sqrt{n_m}}\cos(2\theta_a - \theta_m) \tag{4.13}$$

These equations have two nontrivial solutions:

MSF phase $n_a = 0, n_m = n/2 > 0$. At mean field

$$2\mu - \nu = g_m n_m \tag{4.14}$$

as usual for a weakly interacting Bose gas. The combination $2\mu - \nu$ acts as an effective chemical potential for the molecules.

ASF phase $n_a > 0, n_m > 0$. While there is a closed form expression for n_a and n_m, it is complicated and we omit it. In the large ν limit at fixed density n, we find to lowest order in ν the relations $\sqrt{n_m} = \alpha n/\nu$ and $\mu = g_a n$, which means that the system behaves as a simple atomic BEC.

There is no phase where the atoms are condensed but the molecules are not. Since $\alpha > 0$, in the ASF phase the phases of the atomic and molecular condensates lock together:

$$2\theta_a - \theta_m = 0 \tag{4.15}$$

Eliminating the chemical potential and imposing $n_a = 0$ we find the phase boundary (see Fig.4·1)

$$\left(g_{am} - \frac{g_m}{2}\right) n - 2\alpha\sqrt{2n} = \nu \tag{4.16}$$

The phase boundary crosses the $\nu = 0$ axis at

$$n_\times = 32\alpha^2/(2g_{am} - g_m)^2 \tag{4.17}$$

and the leftmost point is at

$$|\nu^\star| = 4\alpha^2/|2g_{am} - g_m| \tag{4.18}$$

so that using a negative binding energy with $|\nu| < |\nu^\star|$ the reentrant nature of the transition is visible. Finally, we point out that the phase diagram and the order of the transition are sensitive to the sign of $g_a g_m - g_{am}^2$ (for concreteness we assume $g_a g_m > g_{am}^2$) but the realized phases are the same. For a detailed discussion see (Radzihovsky et al., 2008).

4.4 Bogoliubov theory of the Molecular Superfluid

In this section we review the Bogoliubov theory of the molecular superfluid (Radzihovsky et al., 2004), which describes the quadratic fluctuations around the mean field solutions of Sec.4.3. See (Popov, 2001) for a detailed review of the Bogoliubov approach. We expand the action around the mean field configuration

$$\langle \Psi_j \rangle = \sqrt{n_j^0} \qquad j = a, m \tag{4.19}$$

where the two constants (n_a^0, n_m^0) solve Eq.(4.11)-(4.13). We redefine the fields to isolate the deviations ψ_j from equilibrium

$$\Psi_j = \sqrt{n_j^0} + \psi_j \qquad j = a, m \tag{4.20}$$

and we drop from the action all terms of degree higher than two in ψ_j. The result is

$$S = S_2 + \int d\boldsymbol{r} d\tau \, \mathcal{E}_{MF} \tag{4.21}$$

where $\mathcal{E}_{MF}$ is the mean field energy density of Eq.(4.10), there are no terms linear in the fluctuation fields, and S_2 is the quadratic action associated to the fluctuations:

$$\begin{aligned} S_2 = \int d\mathbf{r} d\tau \Big[& \bar{\psi}_m \partial_\tau \psi_m + \bar{\psi}_a \partial_\tau \psi_a \\ & + \bar{\psi}_m \Big(-\frac{\nabla^2}{4m} - 2\mu + \nu \Big) \psi_m + \frac{1}{2} g_m n_m^0 \big(\psi_m^2 + \bar{\psi}_m^2 + 4 |\psi_m|^2 \big) \\ & + \bar{\psi}_a \Big(-\frac{\nabla^2}{2m} - \mu \Big) \psi_a + \frac{1}{2} g_a n_a^0 \big(\psi_a^2 + \bar{\psi}_a^2 + 4 |\psi_a|^2 \big) \\ & + g_{am} \sqrt{n_a^0 n_m^0} \big(\bar{\psi}_m \bar{\psi}_a + \bar{\psi}_m \psi_a + \psi_m \bar{\psi}_a + \psi_m \psi_a \big) + g_{am} \big(n_m^0 |\psi_a|^2 + n_a^0 |\psi_m|^2 \big) \\ & - \alpha \big(2\sqrt{n_a^0} \bar{\psi}_m \psi_a + \sqrt{n_m^0} \psi_a^2 + 2\sqrt{n_a^0} \psi_m \bar{\psi}_a + \sqrt{n_m^0} \bar{\psi}_a^2 \big) \Big] \end{aligned} \tag{4.22}$$

It is convenient to work in momentum space and organize the fields in a Nambu spinor

$$\Phi_{\mathbf{k}}^\dagger \equiv \begin{pmatrix} \bar{\psi}_{a,\mathbf{k}} & \psi_{a,-\mathbf{k}} & \bar{\psi}_{m,\mathbf{k}} & \psi_{m,-\mathbf{k}} \end{pmatrix} \tag{4.23}$$

We have already extracted the spatially uniform part from the fields, so the Fourier expansion of ψ_j does not have a $k = 0$ term. To avoid double counting the anomalous terms we organize the momentum sum as

$$S_2 = \sum_n \sum_{\mathbf{k}, k_z > 0} \Phi_{\mathbf{k}}^\dagger \cdot G_0^{-1} \cdot \Phi_{\mathbf{k}} \tag{4.24}$$

where the inverse G_0^{-1} of the matrix propagator is given in Eq. (4.25). Notice that in the MSF phase $n_a^0 = 0$, so that the matrix is block diagonal. This is a manifestation of $\mathbb{Z}_2$ symmetry: the atom–like Bogoliubov quasiparticles only have overlap with $\psi_{a,\mathbf{k}}$ and $\bar{\psi}_{a,-\mathbf{k}}$, without a molecular component. The molecular block describes a simple weakly interacting condensate of molecules, while the dynamics of the atomic fluctuations is nontrivial: the atoms are not condensed, but the anomalous averages $\langle \psi_a \psi_a \rangle$ acquire a finite value thanks to the off–diagonal Feshbach terms $-2\alpha\sqrt{n_m^0}$ that provide coherent conversion of a condensed molecule into two atoms.

$$G_0^{-1} = \begin{pmatrix} \omega_n + \xi_a + 2g_a n_a^0 + g_{am} n_m^0 & g_a n_a^0 - 2\alpha\sqrt{n_m^0} & g_{am}\sqrt{n_m^0 n_a^0} - 2\alpha\sqrt{n_a^0} & g_{am}\sqrt{n_m^0 n_a^0} \\ g_a n_a^0 - 2\alpha\sqrt{n_m^0} & -\omega_n + \xi_a + 2g_a n_a^0 + g_{am} n_m^0 & g_{am}\sqrt{n_m^0 n_a^0} & g_{am}\sqrt{n_m^0 n_a^0} - 2\alpha\sqrt{n_a^0} \\ g_{am}\sqrt{n_m^0 n_a^0} - 2\alpha\sqrt{n_a^0} & g_{am}\sqrt{n_m^0 n_a^0} & \omega_n + \xi_m + 2g_m n_m^0 + g_{am} n_a^0 & g_m n_m^0 \\ g_{am}\sqrt{n_m^0 n_a^0} & g_{am}\sqrt{n_m^0 n_a^0} - 2\alpha\sqrt{n_a^0} & g_m n_m^0 & -\omega_n + \xi_m + 2g_m n_m^0 + g_{am} n_a^0 \end{pmatrix} \tag{4.25}$$

where ω_n are bosonic Matsubara frequencies, and for brevity we have introduced

$$\xi_a \equiv \frac{k^2}{2m} - \mu \qquad \xi_m = \frac{k^2}{4m} - 2\mu + \nu \tag{4.26}$$

The condition $\det(G_0^{-1}) = 0$ gives the excitation spectrum. Notice that that the G_0^{-1} matrix still depends on the chemical potential μ: when we substitute the mean field value of μ found from Eq.(4.12) and (4.13) we describe the fluctuations around the chosen mean field solution, ignoring the feedback of the fluctuations on the chemical potential itself. The dispersion of the gapless mode is convex in both phases and thus allows spontaneous phonon emission. The lifetime is known at large ν (Beliaev, 1958; Vincent Liu, 1997), either positive or negative, where the gapped mode is inaccessible and the system reduces to a single component BEC. Close to the transition the picture is more complicated, as the phonon and gapped modes are coupled: in this regime,

the low energy behavior of the system is well described by an effective theory of two real fields (Radzihovsky et al., 2008; Lee and Lee, 2004).

4.4.1 Spectrum in MSF phase

In the MSF phase the gapped excitation is protected by $\mathbb{Z}_2$ symmetry, so the only allowed process at low momentum it the emission of a phonon. The kinematics of this decay are such that the line is sharp until the group velocity matches the speed of sound at the critical momentum k_c, then we expect a decay rate proportional to $(k - k_c)^3$, based on general considerations (Abrikosov, 1963) for phonons. There are two modes: one particle–like excitation E_a with odd $\mathbb{Z}_2$ charge and one molecule like E_m with even charge:

$$E_m = \sqrt{\epsilon_m \left(2g_m n_m + \epsilon_m\right)} \qquad \mathbb{Z}_2 \text{ even} \tag{4.27}$$

$$E_a = \sqrt{(\epsilon_a - \epsilon^+)(\epsilon_a - \epsilon^-)} \qquad \mathbb{Z}_2 \text{ odd} \tag{4.28}$$

In these expressions the free atomic and molecular dispersions are

$$\epsilon_a = \frac{k^2}{2m} \qquad \epsilon_m = \frac{k^2}{4m} \tag{4.29}$$

and we have defined

$$\epsilon^{\pm} = \frac{\nu}{2} + \left(\frac{g_m}{2} - g_{\text{am}}\right) n_m \pm 2\alpha\sqrt{n_m} \tag{4.30}$$

The dispersion relations $E_{a,m}$ are plotted in the left inset of Fig.4·1. We note that Eqs.(4.12) and (4.13) have already been used to simplify these expressions. The molecular branch E_m is phonon-like; it is the Goldstone mode arising from the breakdown of $U(1)$ to $\mathbb{Z}_2$, with the speed of sound given by the familiar expression for a single component mean field BEC[1] (the $2m$ in the denominator is the mass of a

[1]For a modern review see for example (Andersen, 2004).

molecule)

$$c_{\mathrm{MSF}} = \left.\frac{\partial E_m}{\partial k}\right|_{k=0} = \sqrt{\frac{g_m n_m}{2m}} \tag{4.31}$$

The atomic branch E_a is gapped, and is characterized at small momentum by a gap Δ_a and an effective mass m_{MSF}

$$E_a \simeq \Delta_a + \frac{k^2}{2m_{\mathrm{MSF}}} \tag{4.32}$$

as $\nu \to -\infty$ we find

$$\Delta_a \simeq \frac{|\nu|}{2} + n_m \left(g_{am} - \frac{g_m}{2}\right) - \frac{4\alpha^2 n_m}{|\nu|} \tag{4.33}$$

The leading term $|\nu|/2$ corresponds to breaking a molecule and creating two atomic excitations. The second term has a simple physical interpretation: removing a molecule from the condensate lowers the energy by $n_m g_m/2$ because that molecule does not interact with the others anymore, and it increases the energy by $g_{\mathrm{am}} n_m$ as now there are two extra atoms interacting with the molecular condensate. In the same limit, the effective mass m_{MSF} of the gapped excitation is

$$m_{\mathrm{MSF}} \simeq m\left(1 - \frac{8\alpha^2 n_m}{\nu^2}\right) \tag{4.34}$$

This reduces to the atomic mass if there is no interconversion or if the binding energy is very large.

4.4.2 Spectrum in ASF phase

The spectrum in this phase has a closed form expression, but it is very complicated and will not be produced here. The qualitative features are the same as in the MSF phase: there is one gapless mode and one gapped one (see right inset of Fig.4·1). The gapless mode is again the Goldstone mode arising from breaking $U(1)$, and we can gain

some insight about the gapped one looking at the mean field energy Eq.(4.10): the Feshbach term is proportional to $\cos(2\theta_a - \theta_m)$, which gaps the out-of-phase oscillation. The excitations are not protected by parity, which is broken. Deep in the ASF phase $\nu \to \infty$, the spectrum reduces to [2]

$$E_\theta = c_{\rm ASF} k + \gamma k^3 \qquad E_\phi = \Delta_\phi + \frac{k^2}{2m_{\rm ASF}} \tag{4.35}$$

The parameters in these expressions are, in the $\nu \to \infty$ limit

$$c_{\rm ASF} = \sqrt{\frac{g_a n_a}{m}} \left(1 - \frac{\alpha^2}{\nu g_a}\right) \tag{4.36}$$

$$\gamma = \frac{1}{8mc^2} \left(1 + \frac{\alpha^2}{\nu g_a}\right) \tag{4.37}$$

$$\Delta_\phi = \nu \left(1 + \frac{(g_{am} - 2g_a)n_a}{\nu} + \frac{8 g_a n_a \alpha^2}{\nu^2 g_a}\right) \tag{4.38}$$

$$m_{\rm ASF} = 2m \left(1 - \frac{4 n_a \alpha^2}{\nu^2}\right) \tag{4.39}$$

As $\nu \to \infty$ the speed of sound c reduces to the expression for a weakly interacting BEC, while the gap and the effective mass show that in this limit the excitation is the formation of a molecule. This intuitive understanding breaks down closer to the transition, where the excitations are linear combinations (Radzihovsky et al., 2008) of all bare atomic and molecular fields $(\psi_a, \bar{\psi}_a, \psi_m, \bar{\psi}_m)$. The convexity of E_θ (since $\gamma > 0$) implies that finite k phonons can spontaneously emit lower momentum phonons. The first subleading correction to the gap has like in the MSF phase a simple interpretations: the excitation energy increases by $g_{am} n_a$ because the newly formed molecule interacts with the atoms, but decreases by $2 g_a n_a$ since two atoms that were interacting with the (atomic) condensate disappeared.

[2] the subscripts match the notation of Sec.4.5.3, where we use θ to denote the phonon and ϕ the gapped mode

4.5 Excitation Lifetimes

In Sec.4.4 we derived the mode structure of the system neglecting the interactions between excitations, which predicts infinitely long lived quasiparticles. This result is far from reality: in both ASF and MSF phases the gapless mode is damped, and the gapped mode may also decay. The field theory predicts finite lifetimes if we include the interactions beyond mean–field; there are three approaches to set up the perturbative calculation: one could diagonalize the matrix in Eq.(4.25), which makes the bare propagator diagonal, but the interaction terms become much more complicated and even the lowest order correction to the lifetime requires the evaluation of many diagrams. Alternatively, one could keep the matrix in Eq.(4.25) unchanged and work with a non–diagonal propagator, keeping the interaction simple but requiring the evaluation of off–diagonal self energies: we have to solve

$$\det(G_0^{-1}(\omega, k) - \Sigma(\omega, k)) = 0 \tag{4.40}$$

for ω, where G_0 and Σ are 4×4 dense matrices. The last approach, the one we use in this section, is to restrict the range of validity of the theory to low momenta, and write an effective theory with fewer degrees of freedom: in terms of these fields the bare propagator is diagonal, and computing the lifetime to leading order requires the evaluation of a single diagram. We use this low energy theory to compute the one-loop decay rate of the gapped modes.

4.5.1 MSF Phase

MSF Kinematics

The dispersion relations for the two modes are given in Eq.(4.27) and (4.28) (see also Fig.4·1). The speed of sound has a simple expression Eq.(4.31), while the group velocity of the atomic excitation is complicated due to the square root, but simplifies

in the large (negative) ν limit

$$v_a = \frac{\partial E_a}{\partial k} = \frac{k}{m} + \frac{8\alpha^2 n_m k}{\nu^2 m} + O\left(\frac{1}{\nu^3}\right) \tag{4.41}$$

The critical momentum k_c where the speed of sound matches the group velocity of the excitation is then

$$k_c \simeq \frac{mc\nu^2}{\nu^2 + 8\alpha^2 n_m} \quad \text{if } |\nu| \gg \left|\frac{4\alpha^2}{2g_{am} - g_m}\right| \tag{4.42}$$

This momentum scale must be compared to

$$k_m = 2\sqrt{2mg_m n_m}, \tag{4.43}$$

the momentum at which the molecular spectrum crosses over from linear to quadratic: taking the ratio

$$\frac{k_c}{k_m} \simeq \frac{1}{2}\left(1 - \frac{8\alpha^2 n_m}{\nu^2}\right) \tag{4.44}$$

shows that $k_m > 2k_c$, so that when the decay is kinematically allowed the dispersion of the molecular excitation is to a good approximation still linear, and we are justified in considering the speed of sound constant up to k_c.

Low energy MSF theory

The first step is to pick the phase for the molecular field so that the vacuum expectation value is real and positive, and reparametrize the fields as

$$\Psi_a = \phi + i\chi \quad \Psi_m = \sqrt{n_m^0 + \rho}\, e^{i\theta} \tag{4.45}$$

where $(\phi, \chi, \rho, \theta)$ are real. Assuming as usual that the fluctuations around the mean field solution are small, we drop from the action terms quartic in χ and ρ, and compute

the resulting Gaussian integrals over these two variables (Radzihovsky et al., 2008). We also drop terms quartic in ϕ, as they cannot give a contribution to the imaginary part of the one–loop self energy. After integration, low energy action is

$$S_{\text{eff}}\left[\theta,\phi\right] = S_{\text{SF}}\left[\theta\right] + S_{\text{I}}[\phi] + S_{\text{int}}\left[\theta,\phi\right] \tag{4.46}$$

where the three contributions are

$$S_{\text{SF}} = \frac{1}{2g_m}\int d\tau d\boldsymbol{r}\ \left(\left(\partial_\tau\theta\right)^2 + c_{\text{MSF}}^2\left(\nabla\theta\right)^2\right) \tag{4.47}$$

$$S_{\text{I}} = \int d\tau d\boldsymbol{r}\left[\frac{1}{2\alpha\sqrt{n_m^0}}\left(\partial_\tau\phi\right)^2 + \frac{\left(\nabla\phi\right)^2}{2m} - \mu_R\phi^2\right] \tag{4.48}$$

$$S_{\text{int}} = \frac{\mathrm{i}}{2}\int d\tau d\boldsymbol{r}\,\phi^2\partial_\tau\theta, \tag{4.49}$$

The shifted chemical potential is $\mu_R = \mu + 2\alpha\sqrt{n_m^0}$. The effective degrees of freedom are a phonon θ with linear dispersion and a Klein-Gordon particle ϕ, which matches the structure of the spectrum discussed in Sec.4.4.1 and Fig.4·1. The form of the vertex is the one we expect for the interaction between a phonon and a massive particle: at $q = 0$ there must be no interaction, as a perfectly uniform medium does not scatter. the S_{int} term couples ϕ to θ: in this effective theory the leading mechanism for sound absorption is the production of a pair of massive particles, not two phonons like in liquid Helium (Bhatt and McMillan, 1974), so that sound absorption measures the decay rate of ϕ. In the on–shell approximation, the decay rate of ϕ is

$$\gamma_{\text{MSF}}(k) = -\text{Im}\Sigma_\phi(E_a(k),k) \tag{4.50}$$

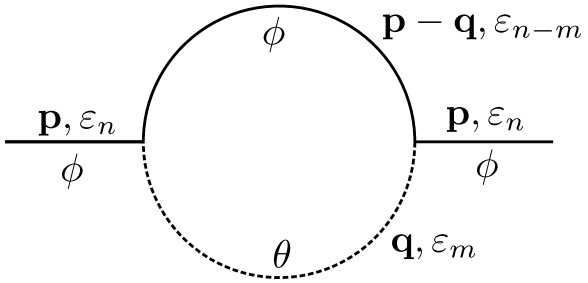

Figure 4·2: One loop diagram contributing to the imaginary part of the self energy Σ_ϕ in the MSF phase. In this diagram a solid line denotes the propagator of the massive mode ϕ, while the dashed line the propagator of the phonon θ.

and the only diagram contributing to Σ_ϕ to one–loop order is the one presented in Fig.4·2. Evaluating the diagram at zero temperature we find

$$\begin{aligned}\gamma_{\mathrm{MSF}}(k) =& \frac{g_m c_{\mathrm{MSF}}}{64\pi^2}\sqrt{\frac{\alpha\sqrt{n_m^0}}{|\mu_R|}} \\ &\times \int d\mathbf{q}\, \delta\big(E_a(k) - c_{\mathrm{MSF}} q - E_a(\mathbf{k}-\mathbf{q})\big)\end{aligned} \tag{4.51}$$

We evaluate the integral in this expression using the technique described in Sec.4.7, which finally gives

$$\gamma_{\mathrm{MSF}}(k) = \frac{m c_{\mathrm{MSF}}^2}{12\pi}\frac{(k-k_c)^3}{n_m^0}\sqrt{\frac{\alpha\sqrt{n_m^0}}{|\mu_R|}} \tag{4.52}$$

This result is compatible with the well–known k^3 dependence for the lifetime at the endpoint of a spectrum due to soft phonon emission (see (Abrikosov, 1963), Sec.(26.3)), and has a few simple experimental consequences: the decay rates are inputs to the calculation of spectral functions, which are directly observable in some experimental setups (for example, see (Valdés-Curiel et al., 2017; Petter et al., 2019; Allard et al., 2016)). Furthermore, the existence of the threshold momentum k_c in the MSF phase (see Fig.4·1, left inset) implies that it behaves as a "momentum funnel" in transmission experiments: neglecting reflection at the phase boundary, an atom propagating with

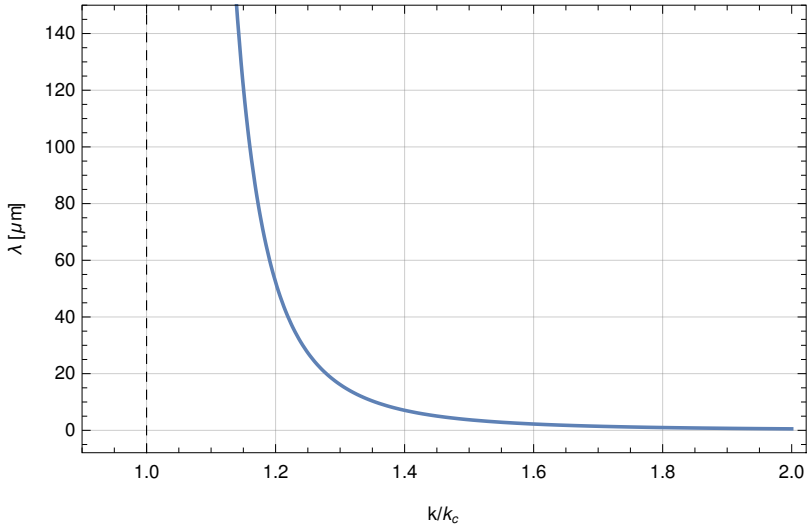

Figure 4·3: Predicted decay length λ of the gapped mode in MSF phase, as a function of momentum (in units of the critical momentum k_c) using data for the 47.97G Feshbach resonance of Cesium (Chin et al., 2010), assuming a condensate density $n_0 = 10^{14}\text{cm}^{-3}$ and a constant magnetic field $B = 47.87$G. The dashed vertical line is the asymptote at $k = k_c$, where the decay length diverges.

momentum k through a cloud of MSF bosons will not lose any energy if $k < k_c$, but emit phonons and decrease its momentum until it reaches k if initially $k > k_c$. To see this effect the cloud has to be thick compared to the absorption length λ, defined as

$$\lambda(k) = \frac{\hbar v_{\text{MSF}}(k)}{\gamma_{\text{MSF}}(k)} \tag{4.53}$$

where $v_{\text{MSF}} = \partial_k E_a(k)$ is the group velocity of the gapped excitation: if the atom cloud is thinner than $\lambda(k)$ the atom leaves the cloud before emitting phonons. To get an idea of the typical size of λ see Fig.4·3, where give an example using data for one of the Feshbach resonances in cesium. Notice that λ is sensitive to the condensate density n_m^0 –a higher density makes the cloud more opaque– and the background magnetic field, through the shifted chemical potential μ_R (see Eq.(4.52)). We also have to keep into account the trapping time: the cloud must remain trapped while the projectile traverses it. In particular, to see the sharp feature corresponding to k_c,

the cloud must survive for a time

$$\Delta t \geq \frac{L}{c} \tag{4.54}$$

where L is the diameter of the sample. Using the same parameters as in Fig.4·3 for the speed of sound and assuming $L \simeq 20\mu$m we must have $\Delta t \geq 5$ms, which is compatible with the current experimental possibilities (Zhang et al., 2021a).

4.5.2 Lifetime of the gapless mode

For completeness we report the analogous result for the decay of one phonon into two phonons. When the binding energy is very large the phonon decay rate is the same as in the single component condensate, and it was first derived by Beliaev (Beliaev, 1958) at zero temperature. The decay rate does not have an elementary expression. In the small and large momentum limits it reduces to

$$\gamma_{T=0}(\mathbf{k}) = \begin{cases} \dfrac{3k^5}{640\pi(2m)n_m^0} & k \ll k_c \\ \dfrac{4\pi a^2 n_m^0 k}{2m} & k \gg k_c \end{cases} \tag{4.55}$$

where a is the s–wave scattering length. We expect this same behavior for the phonon in both phases, as long as $ck \ll \Delta$, where c is the speed of sound in the phase and Δ the gap. For a discussion of the damping properties of the gapless mode in the critical regime see (Lee and Lee, 2004).

4.5.3 ASF phase

ASF kinematics

In the ASF phase the phonons can spontaneously emit other phonons, and so can the gapped mode: there is no symmetry protecting the decay. At large momentum there are two processes available for the decay of a gapped excitation: pair production of two

massive particles, and phonon emission. We focus on the long wavelength physics, and only discuss phonon emission. Deep in the ASF phase at $k = 0$ a gapped excitation emits two back–to–back phonons with momentum k_0, fixed by energy conservation

$$\begin{aligned} \Delta_\phi &= 2c_{\rm ASF}k_0 \\ &\to k_0 \simeq \frac{\nu}{2c_{\rm ASF}} + \frac{\alpha^2 + g_a n_a \left(g_{\rm am} - 2g_a\right)}{2c_{\rm ASF}g_a} \end{aligned} \tag{4.56}$$

and at finite k the emission of two back–to–back phonons is allowed if

$$\begin{aligned} \Delta_\phi + \frac{k^2}{2m_{\rm ASF}} &= c_{\rm ASF}q + c_{\rm ASF}|\boldsymbol{k} - \boldsymbol{q}| \\ &= c_{\rm ASF}(k + 2q) \end{aligned} \tag{4.57}$$

assuming $\boldsymbol{q} = -q\hat{\boldsymbol{k}}$ where $\hat{\boldsymbol{k}}$ is the unit vector in the direction of $\boldsymbol{k}$. Requiring $q > 0$ we get

$$k^2 - 2m_{\rm ASF}c_{\rm ASF}k + 2m_{\rm ASF}\Delta_\phi > 0 \tag{4.58}$$

which is true as long as $m_{\rm ASF}c_{\rm ASF}^2 < 2\Delta_\phi$. Working at leading order in ν and using Eqs.(4.36)-(4.39) this condition reduces to

$$g_a n_a < 2\nu \tag{4.59}$$

and holds if the density is low enough.

Low energy ASF theory

In the ASF phase both the molecules and the atoms are condensed. The Feshbach terms locks the phases of the atomic and molecular order parameters, so it is convenient to redefine the atomic fields as

$$\Psi_a \to e^{i\theta_m/2}\Psi_a \tag{4.60}$$

where θ_m is the phase of the molecular field:

$$\Psi_m = \sqrt{n_m^0 + \rho_m} e^{i\theta_m} \tag{4.61}$$

We choose the phase of the molecular field so that in equilibrium $\theta_m = 0$. Then for small fluctuations around the ASF equilibrium condition

$$\Psi_a = \sqrt{n_a^0} + \psi_a \tag{4.62}$$

and we expand to second order in ψ_a. The terms linear in ψ_a drop out. We further decompose the atomic fluctuations in their real and imaginary parts:

$$\psi_a = \phi + i\chi \tag{4.63}$$

As pointed out in (Radzihovsky et al., 2008), the fluctuations in the ϕ direction reach criticality before the ones in χ, so we drop terms of third and higher in χ and perform the resulting χ Gaussian integral. Deep in the ASF phase the ϕ fluctuations are also small, and integrating over ϕ first will give the same results. After integration the action is

$$S = \int d\tau d\boldsymbol{r} \left[\frac{(\partial_\tau \theta)^2}{2g_m} + \frac{n_m^0}{4m}(\nabla\theta)^2 + i\sqrt{n_a^0}(1-y)\phi\partial_\tau\theta + \frac{(\partial_\tau\phi)^2}{2\alpha\sqrt{n_m^0}} + \phi\left(-\frac{\nabla^2}{2m} - \tilde{\mu}\right)\phi \right.$$
$$\left. + \left(2g_a - \frac{g_m}{2}y^2\right)\sqrt{n_a^0}\phi^3 + \frac{i}{2}(1-y)\phi^2\partial_\tau\theta - y\sqrt{n_a^0}\phi\frac{(\nabla\theta)^2}{4m} \right] \tag{4.64}$$

Where we have relabeled $\theta_m \to \theta$, and we have dropped terms that cannot produce one loop diagrams. We have also defined

$$y = \frac{2}{g_m}\left(g_{am} - \frac{\alpha}{\sqrt{n_m^0}}\right) \tag{4.65}$$

$$\tilde{\mu} = \mu - 3g_a n_a^0 + g_{am} n_m^0 - 2\alpha\sqrt{n_m^0} - \frac{g_m}{2}y^2 n_a^0 \tag{4.66}$$

The low energy description of the ASF phase is an interacting theory of a phonon θ and a gapped Klein-Gordon field ϕ. Unlike in the MSF phase, the decay of one gapped excitation into two phonons is allowed here, and is in fact the only allowed process at low enough momentum. Furthermore, at very small momentum the there is no phase space for the process $\phi \to \phi + \theta$, and energy conservation forbids $\phi \to \phi + \phi$, so we only keep the $\phi(\nabla\theta)^2$ vertex. The term $i\sqrt{n_a^0}\phi\partial_\tau\theta$ mixes the two fields, but it does not gap the phonon and is safe to neglect in a first approximation, as its main effect is to give a correction to the gap and the speed of sound. This approximation simplifies the calculation of the decay rate of the gapped mode: in the on–shell approximation

$$\gamma_{\rm ASF}(k) = -{\rm Im}\Sigma_\phi(E_\phi(k), k) \tag{4.67}$$

We compute the self energy Σ_ϕ to one loop, evaluating the diagram in Fig.4·4 at zero temperature. The decay rate of the gapped excitation is then

$$\gamma_{\rm ASF}(k) = \frac{Z_\theta^2\lambda^2}{32\pi c_{\rm ASF}^2}\int d\mathbf{q}\,\frac{(\mathbf{q}\cdot(\mathbf{k}-\mathbf{q}))^2}{q|\mathbf{k}-\mathbf{q}|}\delta\big(E_\phi(k) - c_{\rm ASF}q - c_{\rm ASF}|\mathbf{k}-\mathbf{q}|\big) \tag{4.68}$$

where we have defined the parameters

$$Z_\theta \simeq g_m + \frac{\alpha n_a^0}{4(n_m^0)^{3/2}} \qquad \lambda \simeq \frac{y\sqrt{n_a^0}}{2m} \tag{4.69}$$

We evaluate the integral using the method described in the Appendix, which finally gives

$$\gamma_{\rm ASF}(k) = \frac{Z_\theta^2\lambda^2}{32\pi c_{\rm ASF}^2}\left(\frac{E_\phi(k)^4}{16c_{\rm ASF}^5} - \frac{E_\phi(k)^2k^2}{c_{\rm ASF}^3} + o(k^2)\right) \tag{4.70}$$

The parametric dependence of $\gamma_{\rm ASF}$ is intuitively clear: when the gap is larger there is more phase space available, which leads to faster decay, while for larger speed of sound there is less phase space and the decay slows down. The dependence on E_ϕ^4

is the same reported in (Bhatt and McMillan, 1974), but in that work the particle disintegrating is itself a phonon, not a gapped excitation. This result implies that the gapped mode is strongly damped, and will be hard to see in experiment.

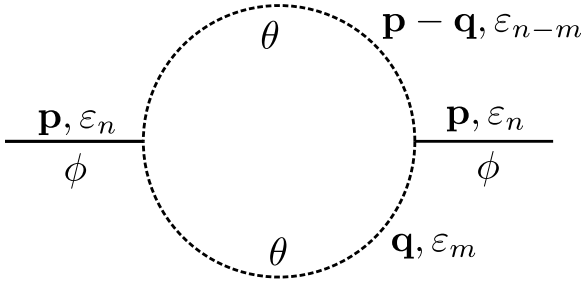

Figure 4·4: One loop diagram contributing to the imaginary part of the self energy in the ASF phase. In this diagram a solid line denotes the propagator of the massive mode ϕ, while the dashed line the propagator of the phonon θ.

4.5.4 Effective theory range of validity

For our approximation to hold, we require the fluctuations of the ϕ_I field, which we integrated out, to remain stable while the ϕ_R field undergoes spontaneous symmetry breaking. Using the mean field value of the chemical potential

$$\mu = g_a n_a^0 + g_{am} n_m^0 - 2\alpha\sqrt{n_m^0} \tag{4.71}$$

the validity condition for the ASF low energy theory is

$$\left(g_{am} - \frac{\alpha}{\sqrt{n_m^0}}\right)^2 > g_a g_m \tag{4.72}$$

which is verified if n_m^0 is small enough.

4.6 Conclusions and Outlook

In this chapter we studied the damping of excitation modes in the ASF and MSF phases of a single-component ultracold atomic gas. In both phases, away from the

critical regime, the phonon damps according to the Beliaev theory (Beliaev, 1958), as expected of a single-component Goldstone mode in a non-relativistic theory. In the ASF phase the gapped mode has a finite lifetime even in the zero momentum limit, while in the MSF phase we find a Cherenkov threshold: below the critical momentum k_c there is no damping, while for $k > k_c$ the dissipation rate is proportional to $(k - k_c)^3$. We discussed how this property of the MSF phase should be observable in experiments in which an atom is transmitted through an MSF cloud: the cloud acts as a momentum funnel, suppressing the transmission amplitude at momenta larger than the threshold and shifting the distribution of transmitted atoms to lower energy.

Such transmission spectroscopy experiments promise to provide great insight into the properties of the MSF and other more exotic ultracold phases. Our work serves as a building block to constructing a complete dissipative transport theory for such near–equilibrium dynamics in the MSF and ASF phases. It would be interesting to understand how our results are modified as the system approaches the critical regime, where the assumption of small fluctuations around the mean-field breaks down. Another promising research direction is the study of heteronuclear condensates (Lam et al., 2022; Thalhammer et al., 2009; Warner et al., 2021; Gröbner et al., 2016), for which strictly speaking our theory does not apply –already at mean field level the phase diagram changes. Nonetheless, kinematic arguments still suggest the existence of a Cherenkov threshold, and a damping structure qualitatively similar to the homonuclear case.

4.7 Off–shell Cherenkov

In this section we catalog some useful tricks for the kind of integration that shows up when dealing with one loop calculations. Consider a massive particle ϕ emitting a

phonon γ:

$$E_\phi(p) = \Delta + \frac{p^2}{2m} \qquad E_\gamma(p) = cp \tag{4.73}$$

We compute the phase space for this process: the process of a particle with momentum p and energy ϵ spontaneously emitting a phonon has phase space

$$g(p,\epsilon) = \int \frac{d\mathbf{q}\, d\omega}{(2\pi)^4}\, \delta(\omega - cq)\delta\left(\epsilon - \omega - \frac{(\mathbf{p}-\mathbf{q})^2}{2m}\right) \tag{4.74}$$

where we allow ϵ to take any value: we include processes where the emitted ϕ is virtual, as is the case in one loop perturbation theory. When evaluating a diagram of the kind discussed in Sec.4.5 the only difference is some extra factor of q in the integrand, the nontrivial part is dealing with the energy–conserving Dirac delta .To evaluate this integral it is convenient to measure the energy ϵ with respect to the threshold energy ϵ_{th}, defined as the lowest energy where the decay is allowed, starting with a particle with momentum p and energy $\epsilon = E_\phi(p)$: the threshold energy is then the minimum as a function of q and Ω of

$$E = \Delta + \frac{p^2 + q^2 - 2pq\Omega}{2m} + cq \tag{4.75}$$

on the minimization domain $q \in [0,\infty), \Omega \in [-1,1]$. The derivatives of E are

$$\frac{\partial E}{\partial \Omega} = -\frac{pq}{m} < 0 \qquad \frac{\partial E}{\partial q} = \frac{q - p\Omega + mc}{m} \tag{4.76}$$

The derivative of E with respect to Ω is always negative, the function assumes its minimum on the upper edge of the domain: the optimal value is $\Omega^* = 1$ (at threshold the phonon is emitted forward). For the other equation we have to discuss two cases separately:

- If $p < mc$ then we always have $\partial_q E > 0$, thus the optimal q and threshold energy

are

$$q^* = 0 \qquad \epsilon_{\rm th} = \Delta + \frac{p^2}{2m} \tag{4.77}$$

which is consistent with the discussion above: when $p < mc$ the on shell process cannot happen (it is only allowed to emit a zero momentum phonon, but there is no such thing). Later we study the off-shell case, which is less trivial.

- If $p < mc$ the minimum is at nontrivial q, and gives

$$q^* = p - mc \qquad \epsilon_{\rm th} = \Delta + pc - \frac{mc^2}{2} \tag{4.78}$$

In the next section we will derive the phase space in these two cases. The space space is 0 when $\epsilon < \epsilon_{\rm th}$ so the formulae we derive should be understood as holding only for $\epsilon > \epsilon_{\rm th}$.

4.7.1 Phase space for $p < mc$

The integral over ω is trivial:

$$g(p,\epsilon) = \int \frac{d\mathbf{q}}{(2\pi)^4}\delta\left(\epsilon - cq - \frac{p^2}{2m} - \frac{q^2}{2m} + \frac{pq\Omega}{m} - \Delta\right) \tag{4.79}$$

use the threshold energy to eliminate Δ and define $\Delta\epsilon = \epsilon - \epsilon_{\rm th}$:

$$g(p,\epsilon) = \int \frac{d\mathbf{q}}{(2\pi)^4}\delta\left(\Delta\epsilon - cq - \frac{q^2}{2m} + \frac{pq\Omega}{m}\right) \tag{4.80}$$

at this point we have two options: integrate over Ω or integrate over q. They are equivalent of course, but it is useful to show the details to understand how the two approaches differ.

Let's integrate over Ω first. The support and Jacobian factor of the Dirac delta are

$$\Omega_0 = \frac{m}{pq}\left(\frac{q^2}{2m} + cq - \Delta\epsilon\right) \qquad \frac{1}{|f'(\Omega_0)|} = \frac{m}{pq} \tag{4.81}$$

where $f(\Omega)$ is the argument of the Dirac delta in the integrand. After integrating over Ω we get

$$g(p,\epsilon) = \int \frac{dq}{(2\pi)^3} q^2 \frac{m}{pq}\left[-1 < \frac{m}{pq}\left(\frac{q^2}{2m} + cq - \Delta\epsilon\right) < 1\right] \tag{4.82}$$

where the square brackets represent the Heaviside theta ([condition] evaluates to 1 when the condition is true and 0 otherwise). The restriction on the q domain is equivalent to

$$\begin{gathered}\left[-1 < \frac{m}{pq}\left(\frac{q^2}{2m} + cq - \Delta\epsilon\right) < 1\right] = \\ \left[\frac{q^2}{2m} + cq - \Delta\epsilon > -\frac{pq}{m}\right]\left[\frac{q^2}{2m} + cq - \Delta\epsilon < \frac{pq}{m}\right]\end{gathered} \tag{4.83}$$

The first condition is equivalent to

$$q > -p - mc + \sqrt{(p+mc)^2 + 2m\Delta\epsilon} \tag{4.84}$$

(notice the right hand side is always positive), and the second to

$$\begin{aligned} q &> p - mc - \sqrt{(p-mc)^2 + 2m\Delta\epsilon} \\ \text{and } q &< p - mc + \sqrt{(p-mc)^2 + 2m\Delta\epsilon}\end{aligned} \tag{4.85}$$

The quantity in the right hand side of the first line is negative, so that condition is automatically verified by $q > 0$. The second condition is complicated, but if we are

only interested in the small $\Delta\epsilon$ limit we expand to first order the square root, and find

$$\begin{aligned}\left[-1<\frac{m}{pq}\left(\frac{q^2}{2m}+cq-\Delta\epsilon\right)<1\right]=\\ \left[\frac{m\Delta\epsilon}{mc+p}<q<\frac{m\Delta\epsilon}{mc-p}\right]\end{aligned} \tag{4.86}$$

so that finally the integral gives

$$\begin{aligned}g(p,\epsilon)&=\frac{m}{2p}\frac{(m\Delta\epsilon)^2}{(2\pi)^3}\left(\frac{1}{(mc-p)^2}-\frac{1}{(mc+p)^2}\right)\\&=\frac{m^4c}{4\pi^3}\frac{(\Delta\epsilon)^2}{((mc)^2-p^2)^2}\end{aligned} \tag{4.87}$$

If we start by integrating over q instead, the support and Jacobian factor of the Dirac delta are

$$q_0=p\Omega-mc+\sqrt{(p\Omega-mc)^2+2m\Delta\epsilon} \tag{4.88}$$

$$\frac{1}{|f'(q_0)|}=\frac{m}{\sqrt{(p\Omega-mc)^2+2m\Delta\epsilon}} \tag{4.89}$$

so after the integration over q we have

$$g(p,\epsilon)=\frac{1}{(2\pi)^3}\int_{-1}^{1}d\Omega\,\frac{mq_0^2}{\sqrt{(p\Omega-mc)^2+2m\Delta\epsilon}} \tag{4.90}$$

The advantage with respect to the previous approach is that there is no condition restricting the integration domain, but the integrand is more complicated. It's convenient to change variable to $x=mc-p\Omega$ (notice that $x>0$) which turns the integral into

$$g(p,\epsilon)=\frac{m}{(2\pi)^3p}\int_{mc-p}^{mc+p}dx\,\frac{(-x+\sqrt{x^2+2m\Delta\epsilon})^2}{\sqrt{x^2+2m\Delta\epsilon}} \tag{4.91}$$

expanding in small $\Delta\epsilon$ again, this integral is approximately

$$\begin{aligned} g(p,\epsilon) &= \frac{m}{(2\pi)^3 p}\int_{mc-p}^{mc+p} dx\, x\left(\frac{m\Delta\epsilon}{x^2}\right)^2 \\ &= \frac{m^3(\Delta\epsilon)^2}{2(2\pi)^3 p}\left(\frac{1}{(mc-p)^2}-\frac{1}{(mc+p)^2}\right) \\ &= \frac{m^4 c}{4\pi^3}\frac{(\Delta\epsilon)^2}{((mc)^2-p^2)^2} \end{aligned} \tag{4.92}$$

as expected from the previous section.

In conclusion, the trade-off we make integrating over q first is that the result integral is harder, but we don't have to think as hard about inequalities that restrict the domain: the $\delta(q-q_0)$ is guaranteed to have the support in the integration interval $[0,\infty)$ as long as we use the positive root q_0.

4.7.2 Phase space for $p > mc$

The starting point is the same as in the previous section

$$g(p,\epsilon) = \int \frac{d\mathbf{q}}{(2\pi)^4}\delta\left(\epsilon - cq - \frac{p^2}{2m} - \frac{q^2}{2m} + \frac{pq\Omega}{m} - \Delta\right) \tag{4.93}$$

but the momentum of the phonon at threshold q^* and the threshold energy are different: (we still have $\Omega^* = 1$)

$$q^* = p - mc \qquad \epsilon_{\text{th}} = \Delta + pc - \frac{mc^2}{2} \tag{4.94}$$

Eliminating Δ using ϵ_{th} we get (as usual $\Delta\epsilon \equiv \epsilon - \epsilon_{\text{th}}$)

$$\begin{aligned} g(p,\epsilon) = \int \frac{d\mathbf{q}}{(2\pi)^4}\delta\Bigg(&\Delta\epsilon - c(q-q^*) \\ &- \frac{(\mathbf{p}-\mathbf{q})^2}{2m} + \frac{(\mathbf{p}-\mathbf{q}^*)^2}{2m}\Bigg) \end{aligned} \tag{4.95}$$

where $\mathbf{q}^*$ is a vector in the same direction as $\mathbf{p}$ of length q^*. The argument of the Dirac delta simplifies a little defining $\delta q \equiv q - q^*$:

$$\begin{aligned} g(p,\epsilon) &= \int \frac{d\mathbf{q}}{(2\pi)^4}\delta\bigg(\Delta\epsilon - c\delta q - \frac{\delta q^2}{2m} \\ &\qquad + \frac{p}{m}(\Omega-1)(\delta q + q^*) + c\delta q\bigg) \\ &= \int \frac{d\mathbf{q}}{(2\pi)^4}\delta\bigg(\Delta\epsilon - \frac{(q-q^*)^2}{2m} + \frac{pq}{m}(\Omega-1)\bigg) \end{aligned} \tag{4.96}$$

Notice that the term quadratic in q is $(q-q^*)^2$, which is *not* a vector difference, it's the difference of two real positive numbers. Again we have two possibilities, integrating over Ω or q first.

Integrating over Ω first, the support and Jacobian factor of the Dirac delta are

$$\Omega_0 = 1 + \frac{m}{pq}\left(\frac{(q-q^*)^2}{2m} - \Delta\epsilon\right) \qquad \frac{1}{|f'(\Omega_0)|} = \frac{m}{pq} \tag{4.97}$$

so integrating over Ω we get

$$g(p,\epsilon) = \int_0^\infty \frac{dq}{(2\pi)^3} q^2 \frac{m}{pq}\big[-1 < \Omega_0 < 1\big] \tag{4.98}$$

The condition restricting the integration domain is equivalent to

$$\begin{aligned} \big[-1 < \Omega_0 < 1\big] &= \bigg[-\frac{2pq}{m} < \frac{(q-q^*)^2}{2m} - \Delta\epsilon\bigg] \\ &\qquad \times \bigg[\frac{(q-q^*)^2}{2m} < \Delta\epsilon\bigg] \end{aligned} \tag{4.99}$$

If $\Delta\epsilon$ is small enough, the first condition is always satisfied, so we only have to consider the second inequality

$$\begin{aligned} [(q-q^*)^2 < 2m\Delta\epsilon] &= \Big[q > q^* - \sqrt{2m\Delta\epsilon}\Big] \\ &\qquad \times \Big[q < q^* + \sqrt{2m\Delta\epsilon}\Big] \end{aligned} \tag{4.100}$$

Notice that $q^* - \sqrt{2m\Delta\epsilon}$ is a strictly positive number for $\Delta\epsilon$ small enough, so the first condition on the right hand side restricts the integration domain more than just asking $q > 0$. The integral is then

$$\begin{aligned} g(p,\epsilon) =& \frac{m}{p(2\pi)^3} \int_{q^*-\sqrt{2m\Delta\epsilon}}^{q^*+\sqrt{2m\Delta\epsilon}} dq\, q \\ =& \frac{m}{2p(2\pi)^3}\left(\left(q^* + \sqrt{2m\Delta\epsilon}\right)^2 - \left(q^* - \sqrt{2m\Delta\epsilon}\right)^2\right) \\ =& \frac{m(p-mc)}{p(2\pi)^3}\sqrt{2m\Delta\epsilon} \end{aligned} \tag{4.101}$$

Integrating over q first, the Dirac delta support and Jacobian are

$$\begin{aligned} q_0^{\pm} =& q^* + p(\Omega - 1) \\ & \pm \sqrt{(q^* + p(\Omega-1))^2 - (q^*)^2 + 2m\Delta\epsilon} \end{aligned} \tag{4.102}$$

$$\frac{1}{|f'(q_0^{\pm})|} = \frac{m}{\sqrt{(q^* + p(\Omega-1))^2 - (q^*)^2 + 2m\Delta\epsilon}} \tag{4.103}$$

using $q^* = p - mc$ and plugging in the phase space integral we have

$$g(p,\epsilon) = m\int_{-1}^{1} \frac{d\Omega}{(2\pi)^3} \frac{(q_0^+[q_0^+ > 0])^2 + (q_0^-[q_0^- > 0])^2}{\sqrt{(mc + p\Omega)^2 - (p-mc)^2 + 2m\Delta\epsilon}} \tag{4.104}$$

and we should also require that the argument in the square root appearing in $q_0^{\pm}$ is positive, which is a condition on Ω. Dealing with these inequalities is complicated, in this case integrating over Ω first is the the best approach.

Chapter 5

Conclusions and Outlook

At the end of this exploration in quantum dynamics, it is clear we left behind countless loose ends. We neglected the role of locality in chapter 2, which is necessary to make the connection to (generalized) hydrodynamics and describe realistic systems. We hope that our treatment will be the starting point of future exploration in this direction.

Our discussion of the amplitude mode in chapter 3 is limited to the simplest BCS case, but commonly used superconductors are much more complex beasts. Much of the knowledge necessary to treat these important problems has been forgotten or is written in a language that is unfamiliar to modern practitioners; we are happy to be part of this process of rediscovery.

In chapter 4 we studied damping in a molecular superfluid of Cesium. The association of these binary molecules is the simplest case of a controlled chemical reaction between ultracold atoms. The natural extension is to different atomic species and more complex molecular structures. Our results are just the first step towards understanding the stability of these rich and interesting systems.

In all three cases we made predictions in highly active areas of research, and we look forward to the experiments that will test them.

References

Abrahams, E. and Tsuneto, T. (1966). Time variation of the ginzburg-landau order parameter. *Physical Review*, 152(1):416.

Abrikosov, A. (1963). *Methods of Quantum Field Theory in Statistical Physics*. Dover Books.

Abrikosov, A. A. (2017). *Fundamentals of the Theory of Metals*. Courier Dover Publications.

Abrikosov, A. A., Gorkov, L. P., and Dzyaloshinski, I. E. (2012). *Methods of quantum field theory in statistical physics*. Courier Corporation.

Allard, B., Fadel, M., Schmied, R., and Treutlein, P. (2016). Sideband Rabi spectroscopy of finite-temperature trapped Bose gases. *Physical Review A*, 93(4):043624.

Andersen, J. (2004). Theory of the weakly interacting Bose gas. *Reviews of Modern Physics*, 76(2):599–639.

Anderson, P. W. (1958a). Absence of diffusion in certain random lattices. *Phys. Rev.*, 109:1492–1505.

Anderson, P. W. (1958b). Random-phase approximation in the theory of superconductivity. *Physical Review*, 112(6):1900.

Aronov, A., Gal'Perin, Y. M., Gurevich, V., and Kozub, V. (1981). The boltzmann-equation description of transport in superconductors. *Advances in Physics*, 30(4):539–592.

Bagrets, D., Altland, A., and Kamenev, A. (2016). Sachdev–ye–kitaev model as liouville quantum mechanics. *Nuclear Physics B*, 911:191 – 205.

Bardeen, J., Cooper, L. N., and Schrieffer, J. R. (1957). Theory of superconductivity. *Physical review*, 108(5):1175.

Basko, D., Aleiner, I., and Altshuler, B. (2006). Metal–insulator transition in a weakly interacting many-electron system with localized single-particle states. *Annals of Physics*, 321(5):1126 – 1205.

Beck, M., Klammer, M., Lang, S., Leiderer, P., Kabanov, V. V., Goltsman, G. N., and Demsar, J. (2011). Energy-gap dynamics of superconducting nbn thin films studied by time-resolved terahertz spectroscopy. *Physical Review Letters*, 107(17):177007.

Beck, M., Rousseau, I., Klammer, M., Leiderer, P., Mittendorff, M., Winnerl, S., Helm, M., Gol'tsman, G. N., and Demsar, J. (2013). Transient increase of the energy gap of superconducting nbn thin films excited by resonant narrow-band terahertz pulses. *Physical Review Letters*, 110(26):267003.

Beliaev, S. T. (1958). Energy spectrum of a non-ideal Bose gas. *Sov. Phys. JETP*, 7(2):299–307.

Bellitti, M., Laumann, C. R., and Spivak, B. Z. (2022). Incoherent excitation of coherent higgs oscillations in superconductors. *Physical Review B*, 105(10):104513.

Bellitti, M., Morampudi, S., and Laumann, C. R. (2019). Hamiltonian Dynamics of a Sum of Interacting Random Matrices. *Physical Review B*, 100(18):184201.

Bernien, H., Schwartz, S., Keesling, A., Levine, H., Omran, A., Pichler, H., Choi, S., Zibrov, A. S., Endres, M., Greiner, M., Vuletić, V., and Lukin, M. D. (2017). Probing many-body dynamics on a 51-atom quantum simulator. *Nature*, 551:579 EP –.

Berninger, M., Zenesini, A., Huang, B., Harm, W., Nägerl, H.-C., Ferlaino, F., Grimm, R., Julienne, P. S., and Hutson, J. M. (2013). Feshbach resonances, weakly bound molecular states, and coupled-channel potentials for cesium at high magnetic fields. *Physical Review A*, 87(3):032517.

Bhatt, R. N. and McMillan, W. L. (1974). Theory of anomalous dispersion in liquid He 4. *Physical Review A*, 10(5):1591.

Brézin, E., Itzykson, C., Parisi, G., and Zuber, J.-B. (1993). Planar diagrams. In *The Large N Expansion In Quantum Field Theory And Statistical Physics: From Spin Systems to 2-Dimensional Gravity*, pages 567–583. World Scientific.

Brézin, E. and Zee, A. (1994). Correlation functions in disordered systems. *Physical Review E*, 49(4):2588–2596.

Bruzda, W., Smaczyński, M., Cappellini, V., Sommers, H.-J., and Życzkowski, K. (2010). Universality of spectra for interacting quantum chaotic systems. *Phys. Rev. E*, 81:066209.

Cea, T. and Benfatto, L. (2014). Nature and raman signatures of the higgs amplitude mode in the coexisting superconducting and charge-density-wave state. *Physical Review B*, 90(22):224515.

Chan, A., De Luca, A., and Chalker, J. T. (2018). Solution of a minimal model for many-body quantum chaos. *Phys. Rev. X*, 8:041019.

Chandran, A. and Laumann, C. R. (2015). Semiclassical limit for the many-body localization transition. *Phys. Rev. B*, 92:024301.

Chang, J.-J. and Scalapino, D. (1978). Nonequilibrium superconductivity. *Journal of Low Temperature Physics*, 31(1):1–32.

Chin, C., Grimm, R., Julienne, P., and Tiesinga, E. (2010). Feshbach Resonances in Ultracold Gases. *Reviews of Modern Physics*, 82(2):1225–1286.

Chin, C., Kerman, A. J., Vuletić, V., and Chu, S. (2003). Sensitive Detection of Cold Cesium Molecules Formed on Feshbach Resonances. *Physical Review Letters*, 90(3):033201.

Choi, S., Turner, C. J., Pichler, H., Ho, W. W., Michailidis, A. A., Papić, Z., Serbyn, M., Lukin, M. D., and Abanin, D. A. (2019). Emergent su(2) dynamics and perfect quantum many-body scars. *Phys. Rev. Lett.*, 122:220603.

Cotler, J. S., Gur-Ari, G., Hanada, M., Polchinski, J., Saad, P., Shenker, S. H., Stanford, D., Streicher, A., and Tezuka, M. (2017). Black holes and random matrices. *Journal of High Energy Physics*, 2017(5).

Duine, R. A. and Stoof, H. T. C. (2004). Atom–molecule coherence in Bose gases. *Physics Reports*, 396(3):115–195.

Giannetti, C., Capone, M., Fausti, D., Fabrizio, M., Parmigiani, F., and Mihailovic, D. (2016). Ultrafast optical spectroscopy of strongly correlated materials and high-temperature superconductors: a non-equilibrium approach. *Advances in Physics*, 65(2):58–238.

Gornyi, I. V., Mirlin, A. D., and Polyakov, D. G. (2005). Interacting electrons in disordered wires: Anderson localization and low-t transport. *Phys. Rev. Lett.*, 95:206603.

Gröbner, M., Weinmann, P., Meinert, F., Lauber, K., Kirilov, E., and Nägerl, H.-C. (2016). A new quantum gas apparatus for ultracold mixtures of K and Cs and KCs ground-state molecules. *Journal of Modern Optics*, 63(18):1829–1839.

Huse, D. A., Nandkishore, R., and Oganesyan, V. (2014). Phenomenology of fully many-body-localized systems. *Phys. Rev. B*, 90:174202.

Katsumi, K., Tsuji, N., Hamada, Y. I., Matsunaga, R., Schneeloch, J., Zhong, R. D., Gu, G. D., Aoki, H., Gallais, Y., and Shimano, R. (2018). Higgs mode in the d-wave superconductor bi 2 sr 2 cacu 2 o 8+ x driven by an intense terahertz pulse. *Physical review letters*, 120(11):117001.

Keldysh, L. V. (1965). Diagram technique for nonequilibrium processes. *Sov. Phys. JETP*, 20(4):1018–1026.

Kemper, A. F., Sentef, M. A., Moritz, B., Freericks, J. K., and Devereaux, T. P. (2015). Direct observation of higgs mode oscillations in the pump-probe photoemission spectra of electron-phonon mediated superconductors. *Physical Review B*, 92(22):224517.

Khemani, V. and Nandkishore, R. (2019). Local constraints can globally shatter hilbert space: a new route to quantum information protection.

Khemani, V., Vishwanath, A., and Huse, D. A. (2018). Operator spreading and the emergence of dissipative hydrodynamics under unitary evolution with conservation laws. *Phys. Rev. X*, 8:031057.

Kitaev, A. (2015). Hidden correlations in the Hawking radiation and thermal noise. *Talk at KITP*.

Kitaev, A. and Suh, S. J. (2018). The soft mode in the Sachdev-Ye-Kitaev model and its gravity dual. *Journal of High Energy Physics*, 2018(5):183.

Köhler, T., Góral, K., and Julienne, P. S. (2006). Production of cold molecules via magnetically tunable Feshbach resonances. *Reviews of Modern Physics*, 78(4):1311–1361.

Kowalewska-Kudłaszyk, A., Kalaga, J., and Leoński, W. (2009). Long-time fidelity and chaos for a kicked nonlinear oscillator system. *Physics Letters A*, 373(15):1334–1340.

Kowalewska-Kudłaszyk, A., Kalaga, J. K., and Leoński, W. (2008). Wigner-function nonclassicality as indicator of quantum chaos. *Phys. Rev. E*, 78:066219.

Kozorezov, A., Volkov, A., Wigmore, J., Peacock, A., Poelaert, A., and Den Hartog, R. (2000). Quasiparticle-phonon downconversion in nonequilibrium superconductors. *Physical Review B*, 61(17):11807.

Lam, A. Z., Bigagli, N., Warner, C., Yuan, W., Zhang, S., Tiemann, E., Stevenson, I., and Will, S. (2022). High phase-space density gas of NaCs Feshbach molecules. *Physical Review Research*, 4(2):L022019.

Lee, Y.-W. and Lee, Y.-L. (2004). Quantum phase transition in an atomic Bose gas near a Feshbach resonance. *Physical Review B*, 70(22):224506.

Lifshitz, E. M. and Pitaevskii, L. P. (1981). *Physical kinetics*. Butterworth Heinemann.

Lighthill, M. J. (1958a). *An Introduction to Fourier Analysis and Generalised Functions*. Cambridge University Press.

Lighthill, M. J. (1958b). *An introduction to Fourier analysis and generalised functions*. Cambridge University Press.

Lin, C.-J. and Motrunich, O. I. (2019). Exact quantum many-body scar states in the rydberg-blockaded atom chain. *Phys. Rev. Lett.*, 122:173401.

Littlewood, P. and Varma, C. (1981). Gauge-invariant theory of the dynamical interaction of charge density waves and superconductivity. *Physical Review Letters*, 47(11):811.

Littlewood, P. and Varma, C. (1982). Amplitude collective modes in superconductors and their coupling to charge-density waves. *Physical Review B*, 26(9):4883.

Mahan, G. D. (2013). *Many-particle physics*. Springer Science & Business Media.

Maldacena, J., Shenker, S. H., and Stanford, D. (2016). A bound on chaos. *Journal of High Energy Physics*, 2016(8):106.

Maldacena, J. and Stanford, D. (2016). Remarks on the sachdev-ye-kitaev model. *Phys. Rev. D*, 94:106002.

Malla, R. K., Chernyak, V. Y., Sun, C., and Sinitsyn, N. A. (2022). Coherent reaction between molecular and atomic Bose-Einstein condensates: Integrable model. *arXiv:2112.12302 [cond-mat, physics:physics, physics:quant-ph]*.

Mark, M., Ferlaino, F., Knoop, S., Danzl, J. G., Kraemer, T., Chin, C., Nägerl, H.-C., and Grimm, R. (2007). Spectroscopy of ultracold trapped cesium Feshbach molecules. *Physical Review A*, 76(4):042514.

Matsunaga, R., Hamada, Y. I., Makise, K., Uzawa, Y., Terai, H., Wang, Z., and Shimano, R. (2013). Higgs amplitude mode in the bcs superconductors nb 1- x ti x n induced by terahertz pulse excitation. *Physical review letters*, 111(5):057002.

Matsunaga, R. and Shimano, R. (2012). Nonequilibrium bcs state dynamics induced by intense terahertz pulses in a superconducting nbn film. *Physical Review Letters*, 109(18):187002.

Matsunaga, R., Tsuji, N., Fujita, H., Sugioka, A., Makise, K., Uzawa, Y., Terai, H., Wang, Z., Aoki, H., and Shimano, R. (2014). Light-induced collective pseudospin precession resonating with higgs mode in a superconductor. *Science*, 345(6201):1145–1149.

Matsunaga, R., Tsuji, N., Makise, K., Terai, H., Aoki, H., and Shimano, R. (2017). Polarization-resolved terahertz third-harmonic generation in a single-crystal superconductor nbn: Dominance of the higgs mode beyond the bcs approximation. *Physical Review B*, 96(2):020505.

Méasson, M. A., Gallais, Y., Cazayous, M., Clair, B., Rodiere, P., Cario, L., and Sacuto, A. (2014). Amplitude higgs mode in the 2 h- nbse 2 superconductor. *Physical Review B*, 89(6):060503(R).

Micheli, A., Daley, A. J., Jaksch, D., and Zoller, P. (2004). Single Atom Transistor in a 1D Optical Lattice. *Physical Review Letters*, 93(14):140408.

Moor, A., Volkov, A. F., and Efetov, K. B. (2017). Amplitude higgs mode and admittance in superconductors with a moving condensate. *Physical review letters*, 118(4):047001.

Morampudi, S. C. and Laumann, C. R. (2018). *arXiv preprint arXiv:1808.08674*.

Nahum, A., Ruhman, J., Vijay, S., and Haah, J. (2017). Quantum entanglement growth under random unitary dynamics. *Phys. Rev. X*, 7:031016.

Nahum, A., Vijay, S., and Haah, J. (2018). Operator spreading in random unitary circuits. *Phys. Rev. X*, 8:021014.

Nakamura, S., Iida, Y., Murotani, Y., Matsunaga, R., Terai, H., and Shimano, R. (2019). Infrared activation of the higgs mode by supercurrent injection in superconducting nbn. *Physical review letters*, 122(25):257001.

Nambu, Y. (1960). Quasi-Particles and Gauge Invariance in the Theory of Superconductivity. *Physical Review*, 117(3):648–663.

Nandkishore, R. and Huse, D. A. (2015). Many-body localization and thermalization in quantum statistical mechanics. *Annual Review of Condensed Matter Physics*, 6(1):15–38.

Nica, A. and Speicher, R. (2006). *Lectures on the Combinatorics of Free Probability*. Cambridge University Press.

Novak, J. and LaCroix, M. (2012). Three lectures on free probability.

Papenkort, T., Axt, V. M., and Kuhn, T. (2007). Coherent dynamics and pump-probe spectra of bcs superconductors. *Phys. Rev. B*, 76:224522.

Pekker, D. and Varma, C. (2015). Amplitude/higgs modes in condensed matter physics. *Annu. Rev. Condens. Matter Phys.*, 6(1):269–297.

Petter, D., Natale, G., van Bijnen, R. M. W., Patscheider, A., Mark, M. J., Chomaz, L., and Ferlaino, F. (2019). Probing the roton excitation spectrum of a stable dipolar Bose gas. *Physical Review Letters*, 122(18):183401.

Popov, V. N. (2001). *Functional Integrals in Quantum Field Theory and Statistical Physics*, volume 8. Springer Science & Business Media.

Radzihovsky, L., Park, J., and Weichman, P. B. (2004). Superfluid Transitions in Bosonic Atom-Molecule Mixtures near a Feshbach Resonance. *Physical Review Letters*, 92(16):160402.

Radzihovsky, L., Weichman, P. B., and Park, J. I. (2008). Superfluidity and phase transitions in a resonant Bose gas. *Annals of Physics*, 323(10):2376–2451.

Rakovszky, T., Pollmann, F., and von Keyserlingk, C. W. (2018). Diffusive hydrodynamics of out-of-time-ordered correlators with charge conservation. *Phys. Rev. X*, 8:031058.

Romans, M. W. J., Duine, R. A., Sachdev, S., and Stoof, H. T. C. (2004). Quantum phase transition in an atomic Bose gas with a Feshbach resonance. *Physical Review Letters*, 93(2):020405.

Rothwarf, A. and Taylor, B. (1967). Measurement of recombination lifetimes in superconductors. *Physical Review Letters*, 19(1):27.

Serbyn, M., Papić, Z., and Abanin, D. A. (2013). Local conservation laws and the structure of the many-body localized states. *Phys. Rev. Lett.*, 111:127201.

Shimano, R. and Tsuji, N. (2020). Higgs mode in superconductors. *Annual Review of Condensed Matter Physics*, 11:103–124.

Srednicki, M. (1999). The approach to thermal equilibrium in quantized chaotic systems. *Journal of Physics A: Mathematical and General*, 32(7):1163.

Thalhammer, G., Barontini, G., Catani, J., Rabatti, F., Weber, C., Simoni, A., Minardi, F., and Inguscio, M. (2009). Collisional and molecular spectroscopy in an ultracold Bose–Bose mixture. *New Journal of Physics*, 11(5):055044.

Timmermans, E., Tommasini, P., Hussein, M., and Kerman, A. (1999). Feshbach resonances in atomic Bose–Einstein condensates. *Physics Reports*, 315(1):199–230.

Tommasini, P., Timmermans, E., Hussein, M., and Kerman, A. (1998). Feshbach Resonance and Hybrid Atomic/Molecular BEC-Systems. *arXiv:cond-mat/9804015*.

Turner, C. J., Michailidis, A. A., Abanin, D. A., Serbyn, M., and Papić, Z. (2018). Weak ergodicity breaking from quantum many-body scars. *Nature Physics*, 14(7):745–749.

Valdés-Curiel, A., Trypogeorgos, D., Marshall, E. E., and Spielman, I. B. (2017). Fourier transform spectroscopy of a spin–orbit coupled Bose gas. *New Journal of Physics*, 19(3):033025.

Vijay, S. and Vishwanath, A. (2018). Finite-temperature scrambling of a random hamiltonian. *arXiv preprint arXiv:1803.08483*.

Vincent Liu, W. (1997). Theoretical Study of the Damping of Collective Excitations in a Bose-Einstein Condensate. *Physical Review Letters*, 79(21):4056–4059.

Voiculescu, D. (1986). Addition of certain non-commuting random variables. *Journal of functional analysis*, 66(3):323–346.

Volkov, A. and Kogan, S. M. (1973). Collisionless relaxation of the energy gap in superconductors. *Zh. Eksp. Teor. Fiz*, 65:2038.

von Keyserlingk, C. W., Rakovszky, T., Pollmann, F., and Sondhi, S. L. (2018). Operator hydrodynamics, otocs, and entanglement growth in systems without conservation laws. *Phys. Rev. X*, 8:021013.

Wang, Z., Xue, J., Shi, H., Jia, X., Lin, T., Shi, L., Dong, T., Wang, F., and Wang, N. (2021). Transient higgs oscillations and high-order nonlinear light-higgs coupling in terahertz-wave drivennbn superconductor. *arXiv preprint arXiv:2107.07488*.

Warner, C., Lam, A. Z., Bigagli, N., Liu, H. C., Stevenson, I., and Will, S. (2021). Overlapping Bose-Einstein condensates of Na 23 and Cs 133. *Physical Review A*, 104(3):033302.

Weinstein, Y. S., Lloyd, S., and Tsallis, C. (2002). Border between regular and chaotic quantum dynamics. *Phys. Rev. Lett.*, 89:214101.

Wigner, E. P. (1958). On the distribution of the roots of certain symmetric matrices. *Annals of Mathematics*, pages 325–327.

Zee, A. (1996). Law of addition in random matrix theory. *Nuclear Physics B*, 474(3):726–744.

Zhang, Z., Chen, L., Yao, K., and Chin, C. (2021a). Atomic Bose-Einstein condensate to molecular Bose-Einstein condensate transition. *Nature*, 592(7856):708–711.

Zhang, Z., Chen, L., Yao, K.-X., and Chin, C. (2021b). Transition from an atomic to a molecular Bose–Einstein condensate. *Nature*, 592(7856):708–711.

Zhang, Z., Nagata, S., Yao, K., and Chin, C. (2022). Many-body Chemical Reactions in a Quantum Degenerate Gas.

CURRICULUM VITAE